Impulsive and Low-Thrust Optimal Trajectories for Asteroid Mining

By

JOSÉ CARLOS GARCÍA MATEAS

In collaboration with

EUROPEAN SPACE AGENCY (ESA)

Tutor: Manuel Sanjurjo Rivo

uc3m | Universidad Carlos III de Madrid

Department of Bioengineering and Aerospace engineering
UNIVERSIDAD CARLOS III DE MADRID

Bachelor thesis submitted to the Universidad Carlos III de Madrid in accordance with the requirements for the degree of BACHELOR IN AEROSPACE ENGINEERING in the Escuela Politécnica Superior.

SEPTEMBER 2018

ABSTRACT

Near – Earth Asteroids (NEA's) are celestial bodies which have ended up falling into orbits in the vicinity of the Earth due to the gravitational interactions these bodies have undergone in the past. As a result, they have posed a new threat to human existence since the risk of collision between the Earth and one of these bodies is certainly possible. Nevertheless, NEA's have also presented humanity with the opportunity of redefining its frontiers and changing the way in which the economical and development system can be conceived, since studies have suggested that these bodies are rich in natural resources such as water and precious metals.

As a result, NEA's have become attractive targets for mining missions. For this operations to be carried out the first step is performing a preliminary study of the trajectories that could take a mission to the asteroid's surface and return it back to Earth once the desired materials have been extracted. To that end, this thesis addresses the determination of optimal trajectories towards ten asteroids selected for the purpose, which include: Ryugu, 1989 ML, Nereus, Didymos, 2011 UW158, Anteros, 2001 CC21, 1992 TC, 2001 SG10 and 2002 DO3.

Results have been obtained for both, chemical propulsion systems and ion engines. Initially, a first study was carried out to determine the pork-chop plots characterizing each of the transfers and the mission with minimum ΔV (including outbound and inbound flights) was analyzed. Then, with the objective of optimizing the whole mission, the Non-dominated Sorting Genetic Algorithm II (NSGA-II) was used so as to broaden the trajectory possibilities and perform a study which also accounted for economical and time factors. With the use of NSGA-II, multi-revolution transfers as well as gravity assist maneuvers around Venus and Mars have been studied. In addition, multi-revolution trajectories using low-thrust were also considered.

The results presented in this thesis show the launching opportunities as well as the optimized asteroid mining missions for both type of propulsion methods being considered. In addition, a full development and analysis of the obtained values is carried out for asteroids Ryugu and Didymos.

DEDICATION AND ACKNOWLEDGEMENTS

Although my years at Universidad Carlos III come to an end with this work, I will never forget the change and impact that I have experienced while I pursued my Bachelor in Aerospace Engineering. It has been hard, but I believe that the effort has been worth it.

This thesis is the final step of the journey I began several years ago and I would like to thank all of those people who have been involved with it. Firstly, special thanks to Dr. Guillermo Ortega, head of the Guidance, Navigation and Control Section of the European Space Agency, for giving me the opportunity to work in such an amazing project. I would also like to thank Celia Yabar from the same organization for her support and help while conducting this thesis.

Huge gratitude also to my tutor, Manuel Sanjurjo, for his counsel and help throughout all the year. He has dedicated uncountable hours to answering my emails, meetings and guiding this project despite the difficulties presented due to me being in Belgium in an Erasmus+ program. Most importantly, he has made me discover my passion for Astrodynamics. I would also like to recognize the work of David Morante, not only for allowing me to use his previous research on low-thrust but also for all his help and support with different aspects of the thesis.

Also, thanks to my friends for the help they have always given me and for the good times we have passed together. In particular, to Andrea Luis, José Medinilla and Juan Manuel Calleja. The hardship of the journey has created strong bonds that will not be broken.

I cannot end up this dedication without recognizing the strength and love that I have received from the most important people in my life. To my parents, who always showed me the path of respect, education and effort. To Tania, whose love and energy has filled me when I wanted to quit. They have pushed me whenever needed. This work is for you.

José Carlos García
Liège, 25th of September, 2018

TABLE OF CONTENTS

LIST OF TABLES

TABLE **Page**

LIST OF FIGURES

Part I

ASTEROID MINING

CHAPTER 1

INTRODUCTION

Context

Since the appearance of the first civilizations in Mesopotamia, Greece, Persia and India during the early stages of history, progress and development of the human species has been intimately linked to the discovery, extraction, processing and usage of the Earth's natural resources. In particular, such activities were thrived with each of the industrial revolutions that took place during the last three centuries, which have been, at the same time, the period of history in which mankind has experienced its fastest growth.

The first industrial revolution, which started in the 1760's decade and lasted until the beginning of the 19th century, saw the birth of the steam engine. Together with the extraction of coal, it produced a change in the world's economic model switching it from agriculture to manufacturing and commercial exchange, which was favored with the development of rail transport [33]. The second industrial revolution took place almost one hundred years later, starting in 1870. It was, once again, linked to the discovery of new energy sources such as oil, gas and electricity, which, together with the development of the combustion engine and with the increased use of steel turned industry into mass production [33]. From 1970 onwards, the world saw the development and growth of electronic devices. Consequently, demand for raw materials such as copper, tin, nickel, aluminum, silver or lead boomed [34].

It is therefore clear that society, as we know it today, relies on natural resources and that this demand will not decay. In fact, taking into account that the world's population is estimated to grow up to 9700 million people by 2050 and up to 11200 million by 2100 [35], it can be expected that the demand for the beforementioned resources will continue to increase. Up to now, extraction of these materials has taken place in Earth. But, what if this process could be performed in space?

Near Earth Asteroids, commonly known as NEA's, present ideal candidates for this purpose. On the one hand, spectroscopic studies have determined that these bodies can be rich in many precious metals as well as water. In addition, the proximity of the orbits to Earth makes access to these bodies easier than going to the Moon [36]. To that end, chemical and ion propulsion methods can be used.

Asteroid mining may therefore revolutionize not only space exploration but also the future of humanity. As a result, interest in this activity has greatly increased in the past years and the European Space Agency (ESA) wants to carry out a preliminary basic analysis on the feasibility of accessing asteroids in order to perform asteroid mining operations.

1.1 Interests in Asteroid Exploitation

At first, speaking about mining an asteroid may sound as a very complex mission in which there are many unknowns and very few certainties. With such an unpromising presentation, it is logical to consider that private investors are not going to be interested in such type of ventures, which may also require considerable amounts of capital. With respect to the different space agencies one may also think that, considering the budget limitations and the existence of many other scientifically promising missions, the interest in asteroid mining can be inexistent.

However, this is not the case. As will be shown later several private companies are currently developing the technology for asteroid mining to become a reality while space agencies are carrying out, or planning to do so, missions to asteroids. The reasons behind this interest are multiple and diverse and will be analyzed below.

1.1.1 Depletion of Earth's resources

The formation of natural resources such as oil or gas occurs through a process that involves millions of years [37]. Similarly, the availability of metals such as iron, copper or cobalt is

defined by the ore reserves existing on Earth. All of these resources are non-renewable and, as a result, will run out in the future. When will this happen depends on two factors: the existing reserves and the rate of consumption. Table 1.1 below shows the extracted quantities for some metals and the corresponding expected year of depletion of such resources.

Metal	Mined Production	Units	Expected Year of Depletion
Copper	20 700 000	tonnes	2048
Lead	4 700 000	tonnes	2029
Gold	3 200 000	kg	2031
Silver	27 461 000	kg	2033
Zinc	12 300 000	tonnes	2031

Table 1.1: Extracted quantities of several metals in the whole world during the year 2016 [1] and expected year of depletion considering the extraction rate of 2014 [2].

As can be appreciated, some of the most commonly used metals such as copper or zinc will face depletion in the near future, while the same occurs with precious metals such as gold or silver. From an economical perspective, one of the conditions required for asteroid mining to be profitable is therefore present: the terrestrial offer will not be able to satisfy the demand since Earth's reserves will be consumed. As a direct consequence, it is expectable that prices of those metals will rapidly grow. Therefore, to the eyes of any private enterprise, being able to supply the Earth with those metals could be very profitable.

This idea has already attracted private businesses into developing the technologies required to do so. In fact, according to the predictions of one of the world's biggest investment banks, Goldman Sachs, the first human to become a trillionaire will be someone dedicated to mining asteroids [38].

1.1.2 Cost of launching payload into space

During the last decade the price for launching payload into space has strongly decreased due to the introduction into the launch market of several private companies. Entry barriers into the mentioned market have been reduced thanks to the support and funding via contracts that space agencies have provided and this has given birth to the development of several rocket vehicles and new technologies, such as reutilization, that have enabled the mentioned price reduction. Table 1.2 shows a comparison between the price per kilogram of launching payloads into low-Earth orbit using different launching systems.

Launcher	**Specific Costs** ($\$/kg$)
Falcon 9	2900
Proton-M	3000
Ariane 5	9000
Long March 3B	6000
Atlas V 551	8500
Delta IV Heavy	10250

Table 1.2: Comparison of the 2017 specific costs associated to different launchers for placing payloads into Low-Earth Orbits (LEO) [3].

Accessing space has therefore become affordable for many institutions, from private companies and space agencies to research centers and universities. However, launching prices are still high, especially in the case in which heavy launchers have to place big payloads into Earth escape trajectories, something common in the case of interplanetary missions.

As a result, an interesting idea for reducing the launching price of this types of missions consists in building some of the spacecraft components in space, with the objective of reducing the mass that the launcher has to lift. Of special interest would be to construct thermal shields. Such components, which are mainly intended to protect spacecraft's during re-entry maneuvers, tend to be heavy and voluminous. For example, in the case of NASA's Mars exploration rover *Curiosity*, the thermal shield (known as *aeroshell*), had a diameter of 4.5 meters and a total mass of 1562 kilograms [39] [40].

The *aeroshell* was constructed using tiles of phenolic impregnated carbon ablator,(*PICA*), a material invented by the NASA Ames Research Center [39]. Although such material cannot be retrieved from an asteroid, studies are being carried out with the objective of creating the mentioned thermal protections from regolith, which can be defined as the granular dust-type material found at the surface of planets, moons and asteroids [41].

Using this material as well as in-situ resource utilization of propellants obtained at the asteroid, it has been estimated that the total cost savings that could be achieved if a 2300 kilogram's regolith-based thermal shield was constructed would be of 161.6 million dollars per mission, considering a price of 5000 dollars per kilogram into LEO [42]. Therefore, regolith obtained from asteroids could be used to construct thermal shields and this would have a considerable impact on the costs of some of the missions space agencies work on.

1.1.3 Fueling spacecraft

As explained in the previous section, reducing a spacecraft mass is one of the possibilities that exist to reduce the cost of launch. Having already talked about the structure of the spacecraft, the other point towards which the aim of reducing mass can be targeted to is the propellant carried by the spaceships. Recalling once again NASA's Mars exploration rover *Curiosity*, one can find that 539 kilograms of propellant were stored for the cruise phase and that 387 kilograms were allocated for the entry, descent and landing phase, totaling 926 kilograms of propellant that had to be lifted-off from Earth by the Atlas V 541 rocket [39].

Similarly, the end-life of a satellite is usually determined by the availability of propellant found in its storage tanks. The reason behind this is that the gravitational pull of the Earth attracts the mentioned satellites towards the surface and therefore forces these systems to perform correction maneuvers so as to regain altitude and be able to maintain current operations. Eventually, the fuel will run out and this will mark the end to the satellite's operational life.

To avoid the two drawbacks explained above a possibility is to generate propellant in space. Doing so would then enable refueling satellites in order to maintain operations and would also save launching costs in future missions. To that end, studies are being conducted in order to develop systems that can generate water-based propellants in space, being the main principle to use electrolysis in order to separate water into hydrogen and oxygen [4]. Table 1.3 shows the expected demand for liquid oxygen (LOX) and liquid hydrogen (LH2) propellants if reusable launcher vehicles replaced the current upper stages to transfer satellites from LEO to geostationary orbit (GEO).

Propellant	**2018**	**2019**	**2020**
LOX [kg]	1 069 231	899 363	926 009
LH2 [kg]	178 205	149 894	154 335

Table 1.3: Predicted propellant demand taking into account commercial and government activities for the period 2018-2020 [4].

In any case, for this idea to be feasible there is the need to supply great amounts of water to the production station. Taking into account that, according to some estimates, near-Earth asteroids can contain up to two trillion tonnes of water [36] and that their corresponding orbits are close to Earth converts these bodies into ideal water supplier candidates for the propellant production in space.

1.2 History of Missions to Asteroids

Interest in asteroids is not new since several missions have been carried out by different space agencies with the objective of studying this type of celestial bodies and retrieving samples for analysis in the Earth. This section aims to provide a brief review of the main missions that have already been conducted.

1.2.1 First missions: NEAR Shoemaker and Deep Space 1

During the 1990 decade, interest in asteroids grew since little was known about the morphology, composition and characteristics of these bodies. As a result, the first missions such as *NEAR Shoemaker* and *Deep Space 1* aimed at studying and analyzing the different features that characterized asteroids. The former was launched the 17th of February of 1996 and was the first mission in history to orbit and touch down on an asteroid [43].

In the case of the latter, it was launched the 24th of October of 1998 and had the objective of studying the chemical composition and atmosphere of asteroid 9969 Braille as well as flying close to comet Borrelly [44]. In addition, this was the first spacecraft to use an ion engine [44].

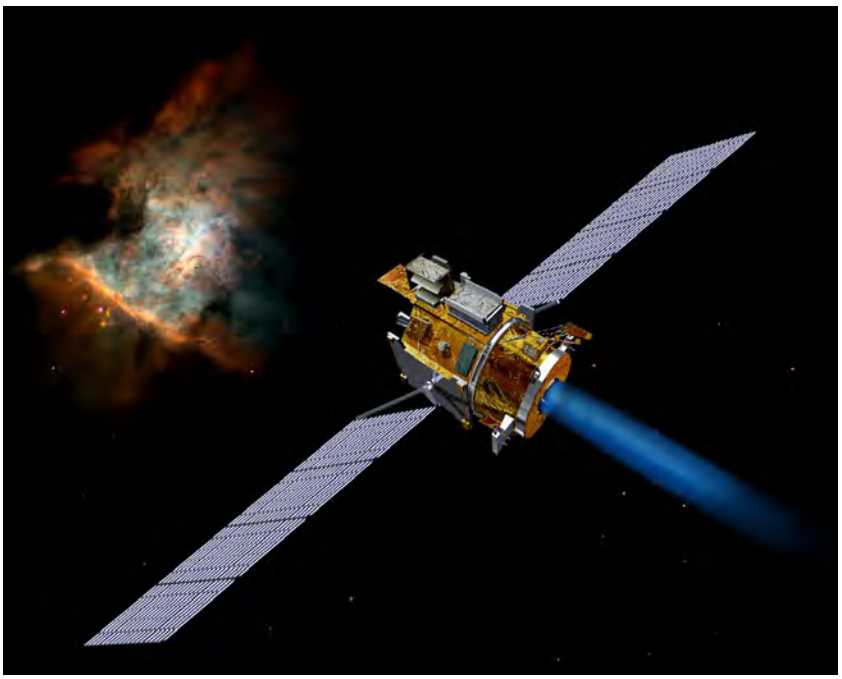

Figure 1.1: High resolution artistic representation of *Deep Space 1* [21].

1.2.2 Missions of the 2000 decade: Hayabusa and Dawn

With the arrival of the new century interest in asteroids did not decay and more missions were designed and launched towards several targets. In general, the main aim of such missions was to continue with the study of asteroid nature and history since there were still many questions to answer.

To that end, it was thought that bringing back samples from asteroids would favor and enhance the study of these bodies and, as a result, the first missions involving landing and returning from asteroids were conceived. This therefore implied developing technologies for anchoring and sample retrieval. The first mission to try to accomplish this task was the Japanese *Hayabusa*, launched the 9th of May of 2003 towards asteroid 25143 Itokawa [45]. Due to the diverse problems that this mission faced, such as the loss of a reaction wheel (that made attitude control more difficult) and the deterioration of the solar panels, the original planning had to be altered.

After remaining on a close orbit for some time, *Hayabusa* attempted several touch down maneuvers but failed either due to attitude control errors or to failure of the anchoring systems and the lander *Minerva* was lost. The sample return capsule arrived back to Earth the 13th of June of 2010 with approximately 1500 dust particles from asteroid Itokawa [45].

On the other hand, *Dawn* was launched September 27 of 2007 with the objective of orbiting around Ceres and Vesta, the two biggest bodies found in the asteroid belt. The aim of this mission was to study the size, shape, composition and characteristics as well as performing an image mapping of the surface and spectroscopic studies. This mission was successful and ended up in June of 2016 [46]. Figure 1.2 shows a topographic study of Ceres performed by *Dawn*, which reveals the altitude variations at the surface.

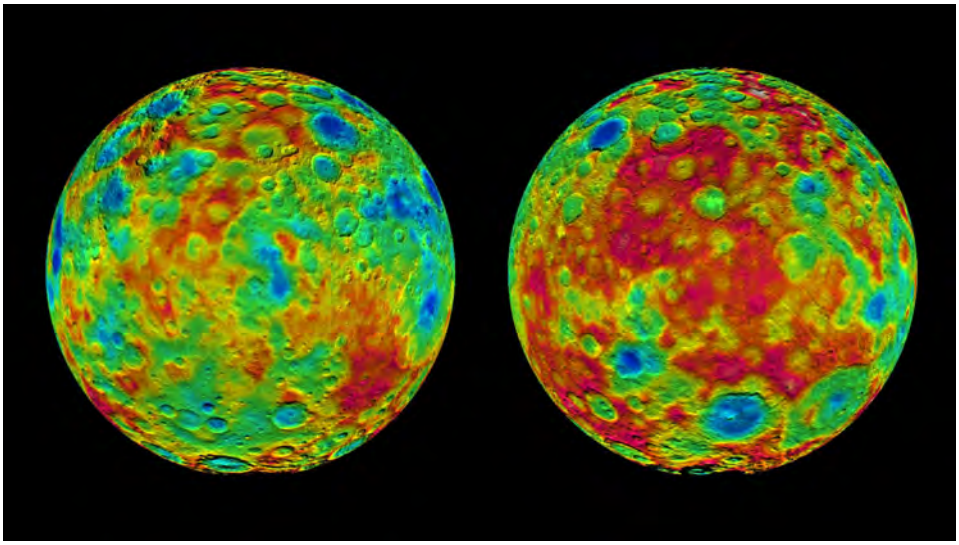

Figure 1.2: Topographic maps of the East and West hemispheres of Ceres [22].

1.2.3 Most recent missions: Hayabusa II and OSIRIS-REx

Despite the landing failures experienced by *Hayabusa*, the last scientific missions to asteroids have been designed with the main objective of returning a sample of asteroid rock back to Earth. Such is the case for *Hayabusa II*, that shares many components with her younger sister mission described in the previous section, and for *OSIRIS-REx*.

The Japanese mission was launched the 3rd of December of 2014 and is designed to meet with asteroid Ryugu, so as to study the asteroid, land and return the sample back to Earth by 2020 [47]. To fulfill these objectives, the mission is equipped with three *Minerva II* landers and a Mobile Asteroid Surface Scout (*MASCOT*) small rover [47].

With respect to NASA's mission *OSIRIS-REx*, the objectives are similar. Launched the 8th of October of 2016, it is directed towards asteroid Bennu with the aims of returning a sample, mapping the asteroid and studying the so-called Yarkosvky effect, that is, the deviation of orbits due to forces not related to gravity [48]. Figure 1.3 below shows an image of the spacecraft before departing from Earth.

Figure 1.3: *OSIRIS-REx* assembled and waiting for encapsulation in its payload fairing at NASA's Kennedy Space Center [23].

1.3 Current Initiatives

Having analyzed the past and the most recent missions to asteroids one may have noticed that all of them correspond to government initiatives either from the American NASA of from the Japanese JAXA. Europe, via the European Space Agency, aimed instead towards a similar type of celestial body such as a comet, with its successful mission *Rosetta*, that was able to study and land in the comet 67P/Churyumov-Gerasimenko.

The lack of private ventures responds to several reasons, among which one can find the big required investment, the degree of risk and uncertainty and the lack of maturity in the anchoring, extraction and processing technologies required to perform asteroid mining operations. Nevertheless, this picture has started to change during the last years with the appearance of new actors in the asteroid mining scenario.

1.3.1 Planetary Resources

One of this new businesses that has entered into this activity is Planetary Resources, a company based in Seattle born in 2009 under the name of Arkyd Astronautics that was brought out into the light of public media with the backup it received in 2012 from Google's founder Larry Page and in 2013 from Richard Branson.

The company is estimated to have around 70 employees and aims to convert asteroid mining into a feasible and profitable activity. To achieve so, it has already developed and launched several spacecraft among which one can find:

- The *Arkyd-3R*, which aimed to test and validate several technologies and subsystems. The first mission failed due to the explosion during lift-off of the *Antares* launcher that had to put it in orbit. Nevertheless, the company was able to send a second, *Arkyd-3R*, which was successfully deployed in 2015 from the International Space Station [24].
- The *Arkyd-6*, a six units CubeSat designed to test a mid-wave infrared imager as well as other communications, avionics and attitude and control systems. It was successfully launched in January 2018 and its systems functioned correctly, being currently in orbit around Earth. An image of this spacecraft can be seen in Figure 1.4.
- The *Arkyd-301*, which is the next generation of spacecraft's and is therefore under current design and development. It will be sent into space with the objective of gathering data on asteroids so as to enable the company to select future targets for the asteroid mining missions.

In addition to this, the company has also signed an agreement with Bayer, which will use the imagery services provided by Planetary Resources to improve agriculture. The government of Luxembourg has also partnered with the company, signing a cooperation agreement and investing up to 25 million euros [49].

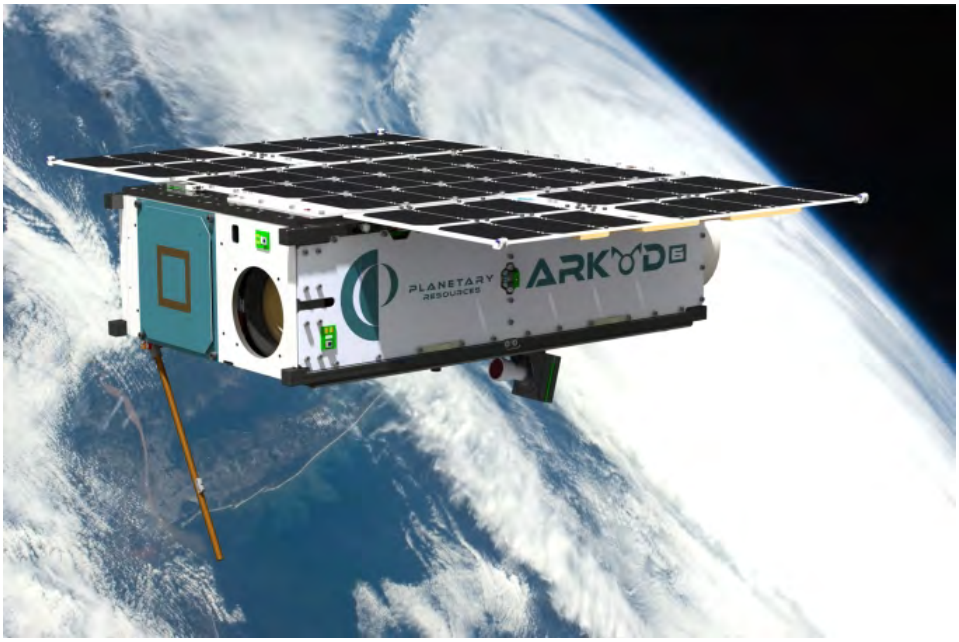

Figure 1.4: Representation of the *Arkyd-6* spacecraft orbiting the Earth [24].

1.3.2 Deep Space Industries

Based in Silicon Valley, California, Deep Space Industries (DSI) is the other main player taking part in the asteroid mining race. It was founded at the end of 2012 with the objective of enabling in-space utilization of resources, therefore entering into the biggest potential market of the next decades.

Nevertheless, before getting directly involved with mining asteroids, the company is first establishing the foundations to make this venture feasible and profitable by developing systems which greatly reduce the costs associated to accessing deep space. Doing so, Deep Space Industries aims to progress towards its ultimate goal of using in-space resources while at the same time generating income to support its activities.

Among the systems mentioned before which intend to reduce the costs of accessing deep space for both private industry and public agencies, one can see that Deep Space Industries has developed the following:

- *Comet* is a water-based propulsion system developed for CubeSat's and microsatellites. According to DSI, this system achieves up to 80% of the specific impulse that is usually reached with mono-propellant systems but with just 20% of the cost [50]. It is non-

toxic and provides more thrust with a lower electrical consumption compared to electric propulsion systems. The price for each unit is 200,000 dollars [50].

- *Xplorer* is the solution proposed by DSI to a achieve low-cost spacecraft's suitable for deep space missions. It is based on the idea of using rideshare launches (also known as piggyback launches) to achieve low Earth orbit. Once there, the spacecraft is designed so as to use its own propulsion system to reach Earth departure trajectories, being able to operate at distances of up to 2.5 astronomical units (AU) from Earth [51]. The spacecraft has 12 units (standard dimensions for CubeSats, being each unit 10×10×10 cm) of inboard volume plus 8 units of outboard available for payload [51].

- DSI has also performed conceptual simple designs of spacecraft exclusively aimed for asteroid mining. Among them, one can find exploration vehicles such as *Prospector's-1A & 1B, Prospector's- XA & XB, Dragonfly's 1 & 2* or extraction spacecraft's such as *Harvestor's 1 & 2*, of which one can see a representation in Figure 1.5 below.

Figure 1.5: Artistic representation of the *Harvestor - 1* spacecraft intended for asteroid mining operations [25].

With respect to financial aspects, Deep Space Industries has already signed several deals to supply its *Comet* propulsion system. Furthermore, it has also signed an agreement with the government of Luxembourg to develop the *Prospector-X* series of exploration spacecraft's so as for them to be operative after 2020 [52].

1.4 Legal Framework for Asteroid Exploitation

The previous section has shown that space agencies are no longer the only organizations interested in asteroids and how some private companies are entering into the asteroid mining nascent industry. From the aspects mentioned above the reader can notice two important facts:

- The two biggest companies dedicated to asteroid mining were created and have their current headquarters in the United States.
- The government of Luxembourg has signed agreement memorandums and invested in both Planetary Resources and Deep Space Industries, being both companies in process of establishing their corresponding European divisions in Luxembourg.

As can be expected, such facts do not correspond to mere coincidences. In order to understand these two points it is therefore necessary to analyze the current state of space law and the legislation changes that have taken place during the last decade.

1.4.1 Main regulatory framework

Space is a vast region with no defined boundaries. Questions regarding space exploration, space utilization and ownership of space started to appear as soon as the first artificial satellites were put into orbit. With the objective of answering all of these issues and establishing a supranational regulatory framework, the General Assembly of the United Nations created in 1959 the so-called Committee on the Peaceful Uses of Outer Space (*COPUOS*) [53]. Since its creation this organism has issued five treaties and five principles for outer space, which have been signed and ratified by variable numbers of countries depending on the treaty. From the asteroid mining perspective the most relevant are:

- **The "Outer Space Treaty"** : passed in October 1967, this document provides the basic legal framework for space activities. As a result, among its articles one can find several which directly affect asteroid mining operations, as it is stated that:

  - Article I states that space is a domain belonging to all mankind and hence that the exploration and usage of the celestial bodies found in outer space has to be carried out so as to benefit humanity as a whole [54].

- Article II affirms that space is a domain in which no country has the right to claim sovereignty over any celestial body, neither to use it nor to occupy it [54].
- Article VI refers to the fact that any national activity carried out in outer space or in celestial bodies is a responsibility of the country where that activity has been originated, independently of whether it is carried out by government agencies or by non-government corporations, and so that the country is responsible for authorizing and supervising them [54].
- Article IX states that contamination of space has to be avoided to the greatest degree possible by the countries accessing this medium [54].

- **The "Moon Agreement"** : approved by the General Assembly of the United Nations in 1979, it did not become effective until 1984. From the point of view of asteroid mining this treaty is very relevant since it contains many articles related to the exploitation of the resources obtained from celestial bodies. The most noticeable articles include:

- Article 2, which states that all the activities to be carried out on the Moon or on other celestial bodies are subjected to international law [55].
- Article 4, where it is mentioned that the exploration and usage of the Moon and the celestial bodies considered in this treaty has to be performed for the benefit of all countries [55].
- Article 8, which indicates that activities can be pursued at any place above or below the surface of the Moon or of the celestial bodies being considered [55].
- Article 9, which enables parties to establish stations on these bodies irrespectively of whether those stations are manned or not [55].
- Article 11, where the first point defines the resources found on the Moon and other celestial bodies as common to all mankind. In addition, point 3 of this article reinforces this idea by stating that no natural resource can become property of a state, international organization or non-governmental entity [55].

However, and in contrast with the "Outer Space Treaty", such agreement has only been signed since its approval by 18 countries due to the fact that no parties involved in the

launching of exploration missions are interested in doing so. As a result, neither the United States, Russia, China nor most of the European Union countries have signed the agreement, meaning that from the practical point of view of asteroid mining operations the existing bounds are those defined in the "Outer Space Treaty".

1.4.2 SPACE Act of 2015

The treaties and articles mentioned above correspond to international laws approved by the United Nations. However, those laws do not imply that countries cannot approve and introduce their own legislation in the matter. As mentioned previously, the fact that both Planetary Resources and Deep Space Industries have their corresponding headquarters in the United States responds to two main reasons: on the one hand, obtaining private funding for such ventures is easier there since the startup culture is more rooted and, on the other hand, their corresponding activities are enhanced and supported by American law.

Responsible of providing such support and stability is the so-called SPACE Act of 2015, officially known as the *U.S. Commercial Space Launch Competitiveness Act (H.R.2262)* [1], approved during the presidency of Barack Obama. Such law contains, under Title IV, the denominated Space Resource Exploration and Utilization Act of 2015, which has two sections that will probably change the future of asteroid mining. These are:

- Section 51302, which states that U.S federal agencies should promote and facilitate citizens to embark on commercial exploration and exploitation missions of outer space resources.
- Section 51303, where it is defined that any citizen from the United States has the right to claim over asteroid and space resources, with the objective of owning, transporting, using and selling the mentioned resource.

With such a legal basis behind, businesses have the framework to develop asteroid mining missions, since U.S law entitles those enterprises to own the resources found in the asteroids or celestial bodies to which they are able to arrive.

[1] Public Law 114-90–NOV. 25, 2015 passed by the Senate and the House of Representatives of the United States of America.

1.4.3 Luxembourg's space law

The approval of American law marked the beginning of the race for asteroid mining and the Grand Duchy of Luxembourg did not want to lose pace. As a result, after 18 months of work, it issued the 20th of June 2017 law regarding the exploration and utilization of space resources [2], with the objective of becoming the European base for space mining companies.

Taking into account that Luxembourg is not one of the signing parties of the "Moon Agreement", it could approve and issue this law with the objective of providing a stable and favorable regulatory framework for the exploration and exploitation of space resources. Such law is comprised of several articles among which Article 1 is of special relevance, since it states that space resources are susceptible to be owned.

Similarly, Article's 2,6,7,8 and 9 define the administrative procedures and requirements for companies and individuals to be granted this right by the government of Luxembourg, who will do so after performing an exhaustive evaluation of the parties and the mission plans and objectives.

In addition, the interest of Luxembourg is further assured by the fact that it is planning to create its own space agency as well as a space investment fund with the objective of providing financial support for future space ventures [56].

[2] Loi du 20 juillet 2017 sur l'exploration et l'utilisation des ressources de l'espace, approved by the House of Deputies of the Grand-Duchy of Luxembourg.

CHAPTER 2

NEAR EARTH ASTEROIDS

Asteroids are small celestial bodies which are generally found in the vicinity of the main asteroid belt, located between Mars and Jupiter. Nevertheless, some of these bodies are also located in the proximity of Earth after having experienced orbit perturbations. This has therefore given mankind the possibility of studying such bodies from a relatively small distance, favoring a better understanding and facilitating the access of scientific missions which have unveiled incredible results.

Such results have made asteroids promising targets for future exploration and exploitation activities such as mining. This chapter therefore aims at presenting and explaining the concepts related to asteroids which have made this bodies interesting for commercial purposes, from the general considerations, compositions, and orbital elements to more exploitation related concepts. Finally, an analysis of the ten asteroids being considered for this thesis is presented.

2.1 General Considerations

Near Earth Objects (NEO's) is the denomination into which asteroids and comets that have orbits close to Earth can be classified. Despite having distinct names, scientist still question what are the differences between such two types of bodies. In general, comets are characterized by having large quantities of volatiles, that is, molecules such as CO_2, CO and H_2O, while asteroids have greater contents of solid rock.

Scientist believe that due to this compositions comets were formed in the outer cold regions of the Solar System and that as a result of the low temperatures the characteristics have been preserved, while asteroids were formed in the closer warmer regions [57]. As a result, it is believed that nowadays existing comets are just the remaining parts of the formation processes that gave birth to Jupiter, Saturn. Uranus and Neptune, while asteroids are considered to be the corresponding counterparts from the formation processes of Mercury, Venus, the Earth and Mars [57].

Asteroids and comets therefore spur scientific interest because getting to know the composition, nature and history of such bodies will probably enable scientist to understand how the Solar System was formed billions of years ago.

2.1.1 The impact threat

Despite the fact that NEO's are extremely interesting from the scientific point of view, it is also true that these bodies pose a threat towards Earth and its inhabitants and the reason for this is no other than the proximity of NEO orbits to Earth.

The Earth gets impacted several times each day by small fragments that disintegrate due to the high temperatures that appear during atmospheric re-entry. This phenomena is not a problem provided that the size of the mentioned fragments is small. If, on the other hand, such fragments are big, an impact could take place against the Earth's surface but, due to the relatively small dimensions, nothing noticeable would happen. The danger appears when the fragments mentioned before turn out to be big asteroids. Table 2.1 shows information regarding impact probabilities of three asteroids, as well as information regarding size and mass.

Object Designation	**Year Range**	**Impact Probability**	**Estimated Diameter** $[km]$	**Estimated Mass** $[kg]$
410777 (2009 FD)	2185-2198	$1.6 \cdot 10^{-3}$	0.160	$3.2 \cdot 10^{9}$
Bennu (1999 RQ36)	2175-2199	$3.7 \cdot 10^{-4}$	0.490	$6.0 \cdot 10^{10}$
Apophis (2004 MN4)	2060-2105	$8.9 \cdot 10^{-6}$	0.370	$6.1 \cdot 10^{10}$

Table 2.1: Examples of NEO's that could impact the Earth. The table shows the time span over which impacts have been detected, as well as the cumulative impact probability and the estimations regarding mass and diameter [5].

In the case in which an impact involves a celestial body of the dimensions shown in Table 2.1, humanity would probably face extinction, just as it is believed that happened to

dinosaurs several millions of years ago. In order to avoid such contingency, NASA created the Planetary Defense Coordination Office, *PDCO*, and the Center for NEO Studies, *CNEOS*. The latter is in charge of studying NEO orbits with the objective of predicting close approaches and calculating the impact probabilities. In addition, NASA will also launch in 2021 its *DART* (Double Asteroid Redirection Test) mission, which has the objective of impacting on a moonlet of the *Didymos* asteroid with the objective of altering its orbit [58].

On the side of the European Space Agency, it has also been working on protecting Earth from this danger. Pioneer in the concept of deflecting an asteroid with its *Don Quijote* project, it now contributes with mission *AIDA* (Asteroid Impact and Deflection Assessment), which has the objective of studying the effect produced by the impact of *DART*. Furthermore, it is in process of developing the so-called NEO Survey Telescope, specially designed for the discovery of new near-Earth objects.

2.1.2 Discovery statistics

In order to be able to prevent impact events from occurring it is necessary to define the orbits of the NEO's and assess the impact probability. To that end, it is essential to find and locate as many near-Earth objects as possible.

Nowadays, the vast majority (up to 90%) of the NEO's which are greater than one kilometer are already known, being efforts placed in discovering the NEO population that is over 140 meters [8] . To achieve so, a series of telescopes are used in order to search the sky. Table 2.2 below shows the statistics concerning the number of these bodies that have been discovered up to now.

	This Month	**This Year**	**All Time**
Number of NEO's discovered	57	1170	18721

Table 2.2: Number of NEO's discovered up to September 12, 2018 [6].

Figure 2.1 below provides a greater insight into the numbers given in Table 2.2. As can be appreciated, almost all the NEO's discovered up to now are asteroids, something logical considering that this bodies were formed in the regions closer to the Sun (and hence to Earth) while comets were created at the outer regions of the Solar System, as was explained at the beginning of Section 2.1. In addition, one can also appreciate that the number of

asteroids with a diameter greater than $1km$ is considerably small, and that the number of known bodies with those characteristics has not significantly varied in the last years.

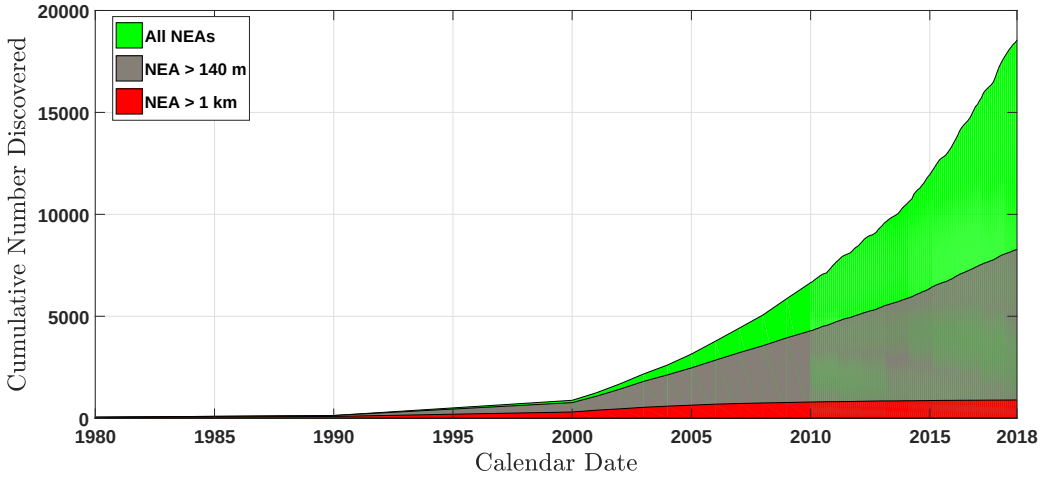

Figure 2.1: Number of near-Earth asteroid known, classified according to date and estimated diameter. Data taken from [8].

2.2 Asteroid Classification

As can be seen in Figure 2.1, there are approximately 18,400 NEA's identified. Despite the fact that each body is unique and different, near-Earth asteroids can be classified into different groups according to criteria based on the orbital elements or to criteria based on the reflectance spectra, which gives an idea about the chemical composition of the body.

2.2.1 Classification according to orbital parameters

In order to classify near-Earth asteroids as a function of orbital parameters there is the need to recall three basic definitions that will ease in the understanding:

- periapsis radius, r_p : it is the distance of the minimum separation point (perihelion), which is the point at which the asteroid comes closest to the Sun.
- apoapsis radius, r_a : it is the distance of the point in the orbit at which the asteroid is furthest apart from the Sun (aphelion).
- semi-major axis, a : it is defined as the sum of the periapsis and apoapsis distances divided by two.

Taking into account that the average distance between the Sun and the Earth is 1 AU[1], near-Earth asteroids are then defined as those which have a perihelion distance smaller than 1.3 AU [7]. Further classification is then performed into the so-called *Atiras*, *Apollos*, *Atens* and *Amors* sub-groups as a function of the three distances defined above. Such classification criteria can be seen in Table 2.3.

Group Type	Classification Criteria
Atiras	$a < 1\ AU$ and $r_a < 0.983\ AU$
Atens	$a < 1\ AU$ and $r_a > 0.983\ AU$
Apollos	$a > 1\ AU$ and $r_p < 1.017\ AU$
Amors	$a > 1\ AU$ and $1.017 < r_p < 1.3\ AU$

Table 2.3: Summary of the classification criteria of near-Earth asteroids according to orbital parameters [7].

Physically speaking, one can then define *Atiras* as asteroids completely found inside the Earth orbit, while *Atens* cross Earth's orbit having a smaller semi-major axis. On the other hand, *Apollos* are asteroids that also cross Earth's orbit while having a greater semi-major axis. Finally, *Amors* are asteroids located outside the orbit of the Earth but inside the orbit of Mars [7]. Table 2.4 below shows the total number of asteroids discovered classified according to the criteria explained in this section.

Group Type	Number Discovered
Atiras	18
Atens	1386
Apollos	10194
Amors	7025

Table 2.4: Total number of NEA's discovered as of September 2018, classified into the corresponding sub-groups according to orbital elements [8].

2.2.2 Classification according to reflectance spectra

The second criteria to classify asteroids, and the most interesting for mining missions, is according to the composition of the body. Determining the composition is no easy task and has to be done by performing what is known as telescopic spectrophotometry.

[1] One astronomical unit is equivalent to 149,598,000 kilometers.

Principally, telescopic reflectance spectroscopy is performed using Earth-based telescopes, although sometimes different spacecraft have been able to perform this studies, either because they were launched with that aim (such as for example the missions described in Section 1.2) or because they performed close approaches to asteroids while on journey to other destinations.

This method is based on the fact that no mineral or component absorbs light at the same wavelenght as another one. As a result, each component has particular absorption features which produce characteristic reflectance spectra. Once this spectra have been obtained, a comparison can be performed with the laboratory results available from experiments and tests carried out on Earth with samples of minerals and fallen meteorites [12].

Nevertheless, one must take into account that this method has two main limitations which are responsible for the uncertainty levels that are found when defining the composition of asteroids. On the one hand, telescopic reflectance spectroscopy only enables a study of the surface composition of the asteroid, which is daily altered and affected by solar radiation, which may cause reactions between components that end up affecting the reflectance characteristics of the asteroid [12].

The second problem is that most of the available meteorite samples correspond to asteroid interiors, which have not undergone the alteration process described in the previous paragraph. Therefore, testing in the laboratory yields results that are different and this makes very complicated the identification of similarities in the composition of the bodies [12]. To all of this one can add that the difficulties are increased by factors such as grain size (because light is reflected by smaller grains faster than by bigger grains, resulting in a reduced absorption) and by the nature of the mineral mixtures [12].

In order to classify asteroids according to the reflectance spectra one must first know which are the mineral groups which are used in order to perform this classification and how do the corresponding reflectance characteristics evolve with wavelength. To that end, Table 2.5 and Figure 2.2 below are provided.

Minerals	Chemical Composition
Pyroxene	Na, Ca, Mg, Fe, Al, $AlSi_2O_6$
Olivine	Mg_2SiO_4, Fe_2SiO_4, $CaMgSiO_4$, $CaFeSiO_4$, Mn_2SiO_4
Plagioclase	Feldspar minerals from $Na(AlSi_3O_8)$ to $Ca(Al_2Si_2O_8)$
Iron	Fe

Table 2.5: Minerals used in the reflectance spectroscopy and the corresponding chemical compositions [9] [10] [11].

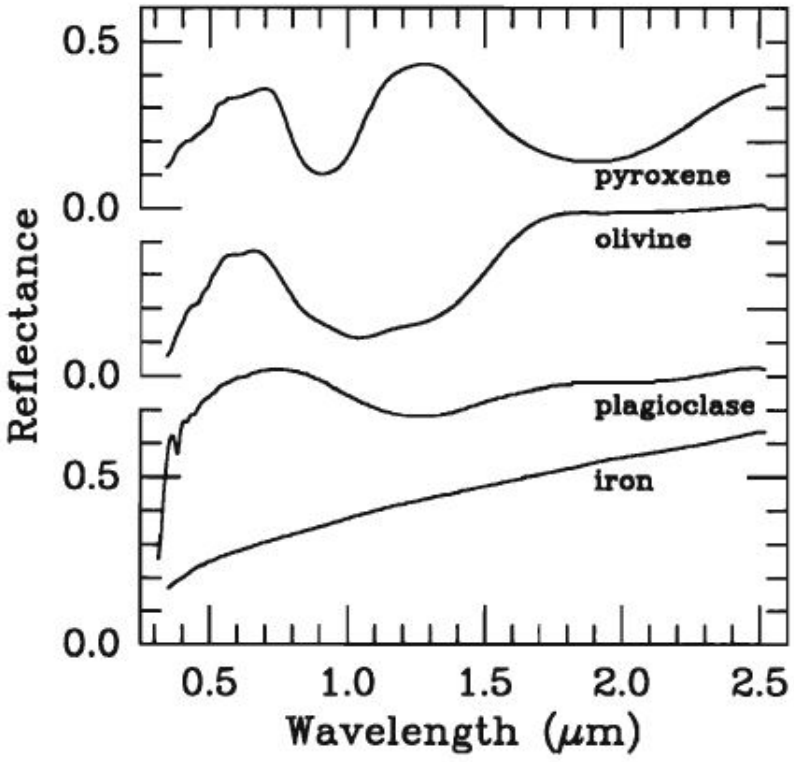

Figure 2.2: Reflectance as a function of the wavelength for pyroxene, olivine, plagiocase and iron [12].

From an analysis of the reflectance spectroscopy asteroids can then be classified into fourteen groups which are labeled with a letter, so that asteroids can be of type A, B, C, D, E, F, G, M, P, Q, R, S, T and V. The surface composition of all of these groups can be appreciated in Table 2.6 below.

Asteroid Type	Surface Mineralogy
A	Olivine or olivine and metal
B, C, F, G	Hydrated silicates, carbon, organic compounds
D	Organic-rich silicates, carbon
E	Enstatite ($MgSiO_3$)
M	Metal, silicates
P	Organic-rich silicates, carbon
Q	Olivine, pyroxene and metal
R	Pyroxene and olivine
S	Metal, olivine and pyroxene
T	Organic-rich silicates, carbon
V	Pyroxene and feldspar

Table 2.6: Interpreted surface composition for each type of asteroid classified according to reflectance spectroscopy criteria [12].

2.3 Selection of Asteroids for Mining Operations

As has been seen in Section 2.1.1, near-Earth asteroids pose a threat to human existence. However, Section 2.2.2 has also shown that asteroids may be rich in resources and that performing asteroid mining may be a profitable activity. In order to carry out such mission, the next step once the composition of the asteroids has been defined is to select the possible target bodies which can be, a priori, interesting, and to do so several factors have to be taken into account.

To begin with, it is necessary to roughly estimate/know the diameter of the asteroid, since it is necessary for the body to be sufficiently big so as for the spacecraft to be able to land and carry out the extraction process (this thesis works with the hypothesis that the spacecraft has to land on the asteroid).

Secondly, since the objective of the transfer trajectory is to be as cost-efficient as possible, the asteroids to be considered should have low inclination angles i. Taking into account that the inclination is defined as the angle between Earth's equatorial plane and the orbital plane, having a low inclination means that the change-of-plane maneuvers the spacecraft has to perform are simple and hence do not involve a big cost in terms of propellant. Furthermore, it is also desirable for the selected asteroids to have a semi-major axis similar to that of the Earth (recall that for Earth $a \approx 1\ AU$), since this implies that the body is relatively close as well as low eccentricities e (the lower e, the closer the orbit is to a perfect circle) [59].

With these premises, ten near-Earth asteroids were selected in accordance with the European Space Agency in order to analyze and optimize the spacecraft trajectories. The ten asteroids considered and some characteristics are shown in Table 2.7 below.

Asteroid Name (ID)	**Asteroid Type (orbit class)**	**Eccentricity** [−]	**Semi-major Axis** [AU]	**Inclination** [$degrees$]	**Orbital Period** [$days$]
Ryugu (162173)	Apollo	0.19022	1.18960	5.88374	473.91484
1989 ML (10302)	Amor	0.13656	1.27246	4.37789	524.28255
Nereus (4660)	Apollo	0.35997	1.48876	1.43155	663.49168
Didymos (65803)	Apollo	0.38383	1.64458	3.40768	770.34333
2011 UW158 (436724)	Apollo	0.37622	1.62064	4.57169	753.57949
Anteros (1943)	Amor	0.25604	1.43044	8.70627	624.89143
2001 CC21 (98943)	Apollo	0.21936	1.03255	4.80853	383.23401
1992 TC (7474)	Amor	0.29227	1.56564	7.08811	715.54396
2001 SG10 (194006)	Apollo	0.42427	1.44853	4.25715	636.78324
2002 DO3 (-)	Apollo	0.49931	1.86023	3.80171	926.71674

Table 2.7: Information on the ten asteroids selected for the analysis of mining missions. Data has been obtained from the *JPL Small Body Database Browser* [13] and rounded up to five decimal places.

2.4 Exploitation

Once the asteroids selected for analysis have been defined, it is then necessary to move on to analyzing the different characteristics, threats and difficulties of carrying out mining operations in an asteroid.

2.4.1 Type of mission: manned, automated or teleoperated

One of the firsts questions to answer is whether the asteroid mining mission is going to involve putting humans on the surface or not, since this has important implications.

On the one hand, sending human miners to asteroids implies many difficulties. This type of missions will normally be long (a complete round trip to an asteroid may take several years) and before being possible will require big investments in developing the necessary technology for sustaining human life for such periods of time. Questions regarding how to protect the crew from solar radiation, how to generate the food and water supplies or even how to treat medical contingencies that may appear during the mission will have to be answered [60]. In addition, sending a group of miners will imply having to design and build big spacecraft, with the consequent technical difficulties as well as launching cost increments. It is true that this type of missions present advantages such as that critical thinking would be available at the asteroid to solve any issues and that maintenance operations could be performed in case of equipment failures, but it is nowadays technically infeasible.

On the other hand, considering a fully automated mission is a very promising idea as, to begin with, most of the problems described in the previous paragraph disappear. However, this type of mission also has its inconveniences, which are mainly related to the fact that it is technically very difficult to automate mining processes. Automation is effective when the operations to be carried out are simple and repetitive [61]. However, whether this is the case for asteroid mining is yet unknown.

As a result, nowadays the most feasible option for asteroid mining is to carry out teleoperated missions, following the principles used for rovers such as *Curiosity*. It is true that this type of mission would face the problem of the delay in the communications because of the separation between the control center in Earth and the different equipment on the asteroid, but it is a problem which has already been solved previously. Maintenance would be, once again, probably difficult to manage but this issues could be addressed just by applying redundancy principles.

2.4.2 Environmental conditions

Once the type of mission has been selected, it is necessary to design equipment and systems in such a way as to be fully operative at the asteroid's surface. To do so, the environmental conditions found at this type of bodies have to be determined and analyzed, since the impact they can have on the operations is very noticeable. Knowing temperatures will surely be necessary, as well as determining the gravitational force of the asteroid or whether there is a great amount of dust, as this may cause maintenance problems.

The strength of the asteroid's gravitational force will determine which type of anchoring method to use as well as the nature of the systems employed for obtaining and storing the desired materials. Although information about this is very scarce, one can logically think that, since asteroids are in general small bodies, the gravitational force will also be considerably small. This will therefore have important implications:

- It will affect the way in which the landing maneuver is performed. Landing on a region of the asteroid full of regolith and hence less consistent can cause a big cloud of dust and small fragments. Besides the fact that the mentioned fragments may damage the spacecraft, the evolution of the dust cloud is unknown and there is the possibility that it remains in the area. As a result, equipment failures may occur more easily since the mentioned dust can block ducts and filters.
- Escape velocities can be very small, of approximately 20 cm/s [62]. This therefore completely eliminates the possibility of performing mining operations based on controlled explosions. In addition, it posses the problem of how to anchor the drilling equipment to the asteroid (on the Earth the equipment's own weight is usually able to counteract the drilling force) and how to collect/retain the broken chunks and prevent them from flying away.

Temperatures are another critical factor to account for. If the temperatures are very low, then problems regarding the brittleness of the material will appear and operations will not be able to be performed. If, on the other hand, temperatures are very high, it is probable that some kind of cooling system will be required by the mining equipments [61] .

2.4.3 Extraction and processing

Once the landing of the spacecraft on the desired location has been achieved, the next step is to deploy the extraction equipment, which has to ensure appropriate traction capabilities so as to be able to move on the asteroid's surface. After the equipment has reached its destination, the first step before starting with the mining operations is to somehow clamp the mentioned systems to the working area.

If the surface is non-consistent, then either contra-rotating screws can be used to burrow the equipment almost completely into the surface or some kind of net/cable can be passed around the asteroid [14]. On the opposite case the mission could be anchored by several

different methods such as by firing harpoons that penetrate into the surface, drilling in screws or even welding the equipment into big metallic rocks [14].

Once the equipment has been successfully secured, the actual mining operations can begin. The method used to extract the material will again depend on the type of surface. Regolith or small rocks can be retrieved using an excavator with a scoop. On the other hand, hard rocks will have to be cutted, drilled or broken into smaller pieces. Table 2.8 summarizes the possibilities regarding the extraction of material.

Type of Material	**Extraction Method**
Unconsolidated / Regolith	Scooped or scrapped
Silicate matrix	Drilling and blasting or cutting
Silicates and ice or hydrocarbons	Vaporization
Silicate and metal	Cutting and crushing
Solid metal	Cutting or melting

Table 2.8: Classification of the possible extraction methods as a function of the type of material to be retrieved [14].

Once the material has been extracted, the last consideration to address is how to process and store the products. The main question will be whether to crush the material or whether to load it directly into the cargo bay. The trade-off here is basically related to the fact that crushing the material would allow a much more efficient use of the volume of the cargo bay while at the same time it would complicate even more the operation, since specially developed machines would have to be used with the consequent increase in costs and also in the probabilities of equipment failure.

CHAPTER 3

PROJECT DESCRIPTION

3.1 Project Objectives

As has been explained in the previous chapters, asteroids pose a threat to Earth's integrity while at the same time present a promising source of resources for mankind that could revolutionize not only space exploration but also people's daily life. Extracting these resources is therefore an attractive activity not only for commercial purposes but also for scientific reasons, making it therefore interesting for private companies as well as space agencies.

Despite this, asteroids present a big number of uncertainties that have to be answered in order for mining operations to become a reality. Nevertheless, with the current information available it is possible to define a basic outline of how an asteroid mining mission could be. Of utmost importance is to perform the preliminary design of the interplanetary trajectories that future spacecraft would have to follow to reach those targets.

As the reader will see in the following chapters, this thesis tries to enlighten the path by performing a preliminary study of the trajectory opportunities to reach ten asteroids which appear to be promising targets for mining operations. After this, focus is placed on optimizing the whole asteroid mining mission by using a genetic algorithm, *NSGA-II*, with the objective of finding the best possible missions for each asteroid. Trajectories are computed and optimized considering both chemical and electric propulsion methods and gravity assist maneuvers are also taken into account.

3.2 Thesis Structure

To accomplish the objectives described in the previous paragraph this thesis has been structured into three main parts: an introduction to asteroid mining, methodology and software description and finally results and conclusions.

The current first part has been devoted to presenting the state of the art regarding asteroid mining. Past exploration missions have been mentioned and the interests that asteroid mining arouses have been explained. In addition, current initiatives were described as well as the legal existing framework for the development of this ventures. Furthermore, asteroids have been presented to the reader: the threats posed, the discovery statistics and the classification criteria have been defined, and the list of the ten targets selected was given. This was all followed by a discussion of the technical challenges that asteroid mining faces.

The second part of this project is focused on explaining to the reader how has the author modeled and solved the problem of optimizing asteroid mining missions. The method of patched conics, *Lambert's problem*, gravity assist maneuvers and the nature of low-thrust trajectories are explained, while justifications are provided for the assumptions introduced. The second part then ends by providing an explanation of the software and tools used to carry out the computations.

Finally, the third part of this thesis is devoted to presenting the results obtained. The optimized asteroid mining mission for two of the ten asteroids are presented and analyzed for both types of propulsion and a final economic study on the profitability and impact of the missions is described. Optimized trajectories for the remaining eight asteroids are provided in Annex A. This thesis ends with an analysis of the budget that has been necessary to carry out this project, detailed in Annex B.

Part II

METHODOLOGY AND SOFTWARE DESCRIPTION

CHAPTER 4

INTERPLANETARY TRAJECTORIES EARTH - NEA'S

Introduction

One of the most important parts of the asteroid mining missions, and the one in which this thesis focuses on, is designing the trajectories that spacecraft would have to follow in order to reach the desired destinations. The idea looks simple: we want to go as fast as possible and at the minimum cost, that is, with the minimum propellant consumption. However, reality proves to be much more challenging since space is a three-dimensional hostile domain full of bodies and in which each one of them has its own particular orbital parameters.

In general, trajectories can be considered to have several characteristic events among which one can find the departure from Earth, the cruise phase (where the flight can be directly towards the target or have intermediate steps) and the arrival at the target body. In the case of asteroid mining missions, since the objective is to return the mined material, the problem has to be solved twice. This chapter focuses on explaining the mathematical and physical concepts employed in order to characterize and design the trajectories for the ten asteroids given in Chapter 2.

4.1 Sphere of Influence

Planets are kept orbiting around the Sun due to the gravitational pull that this body produces. Nevertheless, when a spacecraft sufficiently approaches a planet, the gravitational pull of the planet becomes dominant and hence the motion of the spacecraft is influenced much more strongly by the planet's gravity rather than by that of the Sun.

The limit that differentiates the region where the gravity of the planet becomes stronger than that of the Sun is known as the radius of the sphere of influence. It is measured in km and can be computed using the following equation

$$r_{SOI} = R \cdot \left(\frac{m_p}{m_s}\right)^{\frac{2}{5}} \tag{4.1}$$

where R is the radius of the planet and m_p and m_s are the masses of the planet and the Sun respectively. The sphere of influence is then defined as the region enclosed between the planet's surface and r_{SOI}, and it is important because it directly affects the departure and arrival maneuvers that spacecraft's have to perform.

4.2 Method of Patched Conics

Characterizing interplanetary transfers can be done by using the so-called patched conics method, a simplified model which yields results for interplanetary trajectories and in which it is considered that no propulsion maneuvers are performed during the cruise phase, that is, during the time in between the departure and arrival events. It is known as "patched conics" because the objective of the model is to join three different conics, that is, three different Keplerian orbits [26] that represent the departure, cruise and arrival events:

- First conic: it models departure from Earth, which occurs by means of a hyperbolic departure orbit relative to the Earth.
- Second conic: the cruise transfer phase between the Earth and the asteroid, which is considered to be an ellipse relative to the Sun.
- Third conic: it models the arrival to the asteroid, defined by another hyperbolic orbit which in this case is relative to the asteroid.

The method is said to be a simplification because it is based on two main assumptions: the spheres of influence of the planet's can be neglected and the orbits described by the celestial bodies and the spacecraft are unperturbed. The concept of the sphere of influence was explained previously in Section 4.1. In the patched conics approximation these spheres are neglected due to the fact that it is considered that their dimensions are very small compared to the big distances covered in the interplanetary trajectory. As a result, the planet and its corresponding sphere of influence are modeled as a point in space coincident with the center of the planet.

With respect to the second assumption, the term unperturbed refers to orbits in which the effects of factors such as a non-spherical Sun or solar radiation are neglected. If the orbit is unperturbed then this means that of the six orbital elements that define the transfer orbit from point A to point B, five of them are fixed and only one, the true anomaly θ, is free and changes with time. To understand the concepts of the orbital elements please consider Figure 4.1 below. Taking into account that the ecliptic plane is the plane which contains Earth's orbit around the Sun, the six elements that define the transfer trajectory that the spacecraft has to perform between two points are:

- The eccentricity e , which determines the type of orbit. If $e = 0$, the orbit is circular. If $0 < e < 1$, the orbit is an ellipse. Similarly, $e = 1$ represents a parabolic orbit and $e > 1$ a hyperbolic one.
- The semi-major axis a, which was introduced previously in Section 2.2.1 and that gives an idea about the size of the orbit.
- The inclination i_{tr}, that gives the orientation of the orbit plane with respect to the ecliptic plane.
- The right ascension of the ascending node, Ω_{tr}, which provides the longitude of the intersection between the ecliptic and the orbital planes.
- The argument of the perigee, ω_{tr}, which provides the orientation of the semi-major axis of the orbit with respect to the ascending node.
- The true anomaly, θ, which gives the position of the spacecraft in the transfer orbit.

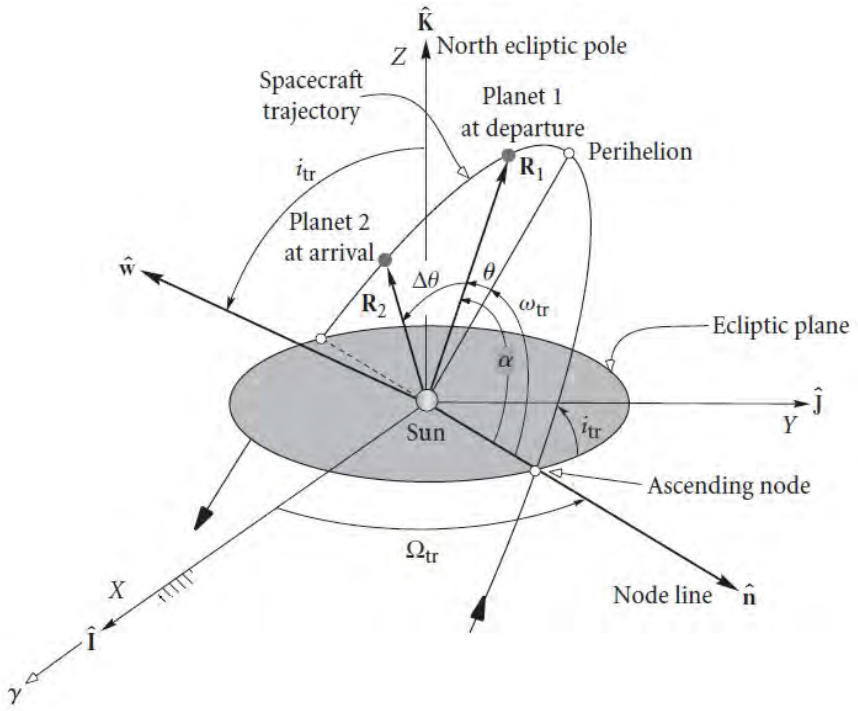

Figure 4.1: Orbital elements with respect to the ecliptic plane [26].

With the two assumptions explained in the previous paragraph the patched conics method then enables the determination of the transfer orbit that the spacecraft would have to follow if it departed from Earth at time t_0 and it arrived at the target body after a certain time of flight, TOF, being the arrival date given by $t_f = t_0 + TOF$. To do so, the heliocentric ecliptic reference frame of Figure 4.1 is considered. Knowing the departure and arrival dates allows the determination of the state vector of the planet and the asteroid, so that the position (r_{planet} and $r_{asteroid}$) and the velocity (V_{planet} and $V_{asteroid}$) vectors of both bodies with respect to the mentioned reference frame are known. Then, *Lambert's Problem*, which will be explained in detail in Section 4.4, has to be solved to obtain the initial and final heliocentric velocities of the spacecraft, V_0 and V_f respectively.

With those values one can then compute the so-called infinity hyperbolic excess velocities, that is, the velocities that the spacecraft has when it exits the sphere of influence of the departure planet and when it arrives at the sphere of influence of the target body. Those velocities are given by the following expressions:

$$V_{\infty_{dep}} = V_0 - V_{planet} \quad and \quad V_{\infty_{arr}} = V_f - V_{asteroid} \tag{4.2}$$

From the values of $V_{\infty_{dep}}$ and $V_{\infty_{arr}}$ one can then compute the cost that performing such interplanetary trajectory has in terms of the velocity change that the propulsion system has to provide, known as ΔV. This velocity change will then be achieved by means of two impulsive maneuvers, one to exit the sphere of influence of Earth and the other to rendezvous with the asteroid (rendez-vous is considered to happen when the spacecraft matches the position and velocity of the asteroid). Therefore, it can be concluded that the first conic to design when constructing a trajectory with the patched conic's method is the cruise phase, since the solution will determine the velocities V_0 and V_f of the spacecraft and hence the hyperbolic velocities at infinity.

4.3 Departing from Earth

The first conic that the method described in Section 4.2 considers is the hyperbolic departure orbit, which the spacecraft has to follow in order to escape from the sphere of influence of the Earth and enter into the cruise phase, that is, the second conic. When analyzing interplanetary trajectories the departure from Earth can be modeled using two different approaches: either it is assumed that the spacecraft is placed into a LEO parking orbit by a launcher and that then it uses its own propulsion system to enter into the escape trajectory or, on the other hand, it is considered that the launcher places the spacecraft into the second conic directly.

The trajectories studied in this thesis work with the second approach. It is assumed that the launchers place the spacecraft into the cruise orbit directly, meaning that the hyperbolic departure orbit is fully performed with the launcher. As a result, the mentioned spaceships do not have to consume propellant for the departure maneuver from Earth. The reader must take into account that not all launchers are capable of carrying out such task. To determine the feasibility of the maneuver and which rocket to use it is necessary to compute what is known as the characteristic energy at departure, *C3*, which is given by the following expression:

$$C3 \quad = \quad V_{\infty_{dep}}^2 \quad \left(km^2/s^2\right) \tag{4.3}$$

With this value, and knowing the mass of the spacecraft, one can then use the corresponding tables provided in the user manuals of the launchers to determine whether the launch is feasible or not. Table 4.1 and Figure 4.2 below show the masses that can be in-

jected by several American and European launchers. In the case of the values of Table 4.1, information was only available for specific mission conditions.

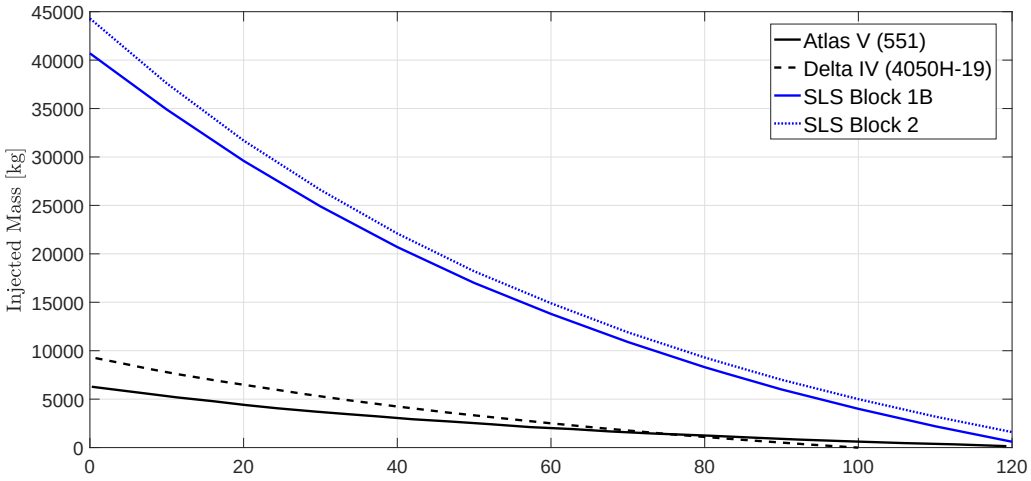

Figure 4.2: Earth escape performance capabilities of several launchers as a function of the characteristic launch energy $C3$. Data taken from [27] and [28].

Launcher Model	**Injected Mass** $[kg]$	**Condition**
Ariane 5 ECA	4550	$V_{\infty_{dep}} = 3.455\ [km/s]$
Falcon Heavy	16800	Mars transfer

Table 4.1: Mass that Ariane 5 ECA and Falcon Heavy can carry into Earth escape trajectories and the associated condition for which the values were found. Data taken from [15] and [16].

4.4 Lambert's Problem

Once the problem of departing from Earth has been presented the next step is to analyze the cruise phase described by the spacecraft, that is, the elliptical orbit connecting the Earth and the asteroid. To do so it is necessary to introduce the so-called *Lambert problem*, which is the basis for interplanetary trajectory determination.

Named after Johann Heinrich Lambert, the problem consists on solving the trajectory that connects the position vector of the departure body at the moment in which the mission is launched, $r_0 = r_1$, and the position vector of the arrival body at the moment of rendez-vous, $r_f = r_2$, for a given time of flight TOF. Doing so yields the orbital elements of the transfer ellipse and, from those elements, one can then obtain the departure and arrival velocity

vectors V_0 and V_f, which can then be substituted into Equation 4.2 to obtain values for ΔV and hence propellant consumption.

Lambert's problem can be formulated as mentioned above due to the fact that it is based on the theorem with which it shares name. This theorem states that the transfer time Δt (also known as TOF) between two points P_1 and P_2 is independent of the eccentricity of the orbit and only depends on the sum of the magnitudes of the positions vectors r_1 and r_2, on the semi-major axis a and on the length of the chord that joins points P_1 and P_2 [26]. The geometry of *Lambert's problem* is presented in Figure 4.3 below.

As the reader can appreciate in the mentioned figure, in each *Lambert problem* the spacecraft has two possible ways of flying from point P_1 to point P_2 in the given TOF. On the one hand, it could follow the shortest route and therefore perform the orbit in the counter-clockwise direction, traveling the arc visible in Figure 4.3. On the other hand, the spacecraft could follow the longest route and travel in the clockwise direction, moving below the fundamental plane and coming back up at the other end. Which type of trajectory the spacecraft follows depends on the value of $\Delta\theta$, the change in true anomaly.

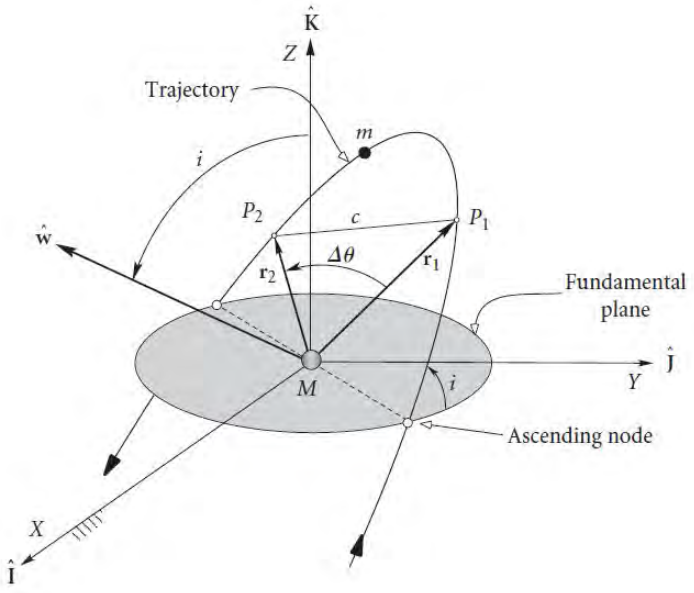

Figure 4.3: Geometry of the *Lambert problem* [26].

Determining whether the spacecraft follows the short arc or the long one therefore reduces to finding the value of $\Delta\theta$. If $0° < \Delta\theta < 180°$, then the spacecraft will follow the short path, while if $180° < \Delta\theta < 360°$ the spacecraft follows the long arc. From trigonometry, the

change in true anomaly is given by:

$$cos(\Delta\theta) = \frac{r_1 \times r_2}{\|r_1\| \cdot \|r_2\|} \tag{4.4}$$

However, Equation 4.4 presents a quadrant ambiguity because if the cosine is positive then $\Delta\theta$ lies in the first or fourth quadrant while if the cosine is negative it lies on the second or third quadrant. Recalling that the vector product $r_1 \times r_2$ yields the vector which is perpendicular to the orbit plane (vector w in Figure 4.3), one can then solve the quadrant ambiguity simply by determining the sign of the Z-component of vector w. If this component is positive, then vector w points out of the plane and hence the spacecraft orbits following a counterclockwise motion, which implies that it travels the short way because $0° < \Delta\theta < 180°$. On the other hand, a negative Z-component implies that vector w points into the plane and hence that the motion occurs in the clockwise direction, so that $180° < \Delta\theta < 360°$. This reasoning and the corresponding formulas to determine $\Delta\theta$ are synthesized in the expression below.

$$\Delta\theta = \begin{cases} cos^{-1}\left(\frac{r_1 \times r_2}{\|r_1\| \cdot \|r_2\|}\right) & if \quad (r_1 \times r_2)_Z \geq 0 \\ 360° - cos^{-1}\left(\frac{r_1 \times r_2}{\|r_1\| \cdot \|r_2\|}\right) & if \quad (r_1 \times r_2)_Z < 0 \end{cases},$$

The reasoning followed in the previous paragraphs was derived for the case of a transfer trajectory with no revolutions. Nevertheless, for the case in which the spacecraft performs one or several revolutions (orbits) around the transfer ellipse, the derivation process is the same. Multi-revolution trajectories usually imply longer times of flight but, on the other hand, may be beneficial because they enable the spacecraft to perform a phasing maneuver, that is, a maneuver with the aim of adjusting the encounter with the target in such a way as for it to occur in a more optimal occasion. As a result, this thesis considers the possibility of performing multi-revolution transfer orbits.

Finally, the reader must consider that only prograde trajectories, that is, trajectories with positive angular momentum, are taken into account in this thesis. Using Figure 4.3, prograde trajectories are those in which the inclination angle i satisfies $0° < i < 90°$. The reason behind this assumption is that prograde trajectories enable the launcher to benefit from Earth's rotational velocity, making it therefore easier to achieve the desired hyperbolic escape.

4.5 Gravity Assist Maneuvers

A gravity assist maneuver, also known as planetary flyby, occurs whenever a spacecraft enters into the sphere of influence of a planet and, instead of perching on the surface (with a controlled landing) or entering into an orbit around it, it just exists the mentioned sphere of influence at the opposite end of the flyby hyperbola.

Performing this type of maneuver can present considerable advantages since it may allow the spacecraft to use the planet's gravitational pull as an external aid for achieving the ultimate goal of arriving to the desired target in the most efficient way. For instance, the spacecraft may be able to perform a change of plane maneuver or gain/lose speed at no cost in terms of propellant. As a result, preliminary trajectory design has to study the possibility of performing gravity assist maneuvers. In the case of this thesis, unpowered three-dimensional flyby's are taken into account in the missions involving chemical propulsion.

4.5.1 Flyby model

The patched-conic flyby model considered in the present work is based on the assumptions that the maneuver occurs instantaneously and that it is unpowered. The first premise implies that the change in heliocentric velocity experienced by the spacecraft is immediate, while the second assumption means that the engines are not used during the maneuver [29]. For the gravity assist to occur at a time t_i, the spacecraft position has to match that of the planet at the same time.

Since the flyby occurs instantaneously the positions of both the spacecraft and the planet relative to the Sun do not change, meaning that, when patching the conics, r_{ship} and r_{planet} at t_f (the end time of the first transfer orbit) are the same as the position vectors at t_0 of the post-flyby transfer leg, which means that $t_i- = t_i+$. This hypothesis can be assumed due to the fact that the time the spacecraft is inside the sphere of influence of the flyby planet is small compared to the duration of the complete transfer trajectory. In addition, the mass of the spacecraft does not change as the engines are not used. The conditions described in these two paragraphs can be mathematically defined as:

$$\begin{cases} x(t_i-) = x(t_i+) \\ m_{sc}(t_i-) = m_{sc}(t_i+) \end{cases} \tag{4.5}$$

Despite the fact that the spacecraft position is constant, the heliocentric velocity of the ship does vary and the post-flyby velocity can be obtained by considering that the spacecraft performs a hyperbolic orbit around the planet. In order to understand the gravity assist problem, please consider Figure 4.4.

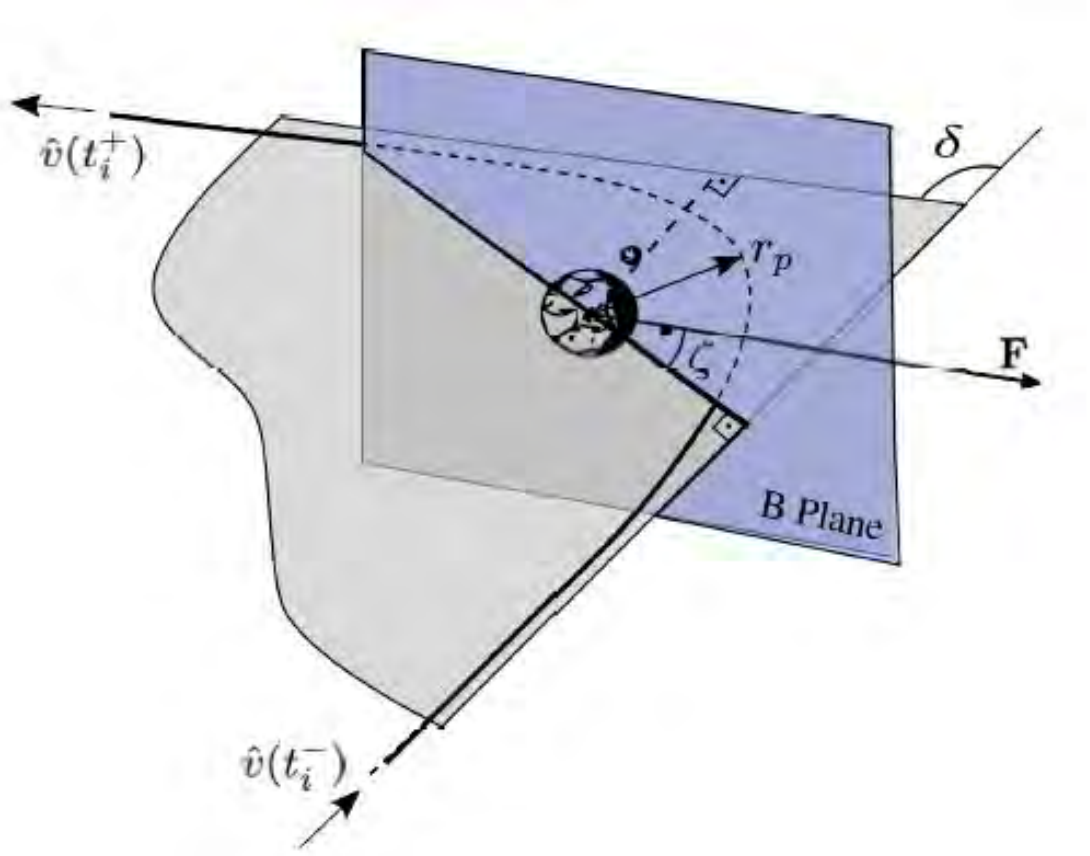

Figure 4.4: Geometry of the gravity assist maneuvers being considered [29].

In the above figure one can appreciate that the hyperbolic trajectory that the spacecraft describes is defined by two angles, δ and ζ (the turn angle and the B-plane angle respectively), and by the radius r_p. Hence, the heliocentric velocity of the spacecraft after the flyby, $V_{ship_{out}}$, and the turn angle δ can be obtained by solving the corresponding flyby equations which make use of the spacecraft velocities relative to the planet, $v(t_i-)$ and $v(t_i+)$, as well as the flyby altitude and target angle, being this two last variables subjects of optimization.

To that end, the first step is computing the spacecraft velocity relative to the flyby planet at the inbound crossing of the sphere of influence. This can be done by applying the following expression, where V_{planet} corresponds to the planet velocity and $V_{ship_{in}}$ is the pre-flyby heliocentric velocity, obtained from the solution to the *Lambert problem* of the transfer leg just before the flyby:

$$v(t_i-) = V_{ship_{in}} - V_{planet} \tag{4.6}$$

The radius of the periapsis of the flyby hyperbola, r_p, is then determined by using the following expression, where R_m is the radius of the planet where the flyby is taking place and h_{pm} is the altitude at which the flyby is performed, which has to be optimized.

$$r_p = h_{pm} + R_m \tag{4.7}$$

Once this two values have been computed, the turn angle delta can be obtained by solving the equation below, where μ is the gravitational constant of the flyby planet:

$$\delta = 2 \cdot arcin\left(\frac{1}{1 + \frac{r_p \cdot v(t_i-)^2}{\mu}}\right) \tag{4.8}$$

The velocity of the spacecraft after the flyby relative to the planet is then given by

$$v(t_i+) = cos(\delta)\vec{i} + cos(\zeta) \cdot sin(\delta)\vec{j} + sin(\zeta) \cdot sin(\delta)\vec{k} \tag{4.9}$$

where the unit vectors are found using the following expressions:

$$\vec{i} = \frac{v(t_i-)}{\| v(t_i-) \|} \quad , \quad \vec{j} = \frac{\vec{i} \times V_{planet}}{\| \vec{i} \times V_{planet} \|} \quad and \quad \vec{k} = \vec{i} \times \vec{j} \tag{4.10}$$

Finally, the heliocentric velocity of the spacecraft after the flyby is computed by applying the equation below:

$$V_{ship_{out}} = v(t_i+) + V_{planet} \tag{4.11}$$

With this formulation, obtained from [29], one can model the patched flyby events. The incoming spacecraft velocity relative to the planet is rotated a turn angle δ on the orbital plane of the flyby hyperbola, and then goes out of the sphere of influence of the planet. The orientation of the orbital plane, as shown in Figure 4.4, is determined by the so-called beta angle ζ, which is the angle between the B-plane and the vector **F** [29]. While the mentioned vector is parallel to the ecliptic plane, the B-plane is perpendicular to the spacecraft velocity that enters into the sphere of influence.

4.5.2 Flyby altitudes

As already explained, for a gravity assist maneuver to take place the spacecraft has to enter into the sphere of influence of the planet. Nevertheless, this event has to be controlled in such a way as to avoid an impact against the planet's surface and, at the same time, enable the spacecraft to benefit from the gravitational pull. To that end, boundaries have to be imposed on both the maximum and minimum altitudes h_{pm}.

With respect to the upper limit one must recall that the gravitational attraction force of a planet decreases with distance, so that the further the spacecraft is from the planet's surface, the smaller the effect it will experience. As a result, the upper bound for the flyby altitude has been set to be two times the radius of the planet at which the flyby is performed. This has been done so as to enable sufficient freedom for the optimization software to considered different possibilities while at the same time reducing the search space.

With respect to the lower bound of the flyby altitude, values have been taken considering several gravity assist maneuvers that were performed in past missions. To that end, the minimum altitude for Mars flyby's was established at 250 km, since it was what the European Space Agency mission *Rosetta* did [63]. For Venus, NASA's *Messenger* June 2007 flyby was considered and the minimum altitude was taken to be 322 km [64]. Table 4.2 below summarizes the upper and lower limits for the flyby altitudes considered in this thesis.

Planet	**Minimum Altitude** $[km]$	**Maximum Altitude** $[km]$
Venus	322	12104
Mars	250	6792

Table 4.2: Flyby altitude intervals considered for each planet.

4.6 Low-Thrust Missions

Previous sections of this chapter have explained many orbital mechanic's concepts. However, when introducing missions which use ion propulsion some of the theorems and ideas have to be adapted. Although the general notions of the sphere of influence, times of flight or number of revolutions are maintained, concepts regarding how to solve each of the trajectory transfer legs have to be re-defined. This is due to the fact that in order to carry out preliminary design of low-thrust missions what is used is a shape-based method: the geometry of the trajectory is assumed and then the problem consists on finding the thrust profile that has to be employed for that trajectory by adjusting a series of shape coefficients [30].

4.6.1 Generalized logarithmic spirals

The main difference between impulsive and low-thrust missions resides in the fact that, while in impulsive trajectories the engines are only fired instantaneously on certain events, in low-thrust trajectories the ion thruster is switched on and generates thrust over sustained periods of time, therefore producing an acceleration on the spacecraft. Following the procedure of reference [30], the dynamics equation of a particle perturbed by a thrust acceleration is given by

$$a_p = \frac{\mu}{r^2}\left[\xi cos(\psi)\vec{t} + (1-2)\xi sin(\psi)\vec{n}\right] \tag{4.12}$$

where μ is the gravitational constant of the main body, ξ is a control parameter, ψ is the spacecraft's flight angle and $\vec{t}$ and $\vec{n}$ are unit vectors in the tangential and normal directions of an arbitrary inertial reference frame, as can be appreciated in Figure 4.5.

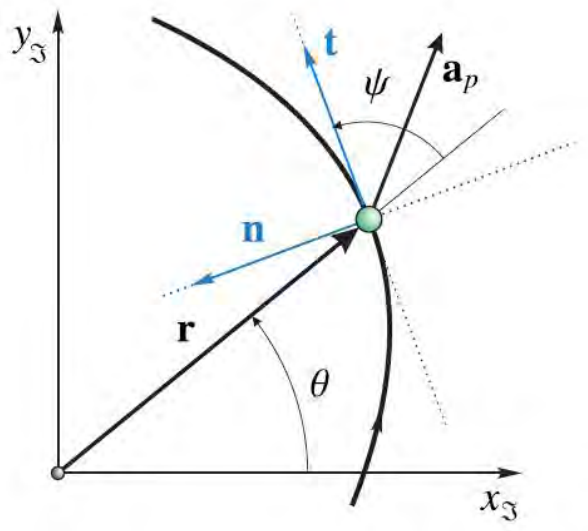

Figure 4.5: Geometry of the problem solved using logarithmic spirals [30].

The so-called generalized logarithmic spirals are therefore obtained from solving Equation 4.12 and represent the thrust arc described by the spacecraft in Figure 4.5. The thrust vector in the low-thrust case lies on the plane in which the spiral is contained, and this therefore converts the problem into 2D. Such spirals can either be elliptic, parabolic or hyperbolic, and the type is determined by the value of the so-called generalized energy constant K_1.

Obtaining the expressions for the generalized logarithmic-spirals is more a mathematical problem and hence is not going to be derived here, since this section aimed at providing the reader with a basic insight into the low-thrust problem. Full mathematical development of the mentioned equations can be found in reference [65].

4.6.2 Analytic design of transfer legs

Modeling the interplanetary transfer between the Earth and the asteroid for a low-thrust mission then reduces to solving, as in the case of chemical propulsion, the trajectory legs between the bodies. The particularity of low-thrust trajectories is that they are a combination of generalized logarithmic spirals with arcs in which the engine is switched-off, therefore leading to trajectories in which one finds what is known as "thrust-arcs" and "coast arcs" [30]. Coast arcs are considered to be Keplerian orbits like the ones explained in Section 4.2.

As mentioned previously, the problem is contained in a two-dimensions domain. As a result, the spacecraft and planet positions will be given in terms of a radius and an angle, $\mathbf{r}$ and θ in Figure 4.5 respectively. Consequently, solving the transfer between the Earth at time t_0 and the asteroid after a certain time $t_f = t_0 + TOF$ reduces to joining the position vectors of both bodies by a combination of coast and thrust arcs, just as shown in Figure 4.6 below where the thrust arcs are θ_0 - θ_A and θ_B - θ_f. Similarly, the coast arc is found between θ_A and θ_B.

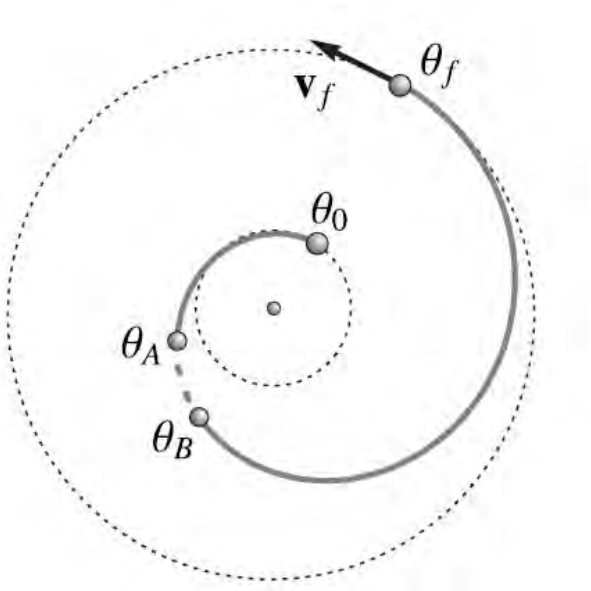

Figure 4.6: Representation of a combination of thrust and coast arcs used by the spacecraft to perform a transfer [30].

Nonetheless, doing so is not as straight-forward as can seem, since, in addition to transitions between thrust and coast arcs one can also find shifts in the type of generalized logarithmic spiral. The former is defined by means of a constant of motion obtained from the initial conditions [65]. The latter is determined by means of the aforementioned control parameter ξ: if its value changes, then the type of logarithmic spiral does too, and this means that the thrust magnitude and its direction are modified [65].

In addition, another consideration to take into account is related to the initial velocity of the spacecraft. In general, the state vector of the spacecraft at a time t is defined by the components $\mathbf{r}, \upsilon, \theta$ and ψ, with ($\mathbf{r}$, θ) describing the position and (υ, ψ) the velocity [30]. If the launch time t_0 is fixed, then the position vector $\mathbf{r}_0$ and θ_0 are known, leaving therefore two degrees of freedom which represent the initial velocity of the spacecraft (υ_0,ψ_0). In the

model considered here, the user has to specify the initial impulse given to the spacecraft. This thesis has therefore assumed that the mentioned departure impulse is provided by the launcher, having a magnitude of $2 km/s$ and being applied in the direction of the Earth velocity at t_0, that is, in the tangent direction. With respect to the asteroid departure, it has been also considered that the spacecraft would receive an initial impulse of $0.1\ km/s$ in the direction of the asteroid velocity, being small due to the reduced asteroid escape velocities which are expected to be found.

Finally, the reader must take into account that this project has considered that the spacecraft used for the low-thrust missions would have a combination of ion and chemical propulsion systems, being the former used for the cruise phases and the latter for the asteroid rendez-vous, departure and Earth arrival. The reason behind this is that the lambert solver used for the low-thrust case did not enable the author to introduce the rendez-vous constrain, that is, it did not allow to fix the final velocity with which the spacecraft had to arrive at the end point of the trajectory. As a result, using a small chemical propulsion system was the only way possible of assuring that the rendez-vous and landing maneuvers would take place.

Indeed, performing all the mission with the ion propulsion system was what should be analyzed in real cases, since the transfer would be characterized as the one shown in Figure 4.6: an initial thrust arc to accelerate the spacecraft followed by a coast arc and then a final thrust arc in which the spacecraft would use the ion engine to gradually slow down (or continue to accelerate) for the rendez-vous to occur. Although this idea could not be modeled due to the lambert solver limitation, Section 4.7.2.3 will explain what was the procedure introduced so as to analyze mission feasibility.

4.7 Spacecraft Propulsion

As stated previously, this thesis addresses solutions with both chemical and low-thrust propulsion methods. Although the idea of these systems is similar, that is, to enable the spacecraft to arrive to the desired destination, the working principle is completely different. In this section both systems are explained and the corresponding information related to the propellant and/or engines considered in this work are stated.

4.7.1 Chemical propulsion

Chemical propulsion engines allow the spacecraft to perform what is known as impulsive maneuvers, that is, maneuvers in which the magnitude and direction of the spacecraft's velocity vector is instantaneously changed by means of short firings of the onboard rocket engines [26]. Since, in general, the time during which the engines are switched on (known as "burn times") is small compared to the time during which the engines are switched-off (known as "coast times"), the impulsive maneuver idealization allows us to consider that the position of the spacecraft remains fixed during the burn.

Whenever one of the mentioned burns is performed the spacecraft velocity experiences a variation $\Delta\mathbf{v}$. Such change can modify the magnitude of the velocity, the direction of the velocity vector or both. In the former, the impulsive maneuver is denoted as a "pumping maneuver"[26], while the latter is known as a "cranking maneuver" [26]. In any case, switching the engine on will cause propellant to be consumed. The relation between the magnitude of the velocity increment, ΔV, and the mass of the propellant used, Δm, is then given by the following equation

$$\frac{\Delta m}{m_0} = 1 - e^{-\frac{\Delta V}{I_{sp} \cdot g_0}} \tag{4.13}$$

where g_0 is the standard acceleration of gravity, m_0 is the spacecraft mass before the maneuver is performed and I_{sp} is the specific impulse of the propellant being used by the engine. This last parameter can be defined as the ratio between the thrust force and the sea-level weight rate of fuel consumption and it is measured in seconds [26]. It is a way of indicating the efficiency of the propellants, since the bigger the value of the I_{sp}, the greater the thrust produced per kilogram of propellant burnt.

The specific impulse achievable by any kind of chemical propulsion system is limited by the amount of energy per kilogram that the elements conforming the propellant have. Nevertheless, considerable amounts of thrust can be obtained due to the fact that the energy that the mentioned elements can release is independent of factors such as the power generation of the spacecraft, since the energy that the chemical reaction produces is a function of the characteristics and kinematics of the combustion reaction (in contrast with what will be explained later for ion-thrusters) [66].

4.7.1.1 Chemical propellant selected

After reviewing different propellants, it was assumed that the spacecraft involved in the asteroid mining missions being analyzed in this thesis would use a chemical propulsion system which had dinitrogen tetroxide, N_2O_4, (usually known as nitrogren tetroxide) as oxidizer and monomethyl hydrazine, CH_3NHNH_2, (referred to as MMH) as fuel.

The reason behind this choice is related with the fact that this is a hypergolic propellant, meaning that it is very reactive and that it spontaneously ignites whenever both the oxidizing and reducing agents come into contact with each other, favoring the reaction [67]. Such characteristic is of special importance since it makes this propellant ideal for the spacecraft maneuvering system, which will undergo long coast times but will have to be fully and rapidly operative when the impulse maneuvers have to be performed.

As a result of the propellant selection, the spacecraft will have to be equipped with one or several liquid propellant engines. Since the selected propellant is hypergolic, mixing of both components will be performed by an injector of the impinging jet type, which will ensure that impinging jets of both components are appropriately arranged [68]. The chemical reaction will take place in the combustion chamber, while the resulting products will be accelerated by the nozzle. The combustion will be described by the following equation [67]:

$$4CH_3NHNH_2 \; + \; 5N_20_4 \longrightarrow 9N_2 \; + \; 4C0_2 \; + \; 12H_20 \tag{4.14}$$

Finally, recalling that the oxidizer is dinitrogen tetroxide and that the fuel is monomethyl hydrazine, the characteristics of the propellant can be seen in Table 4.3 below:

Property	Value	Units
Specific Impulse	336	s
Optimum Oxidizer to Fuel Ratio	2.16	-
Temperature of Combustion	3111.85	$°C$
Oxidizer Density	1450	kg/m^3
Oxidizer Freezing Point	-11	$°C$
Oxidizer Boiling Point	21	$°C$
Fuel Density	880	kg/m^3
Fuel Freezing Point	-52	$°C$
Fuel Boiling Point	87	$°C$

Table 4.3: Properties of the propellant being considered for the asteroid mining missions that use chemical propulsion [17].

4.7.2 Ion propulsion

In contrast with what was explained for rocket engines, electric propulsions systems (also known as ion-thrusters) are considered to be "power limited" [66], since the energy that the spacecraft power unit can supply to the engine determines the output that the thruster will be able to provide. This energy will usually come from the solar panels, and hence will be greatly affected by the distance to the Sun. As a consequence, the power processing units (denoted as *PPU*) associated to these types of engines have to be carefully designed.

4.7.2.1 Working principle of an ion thruster

As the name indicates, ion thrusters work by using ionized propellant and generating the mentioned ions is a process which implies adding or removing electrons from the propellant. To that end, most ion thrusters achieve this by performing what is known as electron bombardment, which consists on forcing a collision between an electron and a propellant atom with the objective of causing the propellant particle to lose electrons and hence become a positively charged ion [69].

Once the collision has taken place, the electrons obtained are then attracted towards the walls of the chamber due to the fact that such walls are positively charged with the power coming from the *PPU* of the system. Nevertheless, the resulting electron motion is not free, since it is guided by magnetic fields created so as to increase the residence time of the electrons in the chamber and therefore improve the ionization process of the propellant that is being injected [69].

Thrust is then generated by accelerating the ions out of the engine. To do so, the end part of the system is composed of several grids. One which is negatively charged, known as the accelerator grid, is then responsible for attracting the positively charged ions and accelerating them to high speeds [69]. Finally, the neutralizer ejects a certain amount of electrons in order to counteract the positive charge that the output ion stream has. This has to be done in order to prevent loss of performance, since having a non-neutral jet would lead to the spacecraft becoming negatively charged [69].

As mentioned, the electrical power required for the walls of the engine to be charged will have to come from either solar panels or an onboard nuclear power system. The availability of this source of energy will then determine the output of the engine. With respect to the propellant, ion propulsion systems usually use xenon. This is due to the fact that it can be

easily ionized and also has a big atomic mass, which causes the amount of thrust generated by the ion acceleration to be bigger compared to other gases [69].

4.7.2.2 Ion thruster selected

Ion thrusters have experienced a very important evolution since the first technology started being developed at the NASA Glenn Research Center in the last years of the 1950's decade, with the first test in space, the Space Electric Rocket Test 1, taking place on July 20 of 1964 [69].

For the low-thrust missions considered in this thesis the ion thruster selected has been NASA's Evolutionary Xenon Thruster-Commercial, *NEXT-C*, which is commercialized by Aerojet Rocketdyne [58]. This choice has been made based on several reasons. On the one hand, this ion thruster has successfully passed NASA's critical design review, (known as *CDR*), meaning that the technology is ready for the production of flight units. Figure 4.7 below shows testing taking place with a NEXT thruster in a single-engine array configuration.

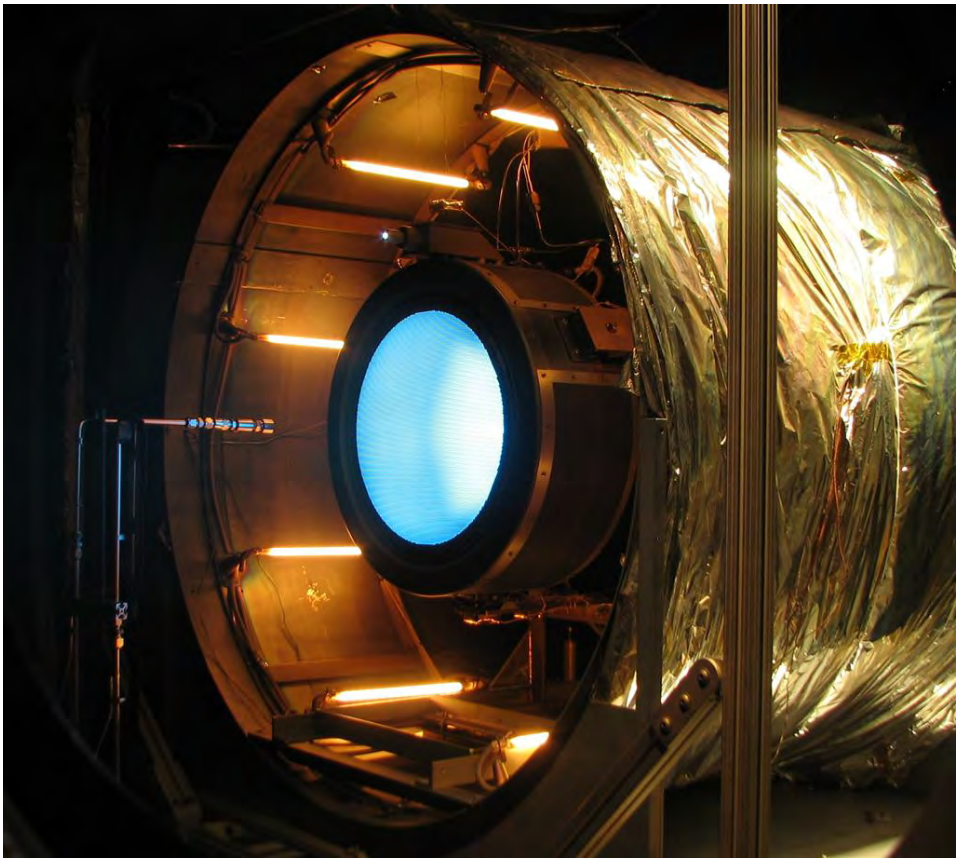

Figure 4.7: Image of environmental testing taking place for the NEXT ion thruster [31].

On the other hand, such system is the one that will equip NASA's forthcoming *DART* (Double Asteroid Redirection Test) mission, which was mentioned previously in Section 2.1.1. Since such mission and the ones being considered in this thesis share a degree of similarity (the type of celestial bodies being involved), it has been considered that the propulsion system used in *DART* could be the same as the one used for the asteroid mining missions. The main performance parameters can be observed in Table 4.4. The trajectories shown later in the result's section have been obtained considering an I_{sp} of 4000 s.

Performance Parameters	Value	Units
Maximum Input Power	6.9	KW
Maximum Specific Impulse	4190	s
Thruster Efficiency at Full Power	71	%
Specific Mass	1.86	kg/KW

Table 4.4: Main performance characteristics of the NEXT ion thruster [18].

Similarly, the design attributes of such system can be seen in Table 4.5, where the values for the diameters and the length include the neutralizer.

Design Attribute	Value	Units
Mass (excluding cabling)	12.7	kg
Beam diameter	36	cm
External diameter	58	cm
Total length	43.4	cm

Table 4.5: Geometrical and mass characteristics of the NEXT ion thruster [18].

4.7.2.3 Verification of low-thrust mission feasibility

In the last paragraphs of Section 4.6.2, the limitation introduced by the lambert-solver with regards to the rendez-vous maneuvers was explained. As stated, this forced the author to consider a spacecraft with both types of propulsion systems: low-thrust for cruise phases and chemical for rendez-vous maneuvers. However, real missions should analyze the possibility of performing all the operations with the ion thruster. Nevertheless, this is not an easy task since ion propulsion is limited by the power that the *PPU* (power-processing unit) would be able to supply. To that end, this section presents the method used in order to verify if the mission could be feasible using only low-thrust propulsion methods.

The idea behind the methodology implemented is based on calculating the ΔV that the NEXT-C engine is able to provide for each of the flight's, so as to compare the value with

the sum of the ΔV that are required for the cruise phases and for the asteroid and Earth rendez-vous. If the ΔV that the NEXT-C engine can provide is greater than that required by the different maneuvers, then the mission is considered to be possible. Mathematically, the two constrains that must be fulfilled for mission feasibility are:

$$\begin{cases} \Delta V_{NEXT_{out}} > \Delta V_{cruise_{out}} + \Delta V_{asteroid_{rdv}} \\ \Delta V_{NEXT_{back}} > \Delta V_{cruise_{back}} + \Delta V_{earth_{rdv}} \end{cases}$$

Although the above criteria is very basic, it can be used to rapidly discard those solutions which are not feasible as well as to determine which trajectories may be possible if two thrusters are used. Nevertheless, the fact that the criteria is satisfied does not guarantee that the missions can be carried out. Determining that would require a more profound analysis of the parameters that falls out of the preliminary trajectory design domain of this thesis.

Applying the criteria therefore requires obtaining the value of the ΔV that the NEXT-C engine can provide. This value can be calculated using the expression below, where T is the thrust generated by the engine and m is the spacecraft mass, which is assumed to remain constant during the outbound and inbound flights (although different mass values are considered for each flight).

$$\Delta V_{NEXT-C} = \int_0^{t_f} \frac{T}{m} \cdot \partial t \tag{4.15}$$

To solve the above equation one must calculate the value of the thrust. This can be done by considering a polynomial expansion as the one of Equation 4.16 and the corresponding curve fit coefficients, which are provided in Table 4.6.

$$T = C_{0T} + C_{1T} \cdot P_a + C_{2T} \cdot P_a^2 + C_{3T} \cdot P_a^3 + C_{4T} \cdot P_a^4 \tag{4.16}$$

Curve Fit Coefficient	**Value (N)**
C_{OT}	1.19388817E-02
C_{1T}	1.60989424E-02
C_{2T}	1.14181412E-02
C_{3T}	-2.04053417E-03
C_{4T}	1.01855017E-04

Table 4.6: Fit curve coefficients for the NEXT-C engine. Values obtained from [19].

Equation 4.16 contains terms which represent the available power, P_a, which is no other than the power that the *PPU* can provide to the engine. As mentioned previously, this quantity will be a function of the distance to the Sun since energy is obtained via solar panels. To characterize the available power Equation 4.17 can be used, where $\gamma = 0.85$ is the efficiency factor, P_0 is assumed as 15 *KW* and r is the modulus of the distance to the Sun. In addition, the available power is bounded due to the limited capacity of the power processing unit, so that P_a will always be between $P_{min} = 0.64$, *(KW)* and $P_{max} = 7.6$ *(KW)* for the NEXT-C engine [19].

$$P_a = \frac{P_0}{r^2} \cdot \gamma \tag{4.17}$$

Once the thrust has been obtained, Equation 4.15 has to be converted into the two-dimensional domain in which the low-thrust trajectories are found in order to be able to solve it, since T is a function of radial position. As a result, there is the need to express ∂t in terms of the angle θ. To do so, one must recall Equation 4.12 and operate following the procedure of reference [65] to obtain the projected equations of motion. This yields that:

$$\frac{\partial \theta}{\partial t} = \frac{v}{r} \cdot sin(\psi) \tag{4.18}$$

Finally, Equation 4.15 can be re-expressed as shown below. Substituting the formulas derived above and integrating then yields the value of the ΔV that the NEXT-C engine can provide.

$$\Delta V_{NEXT-C} = \int_0^{t_f} \frac{T}{m} \cdot dt = \frac{1}{m} \cdot \int_{\theta_0}^{\theta_f} T \cdot \frac{\partial t}{\partial \theta} \cdot \partial \theta \tag{4.19}$$

CHAPTER 5

SPICE

Chapter 4 has presented the main orbital mechanics concepts required in order to solve both the impulsive and the low-thrust trajectories and has provided some insight into the models used in this work. This Chapter therefore focuses now on providing a review on one of the software tools that was used to obtain the trajectory solutions for the outbound and inbound flights of the asteroid mining missions.

5.1 Introduction: what is SPICE?

SPICE is a software which was born with the objective of enabling scientist and engineers design and plan scientific missions and interplanetary trajectories as easily and effectively as possible [20]. It was designed by the Navigation and Ancillary Information Facility (NAIF) from NASA and it permits the computation of position and orientation parameters, not only of celestial bodies but also of spacecraft and their corresponding instruments.

To that end, the software uses what is known as "ancillary data" [20], which is no other than a collection of positions, velocities, orientations, reference systems and associated times. Such data is stored in what is denominated as *kernels*, that is, specific files devoted to providing the SPICE user with the information he desires. The acronym SPICE is directly related to the types of kernels one can find, which provide information about spacecraft (**S**), planets (**P**), instruments (**I**), cameras (**C**) and events (**E**).

The SPICE software (known as toolkit) is free and can be downloaded from the corresponding web page from NASA. It is written so as to be supported in several programing languages and, for this work, the SPICE program has been used in the MATLAB environment. Using SPICE is not a straightforward task since the user has to become familiar with the type of files and the functions to be used. To help with this, the NAIF team provides a series of on-line tutorials.

5.2 SPICE Toolkit architecture

The SPICE version for MATLAB is known as *Mice* and it is no other than a translation from the original program written in *ANSI Fortran 77* into *C* together with the associated specific *wrapper* [1] functions required to adapt the Toolkit into the MATLAB environment [20]. As a result, when the user inputs a certain function MATLAB calls the associated *wrapper*, which then accesses the library, where the user demand is processed. The results are then sent to the *wrapper*, which converts them into MATLAB readable information which is finally available for the user. This sequence is schematically shown in Figure 5.1 below.

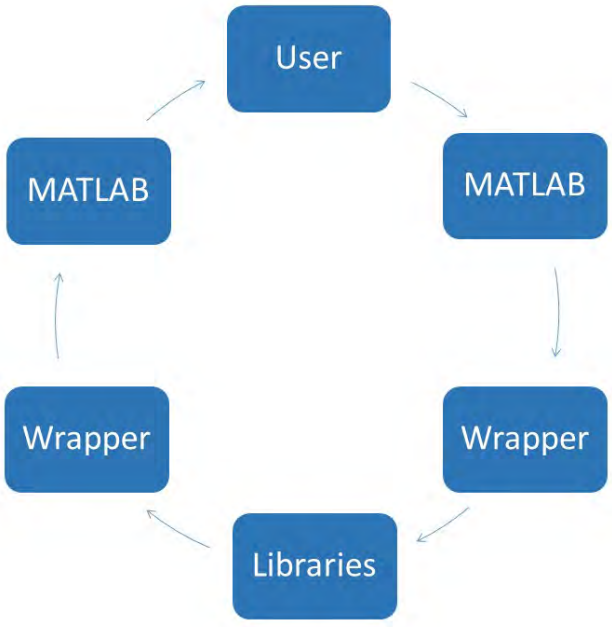

Figure 5.1: Schematic flowchart showing the working philosophy of *Mice*.

[1] A *wrapper* function is basically a routine which is programmed to act as an intermediary between the user and the actual software libraries with the objective of translating and interpreting the user commands so that the libraries can be used.

In order to be able to use SPICE one must understand the different types of *kernels* that there exist, as well as how to obtain and use them. In general, kernels are available for each of the elements that make up the SPICE acronym, that is, there are *kernels* referred to spacecraft, planets, instruments and so on, while the content of the *kernel* varies depending on the type. Table 5.1 below summarizes the existing types of *kernels* and their corresponding content.

Component	**Kernel Name**		**Kernel Content**
S (spacecraft)	SPK		Position and velocity of spacecraft or celestial bodies
P (planet)	PCK		Physical parameters (size, orientation, shape etc) of celestial bodies
I (instrument)	IK		Size, shape and orientation of instruments coverage area
C (camera-matrix)	CK		Orientation of spacecraft or of any of its components
E (events)	EK		Information on events
	Others	FK	Information on reference frames
		LSK	Information for time conversions
		SCLK	Spacecraft clock coefficients
		DSK	Celestial bodies surface shape data

Table 5.1: Table summarizing the different types of kernels available and the content of the information they contain, as obtained from [20].

Knowing the nature of the *kernels* then provides the user with the required information to decide which of these files are going to be needed to satisfy his requirements. For the case of trajectories to asteroids, it is clear that ephemeris data (positions and velocities), physical parameters of the celestial bodies, information for time conversions and reference frames are going to be needed. Therefore, SPK, PCK, FK and LSK *kernels* are required. These can be downloaded from the NAIF web page, available at reference [70].

Nevertheless, and although NAIF provides a wide database, SPK *kernels* for asteroids cannot be downloaded from the source mentioned in the previous paragraph. This is due to the fact that, as was shown in the discovery statistics of Section 2.1.2, the amount of near-Earth asteroids is very big and NAIF is incapable of providing ephemeris data for such number of bodies with its current capacity. Therefore, the user has to generate its own SPK *kernels* for asteroids. This has been done by means of the HORIZONS System of the Jet Propulsion Laboratory (JPL).

5.3 Implementation of Missions into MATLAB

Once all the information regarding the orbital mechanics concepts and SPICE has been provided, the methodology followed in order to determine the asteroid mining trajectories can be explained. SPICE is not a software itself that computes and determines trajectories nor it is a software that optimizes the results, but it provides the necessary tools to develop a MATLAB code which is capable of doing so.

As it was explained in Chapter 4, the trajectories to the asteroids are implemented into MATLAB by using the patched conics approximation. Such method implies solving the well-known *Lambert problem*, which requires position vectors at the start and final times of the transfer, t_0 and t_f respectively, and which can be obtained via SPICE.

In the preliminary stage of trajectory design it is fundamental to perform an analysis of the launch and trajectory opportunities that exist over a wide time interval, with the objective of finding the set of dates at which the configuration of the departure and arrival bodies is the most favorable for the mission to take place. This study basically reduces to obtaining the so-called pork-chop plots, which are graphs that display information regarding launch date, transfer duration and required velocity change, ΔV.

To achieve so, the procedure to follow is to define the time window for Earth departure in which the asteroid mining missions are going to be considered, for example 2018-2028. Then, the resulting time range is divided into a large number of intervals by using a time step. For instance, if the time step is of 4 days then this means that in the example being considered trajectories will be computed taking into account that missions depart from Earth every 4 days from the 1st of January 2018 onwards. Recalling that the final time t_f for the transfer can be computed as $t_f = t_0 + TOF$, the other parameter to set is the TOF, which is done also by considering an upper and lower bound and dividing it into time intervals by means of the time step.

Summing up, obtaining the pork-chop plots for the outbound (Earth - asteroid) and the inbound (asteroid - Earth) flights reduces to defining the launch window, the time step and the time of flight for the two trajectories. Knowing that, an algorithm that solves *Lambert's problem* iteratively can be programed. Please notice that this approach has only been used to consider direct transfers (no gravity assists performed) using chemical propulsion and for trajectories involving 0 or 1 revolution. In addition, the Lambert solver used has been that developed by David Vallado [71], which is an implementation of the *Lambert's problem*

using the concept of universal variables. The following subsections will now explain how was each one of the previously mentioned variables defined.

5.3.1 Defining the launch window

The launch window was established according to the synodic periods shown in Table 5.2, which correspond to the times required for a certain configuration of the asteroid relative to the Earth to repeat [26]. Obtaining the mentioned periods can be done by using Equation 5.1, where T_1 is the orbital period of the Earth (365.25 days) and T_2 are the orbital periods of the asteroids (defined previously in Table 2.7).

$$T_{synodic} = \frac{T_1 \cdot T_2}{\left| T_1 - T_2 \right|} \tag{5.1}$$

Asteroid Name	**Synodic Period** $[years]$	**Synodic Period** $[days]$
Ryugu	4.362	1593.226
1989 ML	3.297	1204.226
Nereus	2.225	812.613
Didymos	1.902	694.777
2011 UW158	1.941	708.830
Anteros	2.407	879.123
2001 CC21	21.322	7787.919
1992 TC	2.043	746.136
2001 SG10	2.345	856.618
2002 DO3	1.651	602.883

Table 5.2: Synodic periods for the different asteroids rounded up to three decimals.

From a physical point of view, the launch window to be considered must correspond to, at least, one synodic period so as to analyze all the possible position configurations between the Earth and the asteroid. Considering the variety of synodic periods shown in Table 5.2, it is decided that the launch window will span from 2018 to 2030 for the ten asteroids being analyzed. Doing this produces a pork-chop plot for a considerable number of years and hence ensures that the most optimum mission in terms of ΔV is retrieved. In addition, it provides project managers with a good general idea of the launching possibilities with the purpose of being able to define schedules for the mission.

5.3.2 Establishing the time step

As mentioned previously, there is the need to specify the time step to use for splitting the launch window and the time of flight. Such time step has to be a compromise between solution quality and computation costs, since smaller time steps imply better solutions (*Lambert's Problem* is solved for more *TOF's* and dates) but also greater computation times. As a reference, NASA's *JPL Small-Body Mission-Design Tool* [72] normally uses a 5 day time step to compute the solutions. Taking all this into account, the time steps shown in Table 5.3 were finally used.

Synodic Period $[years]$	$T_{syn} < 2$	$2 < T_{syn} < 4$	$4 < T_{syn} < 10$	$T_{syn} > 10$
Time Step $[days]$	2	2	4	5

Table 5.3: Time steps used to compute the solutions to *Lambert's Problem* using the SPICE Toolkit *Mice* implemented in MATLAB.

5.3.3 Bounding the time of flight

Once the launch window and the time step have been properly defined, it is also necessary to establish the minimum and maximum duration for the mission in terms of time of flight. This has to be done so that the Lambert solver does not provide solutions which involve the spacecraft flying in space for non-viable periods of time, which could be too long (a mission with a flight time of 5 years to an asteroid with a synodic period of 2 years is meaningless) or too short (a time of flight of 15 days to an asteroid would mean an almost straight trajectory). The values used to bound the time of flight for the *Lambert problem* with zero revolutions are shown in Table 5.4. For cases of one revolution, the lower bounds were kept and the upper were tripled.

Synodic Period $[years]$	$T_{syn} < 2$	$2 < T_{syn} < 4$	$4 < T_{syn} < 10$	$T_{syn} > 10$
Minimum TOF $[days]$	30	30	60	120
Maximum TOF $[days]$	365	365	548	548

Table 5.4: Maximum and minimum time of flight (*TOF*) considered as a function of the synodic periods for the asteroids being analyzed.

5.3.4 Considerations for the inbound flight

As this work aims to model the whole asteroid mining mission, there is the need to also determine the pork-chop plot for the inbound (comeback) flight. For that, the criteria for the time step and the TOF can be maintained. However, when defining the launch window for

the return flight special considerations have to be introduced to represent that the spacecraft will be ready for the asteroid departure once the mining operations have finished. In general, the time intervals to account for will be:

- The time the spacecraft should orbit around the asteroid after arrival, not only to perform scientific research and studies but also to determine the best landing site, $t_{observation}$.
- The precise amount of time that the landing maneuver would take, $t_{landing}$.
- The amount of time required to mine the asteroid and retrieve the desired quantity of materials, t_{mining}. Such value would mainly depend on the payload capacity of the spacecraft and also on the rate of extraction achievable by the mining equipment.

To that end, the European Space Agency mission *Rosetta* has been used as reference to obtain orders of magnitude for $t_{observation}$ and $t_{landing}$, since this mission targeted the comet *67P/Churyumov-Gerasimenko*, a type of body similar to that of an asteroid. For the case of this mission, the mentioned times were approximately $t_{observation}$ = 98 days and $t_{landing}$ = 1 day [73]. With respect to the time required to actually mine the asteroid, that is, to extract, process and load the materials in the spacecraft, it was assumed that the operation would encompass three months. Hence, with this information the durations for the different phases of the asteroid mining missions were defined to be as shown in Table 5.5.

$t_{observation}[days]$	$t_{landing}[days]$	$t_{mining}[days]$
120	1	90

Table 5.5: Estimated duration of the observation, landing and extraction and processing phases of the asteroid mining mission.

The reader must take into account that the mining time was set arbitrarily, since no data was available from the European Space Agency to characterize the vehicle capacity nor the mining rate. With all the information stated above, the start date of the comeback launch window was therefore defined to be 211 days after the asteroid arrival, and was set to span a period of 4 years since longer times imply that the spacecraft would be inefficiently waiting ready for departure for too long, being this an important drawback from the point of view of the profitability of the mission.

CHAPTER 6

GENETIC ALGORITHMS

The methodology presented in Chapter 5 to model the asteroid mining missions has one main flaw: the optimization is performed for both the outbound and the inbound flights in terms of only one parameter, the ΔV, which then determines the propellant consumption and hence the initial mass of the spacecraft.

Nevertheless, when considering asteroid mining missions from an economic perspective, two other factors appear into the equation: on the one hand, the amount of mined material (which determines the income from selling the products) and on the other hand, the total duration of the mission. Hence, the problem is complicated further because finding the optimum mission is now a function of three objectives: minimizing propellant consumption, minimizing mission duration and maximizing the amount of mined material.

In addition, constrains are introduced into the problem because now the spacecraft and mined material masses are being taken into account. Factor such as the maximum cargo capacity of the vehicle or the maximum mission duration have to be introduced. As a result, optimizing the asteroid mining mission requires the use of some kind of optimization tool. This thesis carries out this process by using a genetic algorithm, *NSGA-II*, which will be presented and explained in this chapter.

6.1 Introduction: what are Genetic Algorithms?

Genetic algorithms, usually denoted as *GA*, are tools developed by scientist and engineers with the objective of determining the solution to a certain optimization problem. *GA's* form part of the broader category known as Evolutionary Algorithm's, *EA's*, which is no other than a division where one can find different optimization tools which share one thing in common: the use of natural selection and evolution principles for optimization problem solving.

In general, problems in which optimization only focuses in one objective can be solved relatively easily independently of the number of variables to consider, just by programming the software in such a way as to determine the best solution with respect to the objective. For instance, in the method used in Chapter 5, the problem contained several variables (departure date, TOF, number of revolutions) but only one objective (minimizing ΔV) and so the solution that is obtained is the best solution of all possible.

However, this is not the case when talking about multi-objective optimization. For example, consider a problem in which there are three objectives, x_1, x_2 and x_3: there can exist a solution which is the best with respect to one of the objectives but one of the worse with respect to the other two. Hence, in multi-objective optimization the aim is to find the set of solutions which are globally optimal, that is, the set of solutions which are a trade-off between all the objectives and that show the best response to the problem but as a whole. Such set of solutions are denominated as the *Pareto* solutions, also known as *non-dominated* solutions because none of the objectives dominates over the others [74].

Since in the non-dominated solutions no solution is better than the rest, they are all viable and acceptable and it remains to the criteria of the user which one to select, having to perform a trade-off between the objectives based on other external factors [74]. With this, the multi-objective optimization problem can be mathematically expressed as follows [74], where $f_i(x)$ is the objectives function, x is the set of input variables (known as decision variables) and c_m and h_k are the set of constrains.

$$\begin{aligned} &\text{minimize/maximize} && f_i(x) \\ &\text{subject to} && c_m(x) \leq 0, \quad m = 1, \ldots, M \\ & && h_k(x) = 0, \quad k = 1, \ldots, K \end{aligned}$$

As a result, a user is able to find the solution that most suits him by obtaining the

mentioned *Pareto front* and defining a criteria to select, from that set, the most interesting solution for his aim. Doing so enables the user to then retrieve the combination of input variables that yields the mentioned result.

6.1.1 How do they work?

With regards to how does the *GA* operate in order to determine the *Pareto front*, one must know that the algorithms work in a form which resembles biological evolution. Such process is characterized by individuals, being each individual a combination of input variables. A certain number of those individuals conforms a population. In each iteration loop, the algorithm evaluates, for each individual, the objectives defined by the user. Then, it selects individuals of the population to reproduce them, generating new individuals of the next generation. Mutation of the individuals is introduced (that is, some of the input variables that define each individual are changed) and then the objectives are again evaluated. The process is repeated iteratively until a stopping criteria is fulfilled. Hence, the main steps that the genetic algorithm follows can be summarized as [75]:

- Initiation: in this stage the user has to define the objectives (and whether he wants to optimize/minimize them), the input variables and their corresponding bounds, the constrains (if any) that he wants to impose and finally the function(s) $f_i(x)$ that relate all of these parameters. A first population is then created.
- Fitness function: the population is evaluated, that is, the objectives are computed for all the individuals.
- Selection: individuals from the population are selected for reproduction.
- Crossover: new individuals, and hence a new population are created by reproduction of the "parents" selected in the previous step.
- Mutation: once the new population has been determined, some of the individuals are selected and mutation occurs, that is, some of the input variables of the selected individuals are changed.

6.1.2 NSGA-II

The Nondominated Sorting Genetic Algorithm II, *NSGA-II*, was developed as an improvement to the original *NSGA* introduced in 1994 and explained in reference [74]. It is a genetic

algorithm with several modifications which provide better functionality as well as a faster computation time. For this work, the *NSGA-II* developed by Lin Song (reference [76]) and which is publicly available via MATLAB Exchange was used. The main modifications introduced in *NSGA-II* with respect to the operation procedure described in the previous page are referred to the nature in which the previous steps are performed. The changes are [32]:

- Since the objective is to achieve non-dominated solutions, it introduces a new way of organizing the results by performing a classification according to fronts, where the first front is the one containing the individuals which generate the least-dominated solutions. Elitism is introduced because individuals are discarded or not as a function of the front in which they are found.
- In order to preserve diversity in the populations it uses the concept of the crowding distance, which basically measures the distance between solutions. Those individuals which generate solutions which are further apart have higher probability of surviving and passing onto the crossover phase.

The working process of *NSGA-II* can be better understood by looking at Figure 6.1 below and following the explanation of reference [32]. Consider a population of a generation t which has 1000 individuals, that is, P_t with $N = 1000$. Combining P_t with the offspring population that it generated, Q_t, yields a population R_t of size $2 \cdot N = 2000$. All the individuals in R_t are sorted according to non-domination into the aforementioned fronts (F_1,F_2 etc). Then, to create the population of the next generation, that is, P_{t+1}, 1000 individuals are required. These will start coming from the first front, without need of performing crowding distance sorting because the individuals of this front are the best of all according to the non-domination criteria. If the size of F_1 is smaller than 1000, then individuals are taken from F_2 and so on. Eventually, a front will be reached in which not all the individuals found in it are required since there are not enough spaces to fill population P_{t+1}. It is then when crowding distance is computed and those individuals with the best values survive and reach the new population.

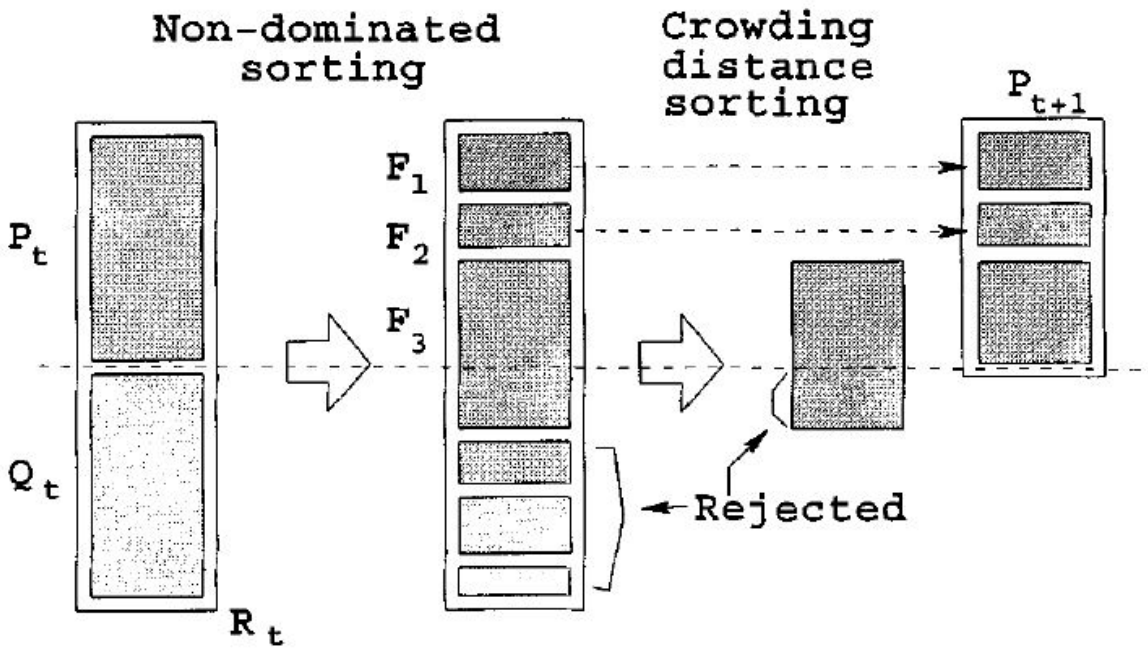

Figure 6.1: Graphical representation of the working principle of *NSGA-II* [32].

Furthermore, *NSGA-II* is a genetic algorithm that can be coded, if desired, to allow the introduction of constrains in order to improve the bounding of the problem and directly neglect those results which do not satisfy certain requirements. Doing so, solutions which may be non-dominated and have a good front position but which do not satisfy the restrictions imposed by the user are directly discarded, therefore not being carried on to the next generations and improving the convergence of the software towards the desired results.

6.2 Implementation of missions in NSGA-II

Once the working philosophy of *NSGA-II* has been explained, it is time to introduce to the reader how has the author used this software to optimize the asteroid mining missions. To that end, explanations are provided regarding which are the objectives defined and why were they chosen, what were the optimization variables considered and how was the mission coded so as to achieve the desired results.

6.2.1 Objective space

As mentioned in the introduction of the present chapter, asteroid mining operations will have to consider three objectives: minimizing the initial mass at Earth departure, m_0, maximizing the mined mass m_{mined} and minimizing the mission duration, being these objectives independent of the type of propulsion method selected.

The reasons behind this choice are related both to economical factors as well as to the capabilities of the current space engineering systems. For instance, there are two main reasons for minimizing the initial mass: on the one hand, to ensure that the spacecraft is as light as possible so that the launcher can escape Earth's gravitational pull, thus ensuring mission feasibility; on the other hand, a minimum initial mass implies smaller launching costs (recall the estimated price of 5000 dollars/kg into LEO from Section 1.1.2 as a reference). Minimizing mission duration is logical from the business perspective as this implies that income flows from selling the products would be more frequent and that the depreciation of the equipment would be smaller.

Finally, maximizing the mined mass is desired so as to obtain the greatest income possible. Nevertheless, please recall that data was not available from the European Space Agency to characterize mining rate nor spacecraft capacity. Therefore, it was assumed that the maximum mineral load that could be allocated in the cargo bay was of 2000 kg, and that the extraction, processing and loading rate would be of 9 kg/day.

6.2.2 Decision variables

The so-called decision space is the domain conformed by the input variables that the algorithm has to optimize. The number and characteristics of the decision variables depends on the type of mission being considered, since missions which involve only multi-revolution trajectories will have a smaller number than those which involve flyby maneuvers. A summary of the decision space for each type of mission would be as follows:

- **Multi-revolution trajectories**: date of Earth departure, time of flight of the outbound flight, date of asteroid departure, time of flight of the inbound flight, number of revolutions for the outbound transfer and number of revolutions for the comeback flight. This sums up to 6 decision variables.

- **Trajectories with one flyby**: date of Earth departure, date of asteroid departure, TOF of the first leg, TOF of the second leg, TOF of the third leg, planet of flyby, flyby altitude, flyby target angle, number of revolutions of the first, second and third leg. This makes up a total of 11 decision variables.

Looking at the variables defined above it is clear that the genetic algorithm will have to deal with a large number of possibilities, that is, with a big decision space. In order to aid the software, it is effective to simplify the dimension of the decision space as much as possible, either by reducing the bounds of the variables (for instance, reducing launch window's, times of flight or possible number of revolutions) or, for the case of the flyby's, by specifying the flyby planet and in which flight (the outbound or the inbound) is it going to be performed. Doing this not only reduces computation times but also facilitates the optimization process.

To that end, the "general" genetic algorithm was decomposed into four different programs: one for the multi-revolution cases with chemical propulsion, one for multi-revolution trajectories with low-thrust, another with the flyby being performed in the outbound flight and a last one in which the flyby was performed in the inbound flight (recall that gravity assist maneuvers were only considered for the chemical propulsion trajectories). In addition, in the case of the *GA's* involving flyby's, runs were performed defining the flyby planet and then changing it as different solution possibilities were explored.

Furthermore, it was considered that the minimum time the spacecraft would be on the asteroid's surface, $t_{mining_{min}}$ was to be 90 days, while the maximum $t_{mining_{max}}$ two years. This was done not for the purpose of extracting material (the cargo bay capacity would be full in less than two years) but to give freedom to the algorithm with respect to the launching date for the inbound flight. Hence, the minimum asteroid departure date would be 211 days after the arrival while the latest date could be 851 days after the encounter.

The limits considered for all the different decision variables presented in this section can be seen in Table 6.1 below. Please notice that, although the mentioned table has been created for the case of missions considering flyby's, the variables for the multi-revolution trajectories are also shown since gravity assist maneuvers just add up new variables to the ones found in the basic problem. Hence, for multi-revolution trajectories the limits are those written in the first five rows of Table 6.1 for both, chemical and low-thrust missions, although the latter enables a greater number of revolutions since low-thrust propulsion methods may

require greater transfer times to achieve the required velocity change. Furthermore, planet identification numbers were assigned to define the body around which the gravity assist maneuver would be performed. ID 2 corresponds to Mars and ID 3 to Venus.

Decision Variable	**Lower Bound**	**Upper Bound**
Earth departure date	01 January 2018	01 January 2028
TOF leg_i	30 *[days]*	1460 *[days]*
Number of revolutions leg_i (chemical propulsion)	0	1
Number of revolutions leg_i (ion propulsion)	0	4
Asteroid departure date	Asteroid arrival date + 211 *[days]*	Asteroid arrival date + 851 *[days]*
Flyby planet ID	2	3
Flyby altitude	See Table 4.2	See Table 4.2
Flyby angle	-180 °	180 °

Table 6.1: Summary of the decision variables considered along with the corresponding upper and lower bounds.

6.2.3 Constrains

The possibility of introducing constrains into the problem is very useful for this study since there are certain limitations imposed by launcher capabilities and by economic aspects which have to be taken into account. For example, missions which involve Earth departure masses (m_0) which are very big, or missions which imply large infinity departure velocities ($v_{\infty_{dep}}$) should not be considered due to the limitations imposed by launcher capacities.

In addition, from an economic perspective the duration of the missions should also be limited to avoid excessive times (specially for the case of missions considering flyby's since there is an extra leg in the trajectory or for the low-thrust missions were up to four revolutions can be considered). Introducing these constrains therefore allows the genetic algorithm to operate more robustly, eliminating solutions which are not desired and hence achieving good degrees of convergence between runs and at a smaller computation time. Table 6.2 presents a summary of the constrains introduced into the problem depending on the type of mission.

Mission Type	**Constrain 1** $[km/s]$	**Constrain 2** $[kg]$	**Constrain 3** $[years]$
Multi - revolutions	$v_{\infty_{dep}} < 7.5$	Initial mass < 20000	-
Low thrust	-	Initial mass < 20000	Duration < 12
Gravity assist trajectories	$v_{\infty_{dep}} < 7.5$	Initial mass < 60000	Duration < 12

Table 6.2: Summary of the constrains considered for each of the different types of missions implemented in the genetic algorithm.

6.2.4 Obtaining the results

The so-called objective function is the part of code of the genetic algorithm were all the decision variables are introduced with the purpose of calculating the values of the three objectives defined in Section 6.2.1 for each of the individuals that conform the population. This function has to be created and customized by the user. For this work the objective function was developed making use of SPICE to retrieve positions and velocities, then solving the *Lambert problem* associated to each of the transfer legs and finally computing the three objectives.

As was explained in Section 6.2.1, two of the objectives that the algorithm had to optimize were the spacecraft initial mass and the mass of mined material. To obtain these values it was decided that the best approach to follow was to use a system of equations which "constructed" the masses for each of the phases of the mission.

This method consists on assuming that the final mass, that is, the mass that remains after the Earth rendez-vous, is just the sum of the mined mass and the structural mass of the spacecraft. From that point of the trajectory, one can then go backwards and construct the masses by applying Equation 4.13, since the values of ΔV are known after solving the *Lambert problem*. To illustrate the mass variables used in the problem please consider Figure 6.2 below, which shows the characteristic events and masses involved in a mission with a gravity assist maneuver in the outbound flight.

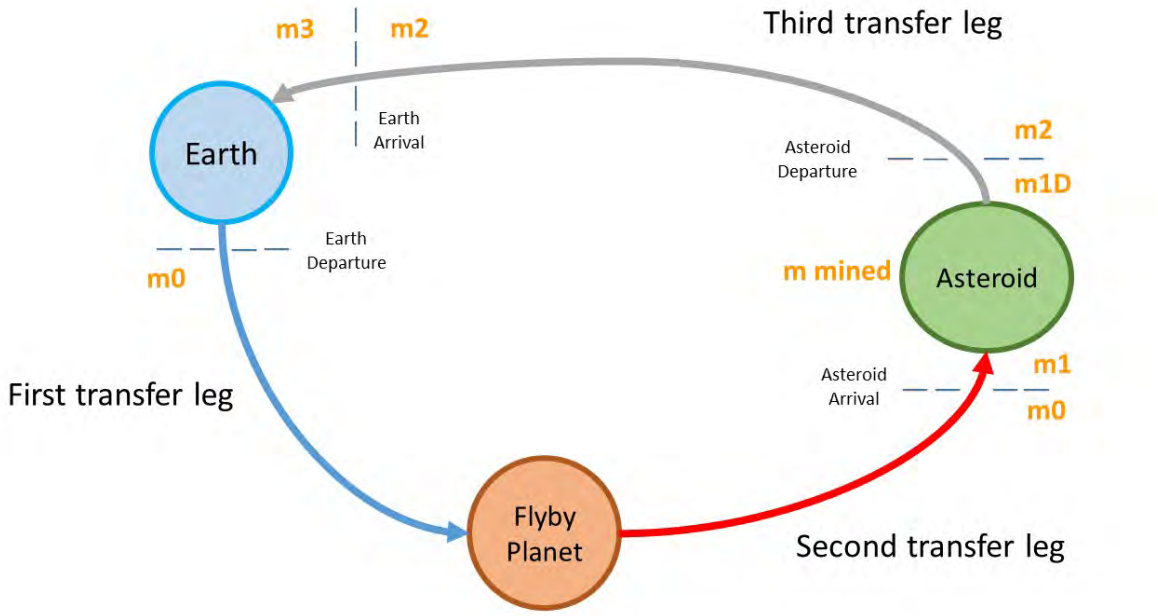

Figure 6.2: Schematic representation of a typical asteroid mining mission with one flyby together with the notation used to describe the trajectory.

Considering the nomenclature of Figure 6.2, the construction process starts by defining a factor to account for the spacecraft mass. It is assumed to be 1.3, meaning that the dry mass (spacecraft structures and components) are considered to be 30% of the total mined mass. Since this is known (recall that the extraction rate was imposed and that the mining time can be computed as the difference between the date of landing and the date of asteroid departure), one can obtain the value of m_3 as:

$$m_3 = m_{mined} \cdot factor \tag{6.1}$$

Then, using Equation 4.13 and the ΔV from the Earth rendez-vous maneuver yields:

$$\frac{m_2}{m_3} = exp\left(\frac{\Delta V_3}{g_0 \cdot I_{sp}}\right) \quad \longrightarrow \quad m_2 = m_3 \cdot exp\left(\frac{\Delta V_3}{g_0 \cdot I_{sp}}\right) \tag{6.2}$$

Similarly, for the asteroid departure we have:

$$\frac{m_{1D}}{m_2} = exp\left(\frac{\Delta V_2}{g_0 \cdot I_{sp}}\right) \quad \longrightarrow \quad m_{1D} = m_2 \cdot exp\left(\frac{\Delta V_2}{g_0 \cdot I_{sp}}\right) \tag{6.3}$$

m_{1D} is the mass at asteroid departure and is given by the following expression, which allows us to find the mass after the asteroid rendez-vous maneuver m_1:

$$m_{1D} = m_1 + m_{mined} \quad \longrightarrow \quad m_1 = m_{1D} - m_{mined} \tag{6.4}$$

Finally, and since the flyby maneuver is unpowered, the initial mass m_0 that the launcher has to place into orbit is given by:

$$\frac{m_0}{m_1} = exp\left(\frac{\Delta V_1}{g_0 \cdot I_{sp}}\right) \quad \longrightarrow \quad m_0 = m_1 \cdot exp\left(\frac{\Delta V_1}{g_0 \cdot I_{sp}}\right) \tag{6.5}$$

The methodology described in this section was employed not only for missions with flyby's but also for the ones involving only multi-revolution trajectories. In those cases, the mass variables were the same as the ones shown in Figure 6.2.

Part III

RESULTS AND CONCLUSIONS

CHAPTER 7

RESULTS FOR ASTEROID RYUGU

This Chapter is now dedicated to presenting the results obtained for the analysis and optimization of the trajectories for asteroid Ryugu. This body has been selected for a complete analysis, along with Didymos which will be presented in Chapter 8, due to the fact that, on the one hand, it is one of the asteroids with the biggest estimated profit according to *Asterank* and, on the other hand, because as presented in Section 1.2.3 mission *Hayabusa II* from the Japanese Space Agency *JAXA* is expected to reach the body at the end of this year.

Firstly, the pork-chop plots obtained following the procedure explained in Chapter 5 will be presented and discussed. Then, the results yielded by the genetic algorithm will be shown, providing the reader with the optimized chemical propulsion mission as well as with the corresponding ion propulsion counterpart. Whenever possible, trajectories will be compared with the values from the *JPL Mission Design Tool*.

7.1 Pork-Chop Plots

Obtaining the so-called pork chop plots is important when performing the preliminary design of interplanetary missions because these graphs provide valuable information regarding the launch epochs, the times of flight and the required ΔV. As a result, the first step for analyzing the asteroid mining missions was to follow the procedure explained in Chapter 5. Doing this yielded Figure 7.1 below, the pork-chop plot for the outbound flight. The mission with minimum ΔV is highlighted by means of a red circle.

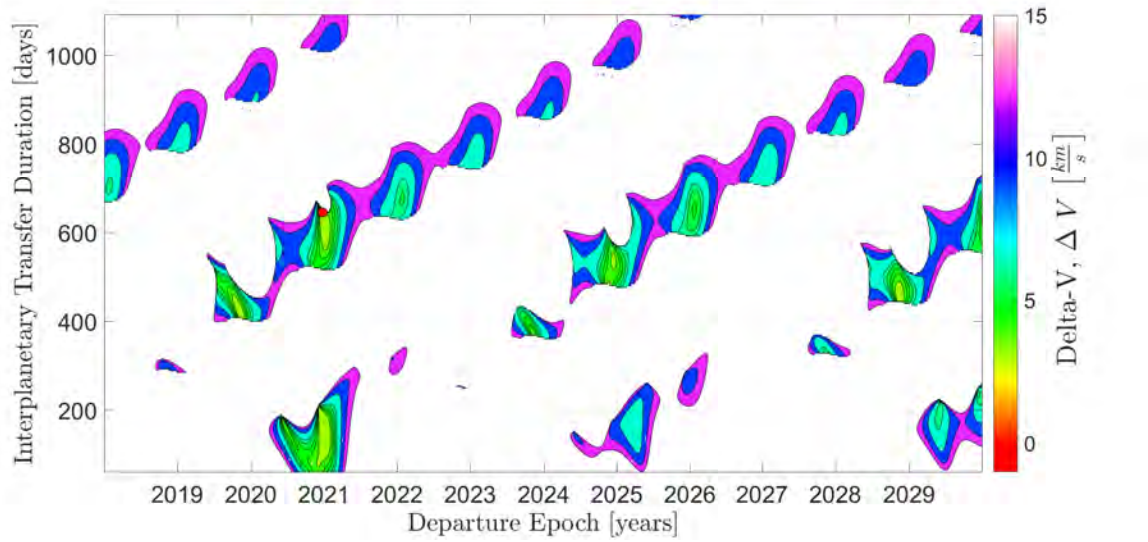

Figure 7.1: Pork chop diagram for the outbound flight to asteroid Ryugu. The mission with smallest ΔV is marked with a red circle.

The diagram obtained shows the evolution of the outbound flight possibilities for the twelve-year launch window being considered. As can be appreciated, the results follow trends that repeat every four years, something expected since the synodic period of the asteroid with respect to Earth is approximately equal to that value. In addition, one can see how the transfer possibilities increase considerably for multi-revolution trajectories, which imply longer transfer times.

Furthermore, the reader may be able to appreciate some small imperfections in the diagram which appear as colorless regions in the middle of the contour (for instance, there is one in 2021 and for a transfer duration of approximately 100 days). The reason behind this is that for such trajectory the Lambert solver was unable to converge and retrieve a solution. Such case appears whenever the change in true anomaly of the trajectory is $\Delta\theta = \pi$, since what happens is that the so-called Gauss function g is equal to zero for such angle and hence no velocity vectors v_1 and v_2 can be retrieved. Mathematically, using the notation of Section 4.4, this can be expressed as:

$$g = \frac{r_1 \cdot r_2}{h} \cdot sin(\Delta\theta) \quad \longrightarrow if \quad \Delta\theta = \pi \quad \longrightarrow \quad g = 0$$

$$v_1 = \frac{(r_2 - f \cdot r_1)}{g} \quad and \quad v_2 = \frac{(\dot{g} \cdot r_2 - r_1)}{g}$$

From Figure 7.1 it can also be appreciated that the trajectory with minimum ΔV is located approximately in 2021 and involves a time of flight greater than 600 days. Such year appears to present very good launching opportunities since, in addition to the mentioned transfer, there is also a region in the vicinity of the 200 days duration which shows interesting values of ΔV for trajectories involving zero revolutions, something which is not the case neither in 2025 nor 2029.

To characterize the two transfers that have been mentioned Table 7.1 is provided, where the reader can appreciate also a comparison with the equivalent flights retrieved from the *JPL Mission Design Tool*. Since the flight with minimum ΔV is the one corresponding to the multi-revolution transfer, the trajectory plots shown in Figure 7.2 and 7.3 have been obtained. The reason behind this is that, although the zero revolution transfer may seem better (almost identical cost but much lower time of flight), the whole mission has to be considered and it is in the inbound flight where substantial differences are found.

Variable	**MATLAB (0 revs)**	**JPL (0 revs)**	**MATLAB (1 rev)**	**JPL (1 rev)**
Launch Date	28 - Dec - 2020	26 - Dec - 2020	24 - Dec - 2020	26 - Dec - 2020
TOF $[days]$	168	170	644	640
C3 $[km^2/s^2]$	7	7.19	6.34	6.41
$V_{\infty_{dep}}$ $[km/s]$	2.65	2.7	2.52	2.5
$V_{\infty_{arr}}$ $[km/s]$	1.79	1.7	1.86	1.8
Total ΔV $[km/s]$	4.43	4.4	4.37	4.4
Sun phase angle [°]	92.98	94.1	120.03	118.4
Range to Earth $[AU]$	0.55	0.55	2.09	2.08
Approach angle [°]	88.19	88.5	95.44	95.2
Declination of the launch asymptote [°]	-29.97	-31.1	-30.01	-30.1

Table 7.1: Comparison between the values retrieved from the *JPL* and those obtained from MATLAB for the zero and one revolution transfers.

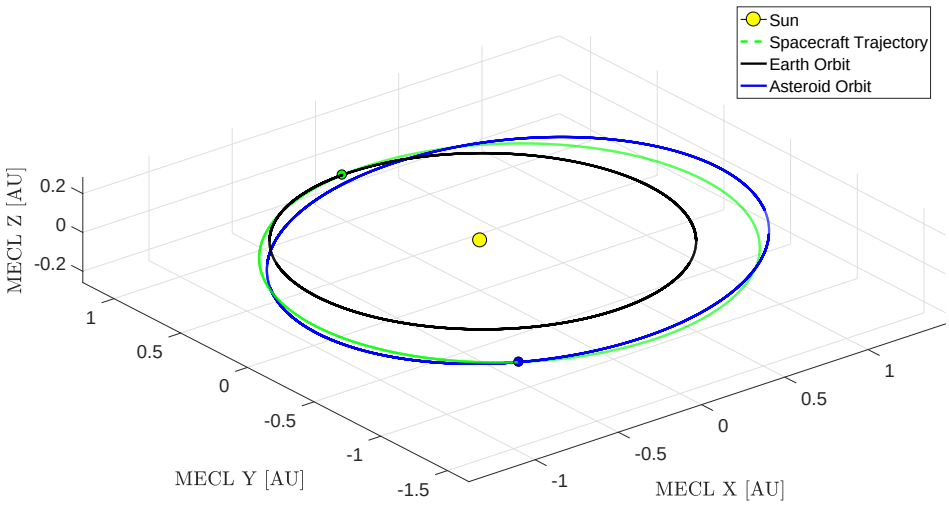

Figure 7.2: Three-dimensional plot of the outbound transfer with minimum ΔV to asteroid Ryugu.

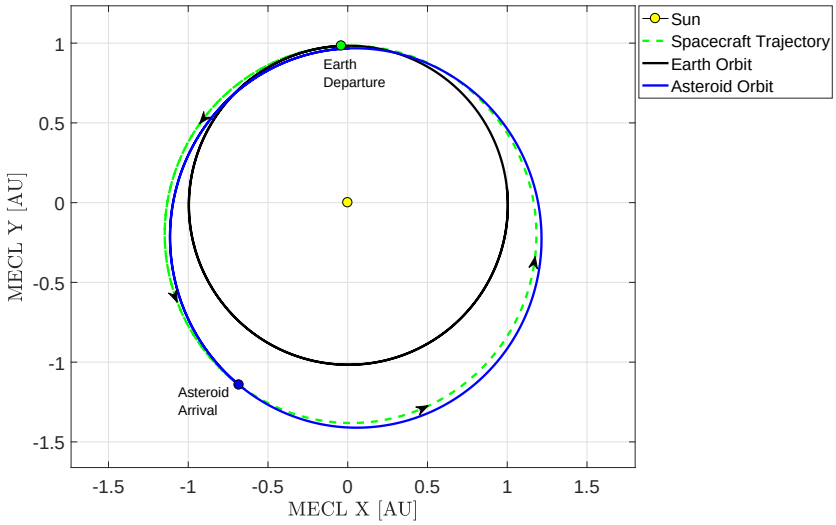

Figure 7.3: Outbound trajectory projected onto the ecliptic plane for asteroid Ryugu.

To conclude with the analysis of the outbound transfer, Figure 7.3 provides further understanding on why is the value of ΔV for the outbound flight small. Although Figure 7.2 clearly shows that the Earth and asteroid orbits are not coplanar (recall that the inclination is of 5.88 ° for asteroid Ryugu) and that hence performing a *Hohmann* transfer (the most energy-efficient trajectory) is impossible, the projected view provided in Figure 7.3 shows

characteristic features of this type of trajectory, since a considerably circular orbit in which departure from Earth occurs at one of the points of the apse line is obtained for the outbound flight.

After the analysis of the Earth - asteroid flight, it is now time to present the results for the inbound trajectory. To that end, the pork-chop plot is shown in Figure 7.4 for the 4-year launch window considered.

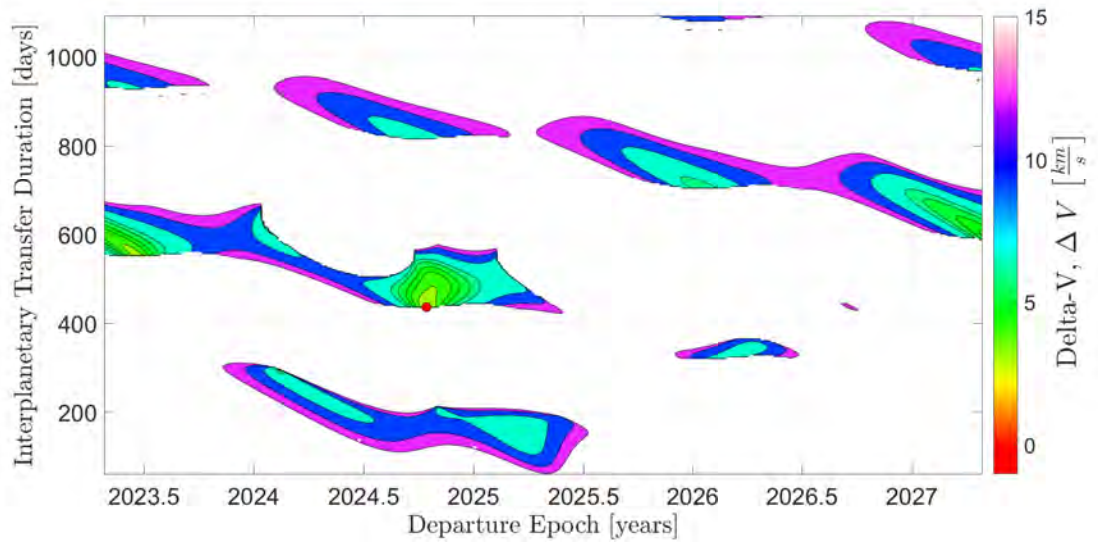

Figure 7.4: Inbound pork-chop plot for asteroid Ryugu.

As can be appreciated, the trajectory with minimum ΔV is found at the end of 2024. Nevertheless, Figure 7.4 also shows that there is an acceptable region with low velocity change exactly one year before, although the time of flight involved is approximately 100 days greater. Therefore, stating which is the optimum date for the return flight is not straightforward, but one can imagine that, due to economic reasons, asteroid mining companies would probably prefer launching the inbound flight in mid 2023 so as to be able to reduce mission duration an increase the rate of income flows, paying-off the drawback of a greater velocity change.

In any case, choosing the best transfer would require a more profound trade-off study. Hence, continuing to apply the criteria of minimum ΔV yields the following trajectory plots for the inbound flight, shown in Figures 7.5 and Figure 7.6, where as can be seen the transfer performs one revolution in the short-arc direction.

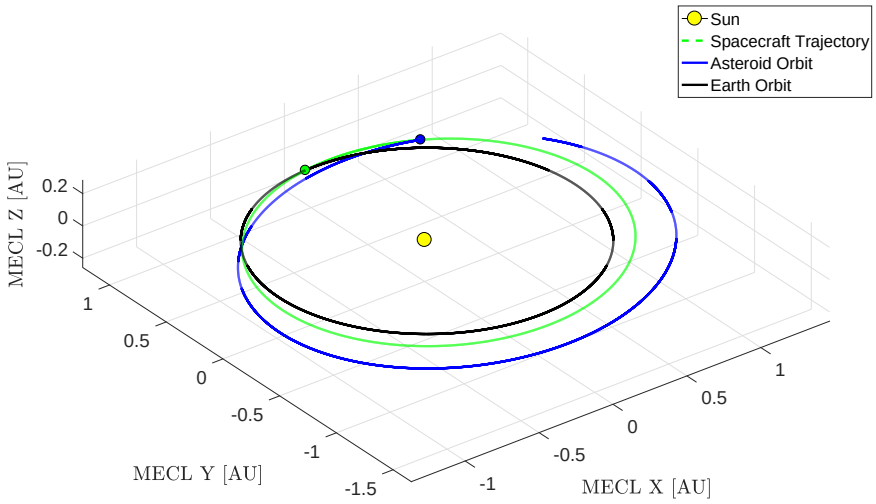

Figure 7.5: Inbound flight trajectory for asteroid Ryugu.

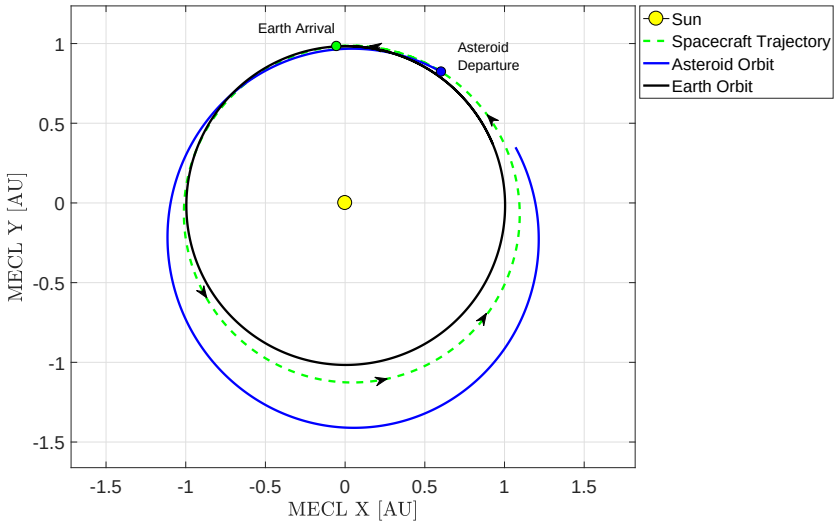

Figure 7.6: Ryugu - Earth transfer projected onto the ecliptic plane.

The values characterizing the flight shown above can be seen in Table 7.2, where a relatively long time of flight is necessary to perform the revolution for phasing purposes.

Variable	MATLAB (1 rev)
Launch Date	15 - Oct - 2024
TOF $[days]$	436
C3 $[km^2/s^2]$	8.98
$V_{\infty_{dep}}$ $[km/s]$	2.99
$V_{\infty_{arr}}$ $[km/s]$	1.93
Total ΔV $[km/s]$	4.93
Sun phase angle [°]	119.58
Approach angle [°]	68.06

Table 7.2: Results for the Ryugu - Earth tranfer.

7.2 Pareto Fronts

To avoid the optimization problem presented for the inbound flight described in the previous section, multi-objective optimization using *NSGA-II* was performed and the resulting pareto plots are presented and discussed in this section. To that end, the analysis can begin by considering Figure 7.7 below.

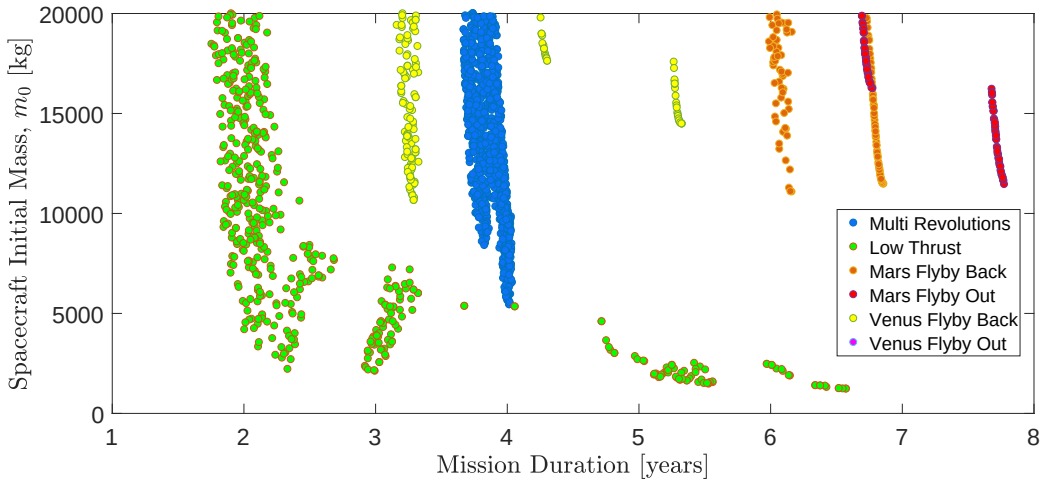

Figure 7.7: Pareto plot of the initial spacecraft mass as a function of the mission duration for asteroid Ryugu. All types of trajectories are plotted and represented according to the legend.

The first thing to point out for the results shown is the apparent contradictory behavior that can be appreciated when comparing the multi-revolution transfers with low-thrust and their corresponding counterparts with chemical propulsion. In principle, one would expect for the chemical missions to imply smaller transfers times, since achieving the ΔV would not require a long sequence of thrust and coast arcs and, in addition, the genetic algorithm is given the possibility of performing more revolutions in the low-thrust case.

The reason behind the yielded values resides in the fact that chemical propulsion missions are modeled with the constrain that the maximum departure infinity velocity is of 7.5 km/s, in contrast with low-thrust missions in which the initial impulse is considered to be 2 km/s at Earth departure. This constrain eliminates many of the possible missions involving multi-revolutions with chemical propulsion, and, in particular, does so with all the solutions implying less than 3 years, since the launchers would not be able to place the mission into the desired injection point.

With respect to the rest of possibilities, Figure 7.7 discards all implying gravity assist maneuvers in Mars due to an excessive mission duration. In addition, all missions with a flyby in Venus in the outbound flight are also eliminated due to excessive spacecraft initial masses. Therefore, only multi-revolution trajectories with low-thrust and with chemical propulsion as well as missions involving a Venus flyby in the inbound transfer should be considered for further study. With the objective of doing so, Figure 7.8 is provided.

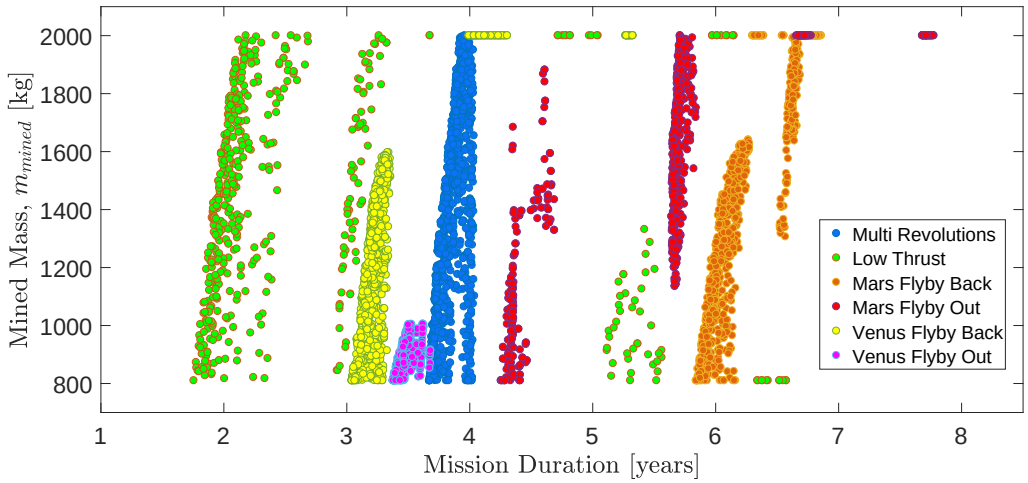

Figure 7.8: Pareto plot showing mass of mined material as a function of mission duration for asteroid Ryugu.

With the results shown in Figure 7.8 one can conclude that missions which perform a Venus flyby in the comeback flight should not be further analyzed since the masses of mined material that can be retrieved are limited. This is probably due to the fact that the date interval in which the flyby maneuver is advantageous is small, meaning that the time the spacecraft can remain at the asteroid for mining operations is constrained, hence yielding smaller values of mined material.

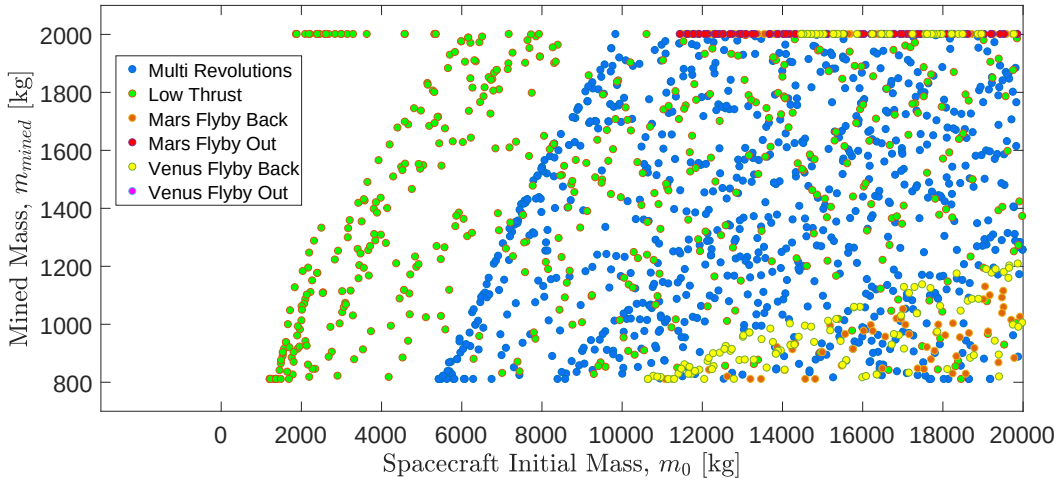

Figure 7.9: Results for mass of mined material as a function of the spacecraft initial mass for asteroid Ryugu and for all the types of transfers.

Finally, Figure 7.9 can be used to determine which type of missions are the most favorable from the two that remain, since an asteroid mining company would desire to achieve the highest possible ratio mined-initial mass. Hence, low-thrust missions can be defined to, in principle, be the best ones. Please notice also how the evolution of the ratio is as expected: bigger mined masses imply longer stay times at the asteroid, which in turn cause bigger spacecraft masses at the Earth rendez-vous and hence a bigger initial mass m_0 after performing the construction method explained in Section 6.2.4.

7.3 Optimized Chemical Propulsion Mission

The analysis of the pareto plots performed in the previous section has yielded that, in principle, the most advantageous missions involving chemical propulsion are those which perform only multi-revolution transfers. Selecting the criteria of minimum spacecraft initial mass leads to obtaining a particular trajectory which will now be presented. The reason

behind considering this objective as the dominant one with respect to mined mass or mission duration is due to the fact that, as mentioned before, launcher capacities posed the most important constrain on the feasibility of the mission. The outbound trajectory is shown in Figures 7.10 and 7.11.

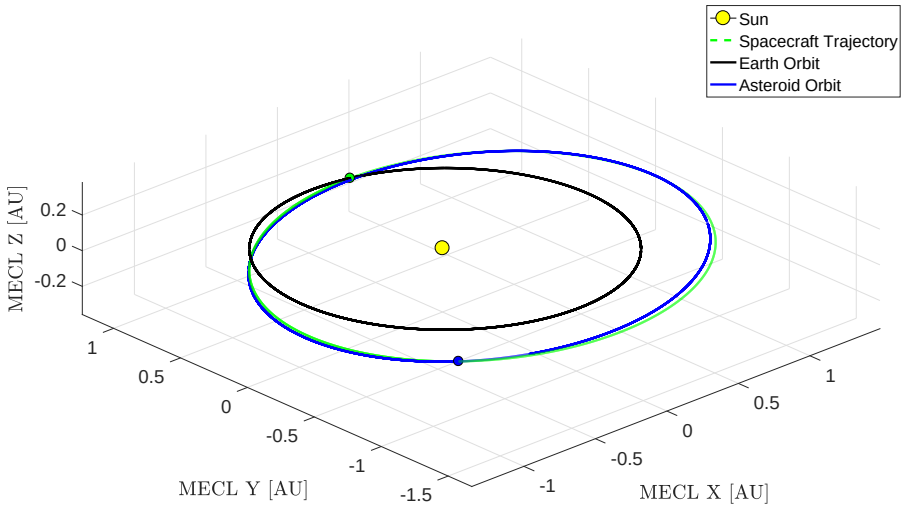

Figure 7.10: Outbound three-dimensional plot of the optimum chemical propulsion trajectory to Ryugu.

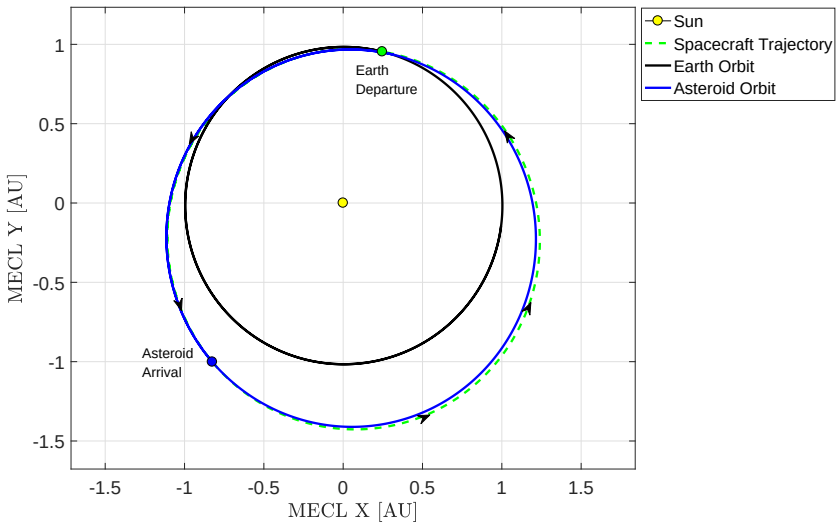

Figure 7.11: Earth - Ryugu projected trajectory for the optimal chemical propulsion mission.

Visualizing the trajectory is not simple due to the superposition of the line representing the spacecraft motion and the different orbits. Nevertheless, this flight corresponds to a short arc transfer which is characterized by the values shown in Table 7.3, where a comparison with the parameters from the *JPL* is provided. The outbound flight is performed in a very optimum way since departure from Earth occurs at a point in which the planet is very close to the asteroid orbit, enabling the mission to enter a trajectory almost identical to that of the small body (hence the superposition of lines), where it performs a phasing maneuver by means of one revolution before the rendez-vous.

Variable	**MATLAB**	**JPL**
Earth Launch	07 - Dec - 2020	06 - Dec - 2020
TOF $[days]$	646	640
C3 $[km^2/s^2]$	18.93	20.88
$V_{\infty_{dep}}$ $[km/s]$	4.35	4.6
$V_{\infty_{arr}}$ $[km/s]$	0.54	0.4
Total ΔV $[km/s]$	4.89	5.0
Sun phase angle [°]	53.59	35.9
Range to Earth $[AU]$	2.01	1.97
Approach angle [°]	78.19	74.4
Declination of the launch asymptote [°]	-50.24	-51.6

Table 7.3: Values characterizing the outbound trajectory and the corresponding comparison with those retrieved from the *JPL Mission Design Tool*.

Once the outbound trajectory has been defined, Figures 7.12 and 7.13 show the plots for the asteroid - Earth flight. The resulting transfer is considerably similar to that found in the outbound trip, since the arrival at Earth occurs at the region in which the orbits come closest and it also implies a one revolution flight, which, as can be seen looking at the values of Table 7.4 results in a long time of flight.

Finally, the reader must know that the mission described in this section is capable of retrieving 810 kg of mined material and that the total duration corresponds to 1465 days. For this mission to be possible, the launcher has to place 5452 kg into orbit, being the launch energy C3 = 18.93 $[km^2/s^2]$. With such values, Table 4.1 and Figure 4.2 show that the spacecraft can use the SLS Block 1B and 2, Falcon Heavy or Delta IV as launchers.

Variable	Value
Asteroid Departure	13 - Apr - 2023
Earth Arrival	11 - Dec - 2024
$V_{\infty_{dep}}$ $[km/s]$	1.07
$V_{\infty_{arr}}$ $[km/s]$	4.34
TOF $[days]$	608
Sun phase angle [°]	101.95
Approach angle [°]	52.65

Table 7.4: Values that define the inbound flight for the chemical propulsion mission with minimum m_0 to asteroid Ryugu.

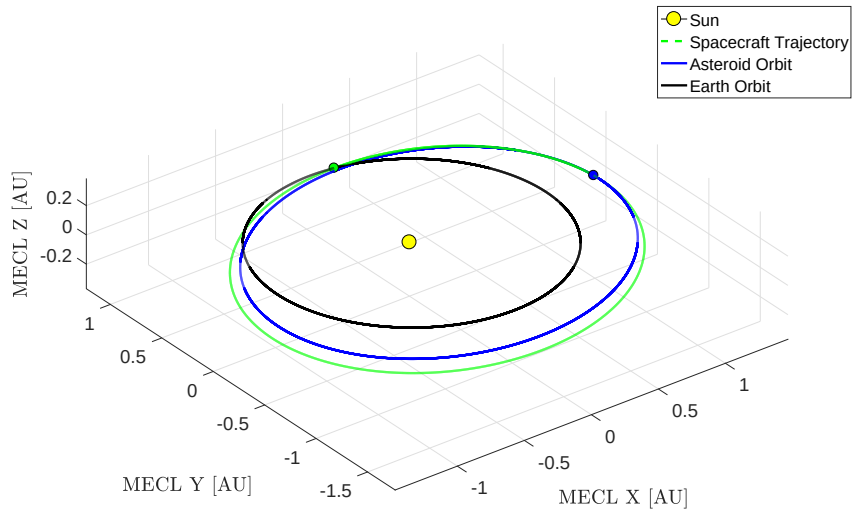

Figure 7.12: 3D view of the inbound trajectory for the optimal chemical propulsion mission.

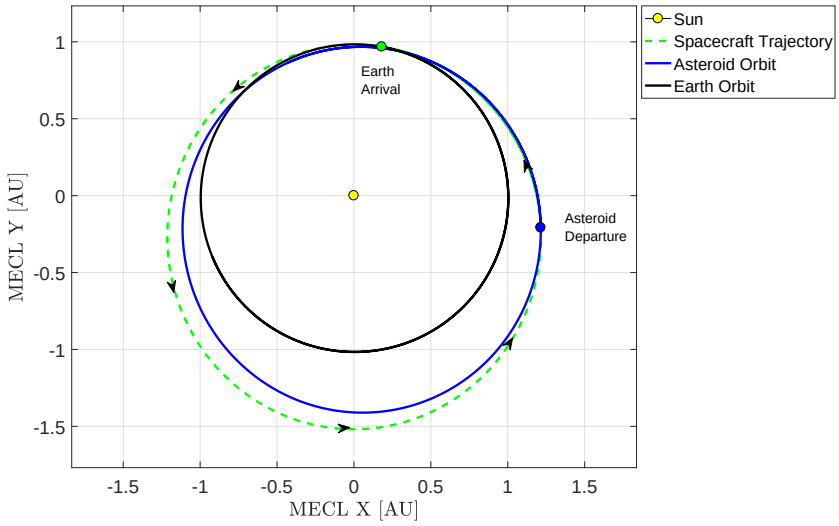

Figure 7.13: Ryugu - Earth projected view of the trajectory for the optimal chemical propulsion mission.

7.4 Optimized Mission with Low-Thrust

As reasoned in Section 7.2, low-thrust missions presented the best compromise between the three objectives being considered. This section will now complete the analysis of asteroid mining trajectories to Ryugu by providing the values and plots which characterize the low-thrust mission involving minimum spacecraft initial mass m_0.

The outbound trajectory is represented in Figure 7.14 below, where the reader can see the thrust-coast arc sequence which enables the spacecraft to encounter the asteroid. As was explained in Section 4.6.2, the final thrust arc before asteroid arrival does not appear. In addition, one can also see how the thrust arc corresponds to a logarithmic spiral in raising regime, as it propagates away from the attraction center. The values characterizing this transfer are provided in Table 7.5.

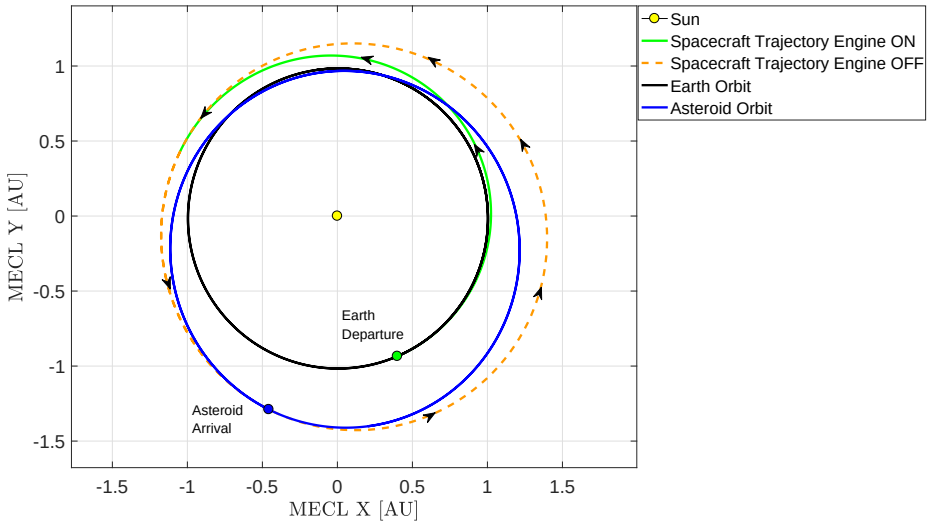

Figure 7.14: Outbound trajectory for the low-thrust mission to asteroid Ryugu.

Variable	**Value**
Earth Launch	15 - Jul - 2025
Asteroid Arrival	30 - Dec - 2027
Asteroid Landing	29 - Apr - 2028
$V_{\infty_{arr}}$ $[km/s]$	1.35
ΔV_{ion} $[km/s]$	11.39
TOF $[days]$	898
Number of revolutions	1
Range to Earth at asteroid arrival $[AU]$	2.28

Table 7.5: Parameters characterizing the outbound flight for the low-thrust mission to Ryugu.

With respect to the comeback flight, Figure 7.15 shows the nature of the trajectory. The coast arc appears as a continuous orange line due to the fact that, since it is a multi-revolution trajectory, the dashed lines superpose each other. For the sake of clarity a zoomed view of the thrust arc has been provided in Figure 7.16. As can be seen, the ion engine is switched on for a considerably small period of time and the generalized logarithmic spiral is found to be in lowering regime, since it approaches its attraction center.

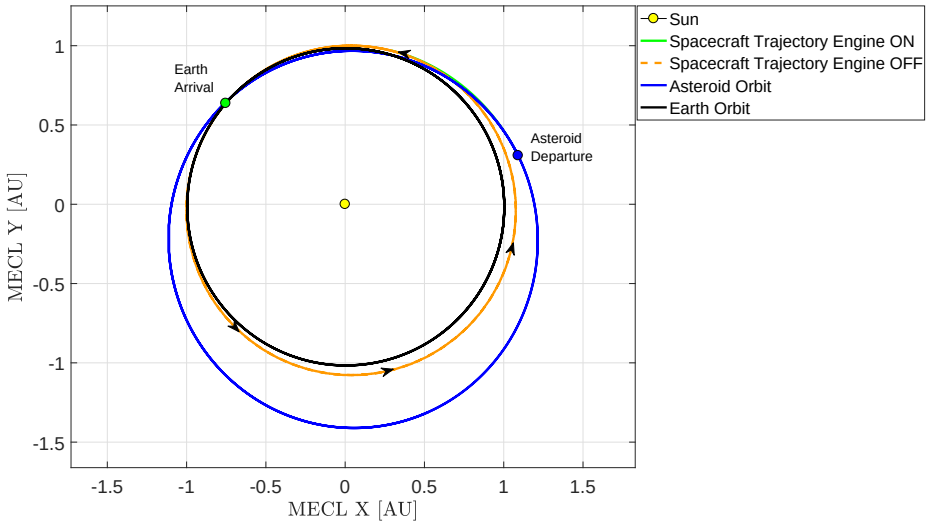

Figure 7.15: Inbound trajectory for the low-thrust mission to asteroid Ryugu.

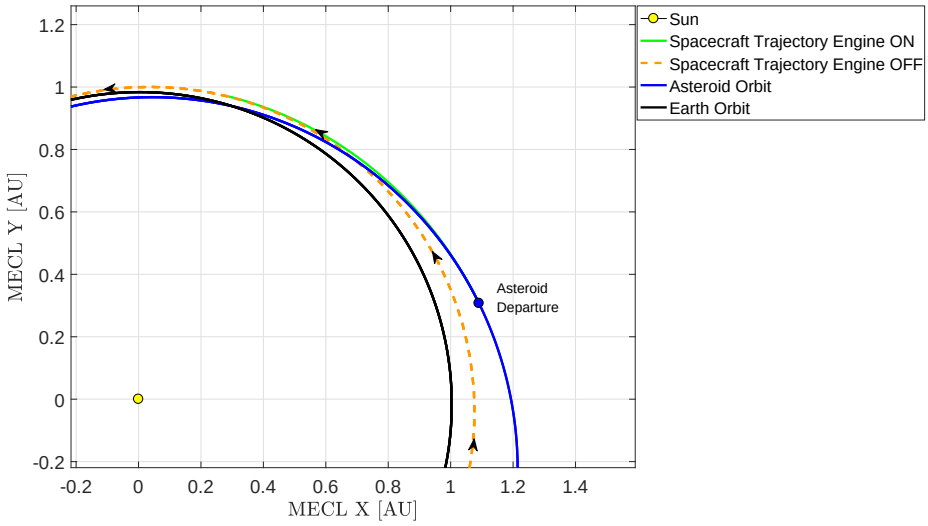

Figure 7.16: Zoomed view of the thrust arc corresponding to the Ryugu-Earth transfer.

Finally, Table 7.6 shows the values of the parameters that define the comeback flight. In accordance with the trajectory plot, the transfer involves 3 revolutions and hence a very long time of flight. This, on the other hand, has the advantage that the infinity arrival velocity that the chemical propulsion system must counteract is considerably small. Furthermore, since the thrust arc is short, the ΔV obtained with the ion engine is low.

Variable	Value
Asteroid Departure	28 - Jul - 2028
Earth Arrival	09 - Feb - 2032
$V_{\infty_{arr}}$ $[km/s]$	0.57
ΔV_{ion} $[km/s]$	3.61
TOF $[days]$	1290
Number of revolutions	3

Table 7.6: Data characterizing the inbound transfer leg for Ryugu.

Having provided the trajectory plots and the parameters characterizing the mission, the final study consists on determining whether the thrust profile associated to this solution is feasible or not. To that end, the procedure described in Section 4.7.2.3 has been followed and the values shown in Table 7.7 have been obtained. Comparing the required ΔV values with those that could be provided by the NEXT-C engine shows that the mission described in this section could be feasible with one engine.

$\Delta V_{req_{out}}$ $[km/s]$	$\Delta V_{NEXT_{out}}$ $[km/s]$	$\Delta V_{req_{back}}$ $[km/s]$	$\Delta V_{NEXT_{back}}$ $[km/s]$
12.74	15.44	4.19	18.46

Table 7.7: ΔV required in both flights and actual output of one NEXT-C engine.

Finally, since the required initial spacecraft mass m_0 is 1222 kg, the mission could be perfectly launched by any of the rockets mentioned in Section 4.3. The amount of mined material m_{mined} retrieved would be 810 kg and the total mission duration would amount to 2399 days. Compared to the mission with chemical propulsion described in the previous section, the drawback is that the duration is considerably longer. This is due to the fact that imposing the criteria of minimum m_0 yields a mission which corresponds to the ones found in the 6-year duration region of Figure 7.7. As can be seen in that plot, there are low-thrust missions in which, although the mass may be larger, the duration is almost halved. Nevertheless, determining which mission is best would require an extensive analysis of the 2-3 year duration region, and, in particular, of the NEXT-C engine performance, since the fact that the mission implies smaller flight times may lead to infeasible thrust profiles.

CHAPTER 8

RESULTS FOR ASTEROID DIDYMOS

This Chapter will now present and discuss the results for the optimized asteroid mining missions to Didymos. Such body has been selected from the list due to the fact that, as mentioned in Section 4.7.2.2, NASA's mission *DART* is targeting this asteroid.

As was done in the previous chapter, pork-chop plots will be presented and the results obtained for the mission with minimum ΔV discussed and compared. Then, focus will be placed on the values yielded by the genetic algorithm. To that end, the pareto plots and the optimal missions involving chemical and low-thrust propulsion will be defined and analyzed.

8.1 Pork-Chop Diagrams

The procedure described in Chapter 5 optimizes the asteroid mining missions in terms of ΔV and at the same time yields the pork-chop plots for the transfers. For asteroid Didymos, the outbound mission with minimum velocity change is found to involve a transfer with one revolution. The corresponding pork-chop plot is shown in Figure 8.1, being the optimum mission marked with a red circle.

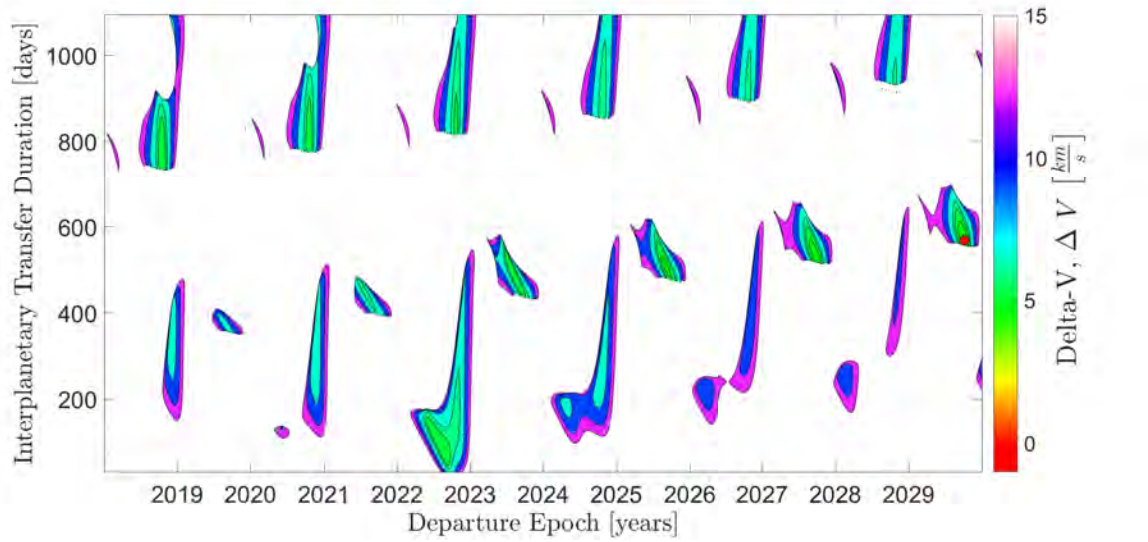

Figure 8.1: Pork chop diagram for the outbound flight to asteroid Didymos. The mission with minimum ΔV is represented with a red circle.

Figure 8.1 shows the different launching possibilities for the 12-year period considered. It is interesting to note that the mentioned opportunities are found every two years approximately, something logical considering that the synodic period of the asteroid is 1.9 years. Please notice that only results with a ΔV smaller than 15 km/s have been considered. With respect to the mission with minimum velocity change it is found at almost the upper limit of the launch window. This is beneficial since, if a mission was to be seriously considered, there would be sufficient time margin so as to carry out the different development and preparation steps.

Nevertheless, if one assumes that technology is already available for asteroid mining then the aim would be to launch the mission as soon as possible. This could be done in the vicinity of 2023, since it presents a favorable opportunity for non-revolution trajectories and with considerably small times of flight. This mission can be retrieved from the zero-revolution problem solved for the asteroid.

The two opportunities and all the corresponding parameters that have been obtained for each trajectory can be found in Table 8.1, where the data retrieved from the *JPL Mission Design Tool* is also provided for comparison. Then, focus is placed on the trajectory with lowest ΔV and plots for the transfer can be seen in Figures 8.2 and 8.3, where a three-dimensional graph and a projected view on the mean ecliptic plane can be observed.

Variable	**MATLAB (0 revs)**	**JPL (0 revs)**	**MATLAB (1 rev)**	**JPL (1 rev)**
Launch Date	20 - Aug - 2022	18 - Aug - 2022	04 - Oct - 2029	28 - Sep - 2029
TOF $[days]$	80	80	568	570
C3 $[km^2/s^2]$	11.13	10.31	8.4	9.09
$V_{\infty_{dep}}$ $[km/s]$	3.34	3.20	2.9	3.0
$V_{\infty_{arr}}$ $[km/s]$	3.78	3.9	3.37	3.3
Total ΔV $[km/s]$	7.12	7.1	6.27	6.3
Sun phase angle [°]	86.48	84.8	110.1	104.1
Range to Earth $[AU]$	0.125	0.122	1.987	1.976
Approach angle [°]	150.6	151.3	141.7	141.4
Declination of the launch asymptote [°]	10.72	9.3	17.84	14.3

Table 8.1: Results obtained for the single and multi-revolution outbound transfer to asteroid Didymos, compared to the values retrieved from the *JPL*.

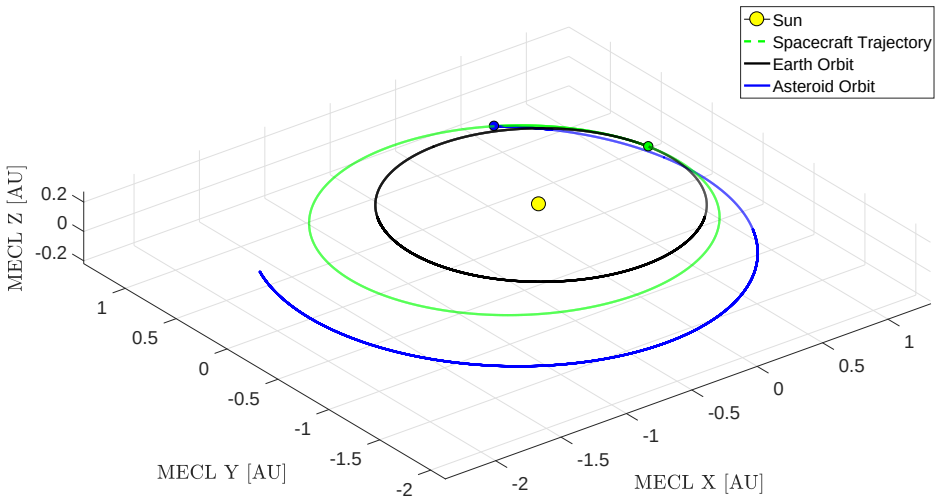

Figure 8.2: Three-dimensional plot of the outbound trajectory with one revolution for asteroid Didymos.

In Figure 8.2 the reader can appreciate that the trajectory is contained in a plane which has a similar inclination to that of the Earth. Indeed, this is an expected result since, as provided in Table 2.7, the inclination of the plane containing the asteroid orbit is only 3.41°. In addition, Figure 8.3 shows that it is a short-arc trajectory and that the revolution is performed with the objective of resembling a phasing maneuver.

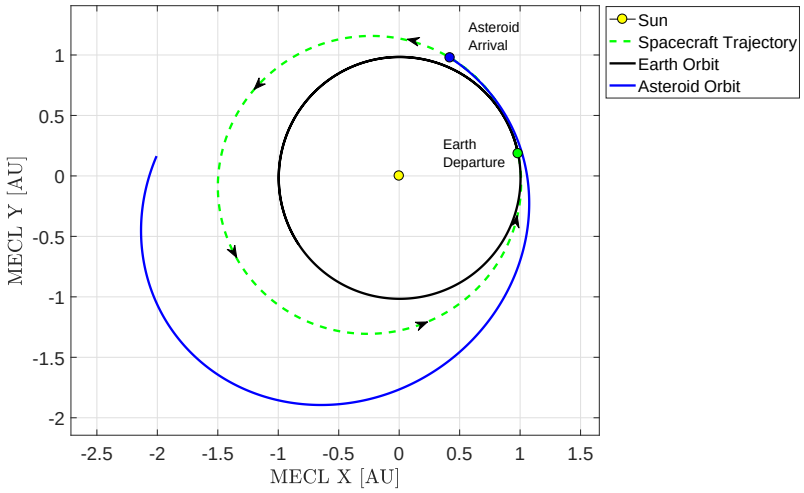

Figure 8.3: Projected view of the outbound transfer with one revolution for asteroid Didymos.

Once the outbound flight has been discussed, one can now analyze the results for the inbound trajectory. To that end, Figure 8.4 shows the opportunities for the departure from the asteroid. The mission with minimum ΔV is again highlighted with a red circle.

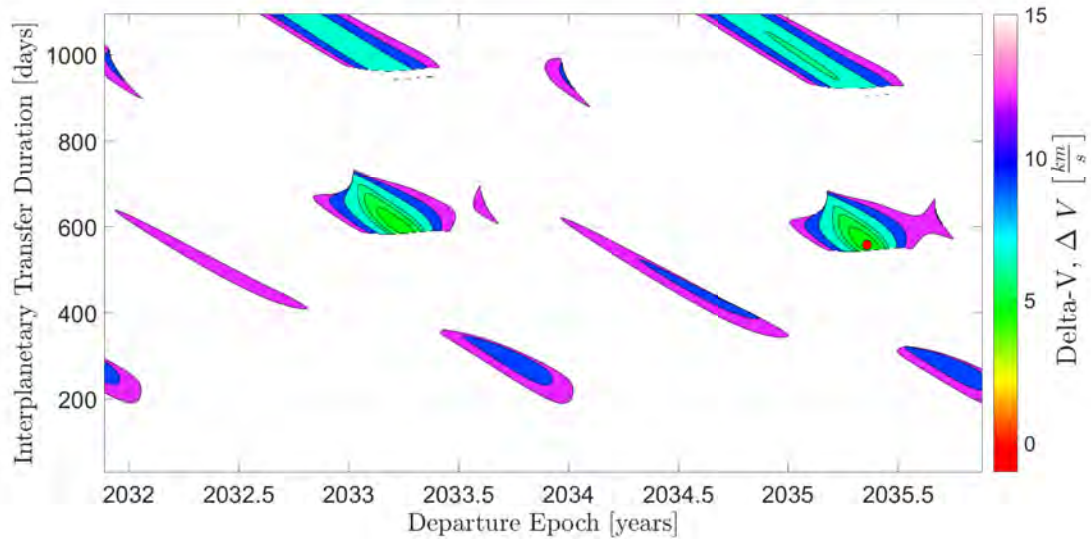

Figure 8.4: Pork chop diagram for the inbound flight of asteroid Didymos. Mission with minimum ΔV is shown with a red circle.

Launching opportunities for the inbound flight appear every two years due to the synodic period of the asteroid, while results below a transfer duration of approximately 350 days correspond to trajectories with 0 revolutions. As can be appreciated, the return flight with minimum ΔV is found in 2035. Nevertheless, this may not be the best trajectory to consider since in the vicinity of 2033 there is another region in which low ΔV trajectories with similar transfer times are found.

Taking into account that the optimum outbound flight would depart from Earth the 4th of October of 2029, that the TOF would be of 568 days, and that the observation, landing and minimum mining time would add 211 days (as explained in Section 5.3.4), the spacecraft would be ready for departure on the 22nd of November of 2031. As a result, it is possible that departing from the asteroid on 2033 is more efficient from an economical perspective than waiting until 2035. This trade-off possibility should indeed be analyzed in a future work.

Finally, Table 8.2 shows the results obtained for the inbound flight. No comparison has been provided since the *JPL Mission Design Tool* does not consider a complete round-trip, just the outbound flight. Similarly, Figures 8.5 and 8.6 on the next page show the 3D and projected trajectories for the inbound flight.

Variable	**MATLAB (1 rev)**
Launch Date	12 - May - 2035
TOF $[days]$	558
C3 $[km^2/s^2]$	7.67
$V_{\infty_{dep}}$ $[km/s]$	2.77
$V_{\infty_{arr}}$ $[km/s]$	3.55
Total ΔV $[km/s]$	6.32
Sun phase angle [°]	75.37
Approach angle [°]	42.39

Table 8.2: Table summarizing the results for the inbound trajectory for asteroid Didymos.

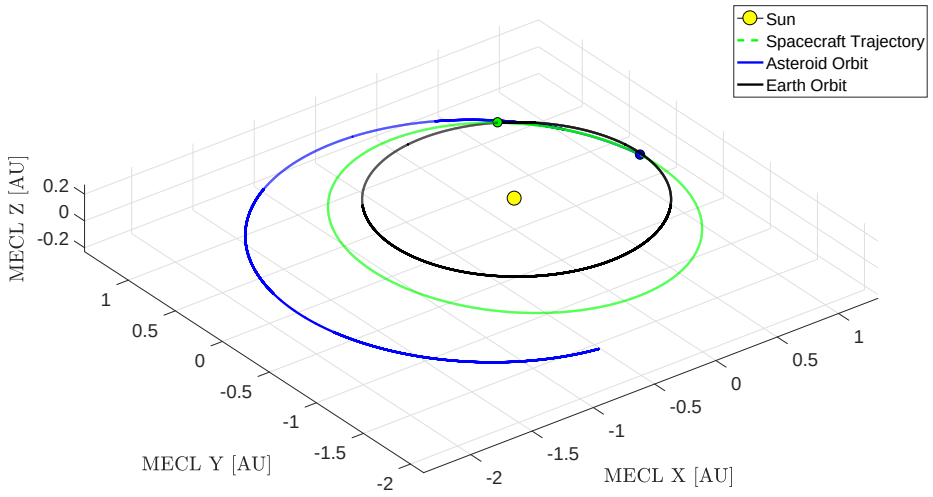

Figure 8.5: Three-dimensional view of the inbound trajectory for asteroid Didymos.

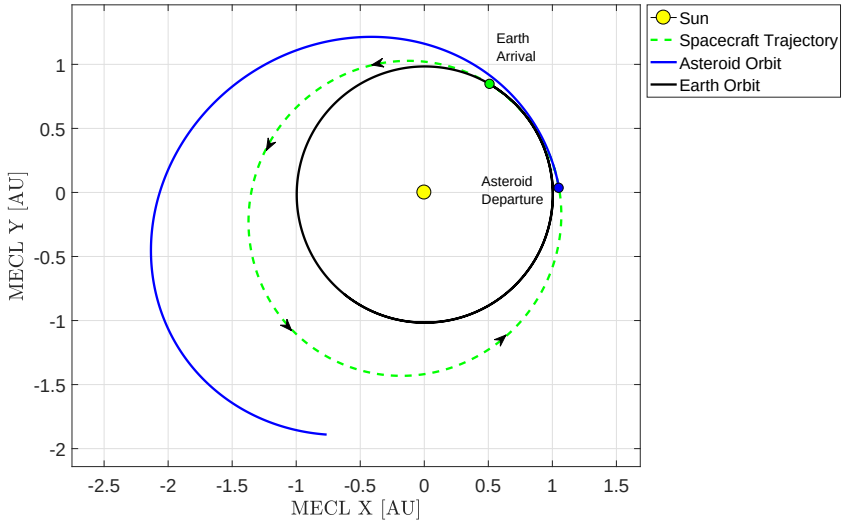

Figure 8.6: Inbound trajectory projected on the mean ecliptic plane for asteroid Didymos.

8.2 Pareto Plots

As has been shown in the previous section, optimizing missions considering only the criteria of minimum ΔV can lead to problems regarding the time efficiency of the mission. To overcome this, *NSGA-II* has been used not only to optimize the mission according to three objectives but also to consider more transfer possibilities apart from single and multi-

revolutions with chemical propulsion. This section will present the Pareto plots obtained for the missions to asteroid Didymos.

To begin with, Figure 8.7 compares the different mission possibilities with respect to spacecraft initial mass and to mission duration. The behavior appreciated is the one expected since there are missions involving multi-revolutions with chemical propulsion which lead to the smaller durations, while multi-revolutions with low-thrust require more time so as to adjust the sequence of thrust and coast arcs and achieve the necessary velocity changes. In addition, trajectories with gravity assist maneuvers are also longer, since they contain an extra leg compared to the multi-revolution transfers.

Furthermore, two sets of solutions are found for multi-revolutions with chemical propulsion which are separated by 2 years, being this related once again to the synodic period. With respect to the time difference between the two sets of low-thrust missions, this is caused by the fact that one of them considers one more revolution than the other in one of the flights.

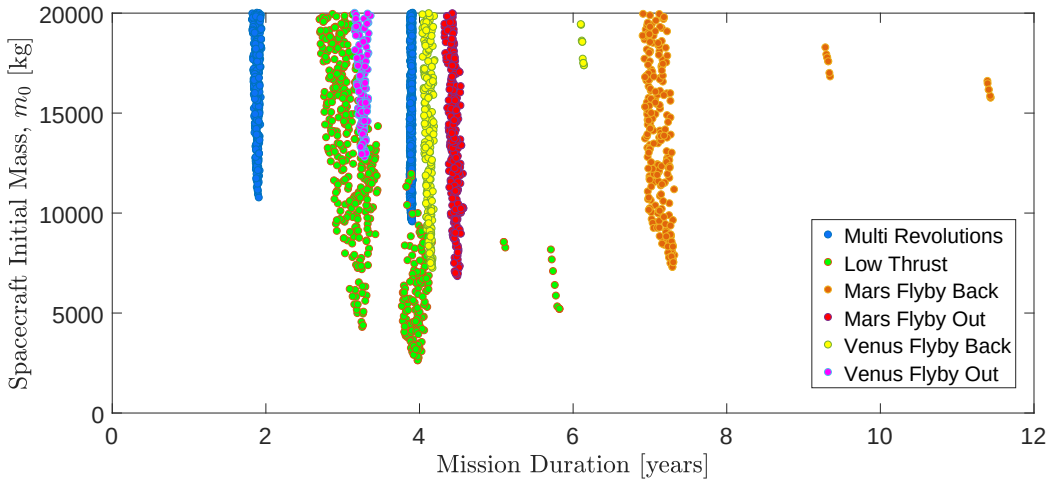

Figure 8.7: Pareto plot showing mission duration versus initial mass obtained for asteroid Didymos. All the types of missions considered are plotted.

From Figure 8.7 one can discard missions involving a flyby maneuver around Mars in the comeback flight, as the duration is too long compared to other possibilities. After that, one can search for the missions with lowest initial mass, as one of the biggest limitations to mission feasibility is ensuring that the spacecraft can escape Earth with the launcher. With this criteria the mission possibilities are reduced to either performing a low-thrust multi-revolution transfer, a chemical mission with a flyby in Mars in the outbound flight or

a flyby in Venus in the inbound flight, although multi-revolutions with chemical propellant could also be considered in case smaller times were essential (compared to the Mars flyby there is a reduction of approximately 180 days). Determining which to carry out would then depend on other factors such as the amount of mined material or the feasibility of the low-thrust mission.

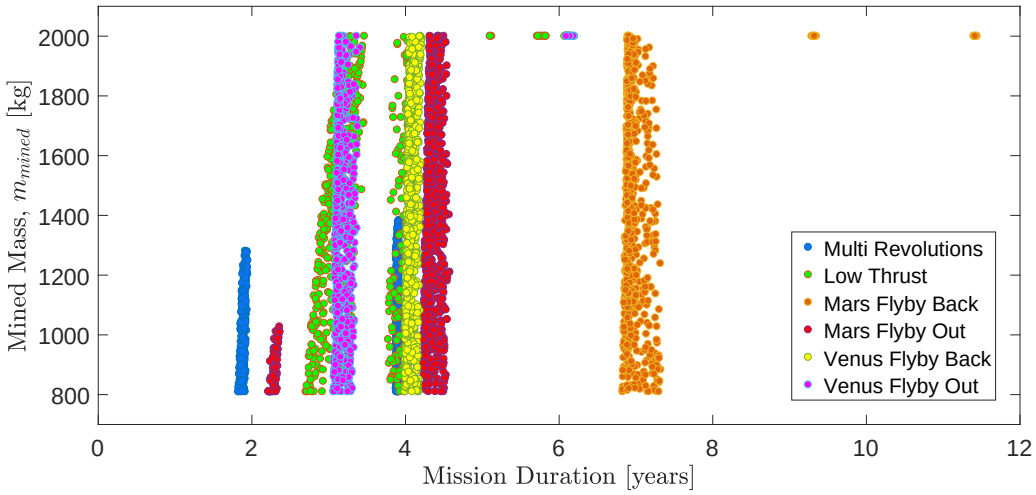

Figure 8.8: Graph showing the evolution of mined mass with mission duration for all types of trajectories.

Hence, Figure 8.8 can then be used to continue with the study. As can be seen, the missions involving multi-revolutions with chemical propulsion should be discarded if it is desired to maximize mined mass, since the set of solutions in the vicinity of a 4 year duration can only achieve up to 1400 kg of material, in contrast with low-thrust missions and the Mars and Venus flyby's mentioned previously, which can retrieve up to 2000 kg.

Finally, with Figure 8.9 one can finally find which is, a priori, the best type of mission to analyze in detail. As can be appreciated, low-thrust missions are able to achieve greater mined masses with smaller m_0 compared to the chemical propulsion trajectories that involve the Mars flyby in the outbound flight and to the missions in which a Venus gravity assist is considered in the comeback flight, being the Mars flyby better than the one in Venus from the point of view of achieving minimum m_0 for the same value of m_{mined}.

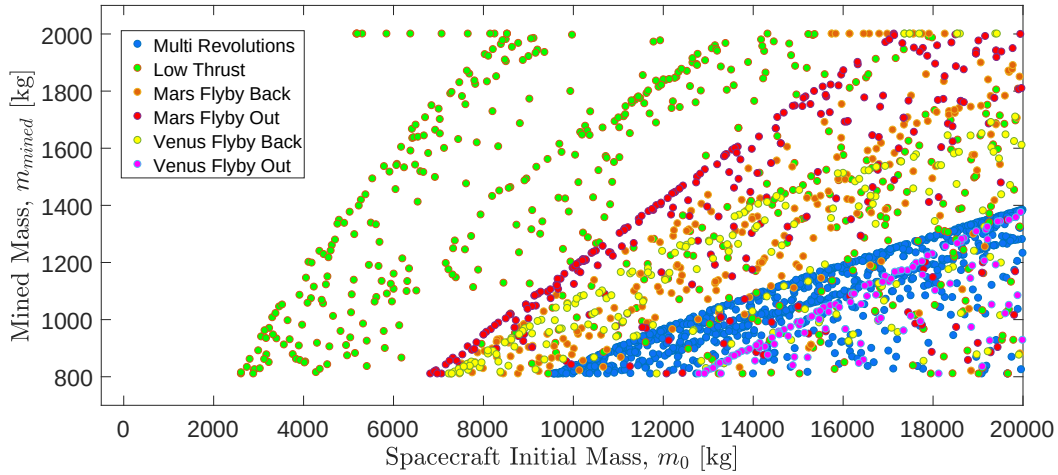

Figure 8.9: Results for mass of mined material as a function of the spacecraft initial mass for all possibilities.

8.3 Optimized Mission with Chemical Propulsion

From the analysis of the pareto plots one can infer which appear to be the best type of trajectories for the asteroid mining missions. In the case of Didymos, it has been reasoned that, for chemical propulsion systems, one with a Mars gravity assist maneuver in the outbound flight presents the best compromise between the three objectives analyzed. However, as explained when talking about genetic algorithms, the user must select which of the objectives is dominant for his interests. Due to the launcher limitations, the initial spacecraft mass, m_0, has been defined as the most important. Hence, this section now provides the information regarding the Mars gravity assist trajectory involving minimum initial mass.

The three-dimensional view of the mentioned transfer can be appreciated in Figure 8.10, while the corresponding projected two-dimensional view is provided in Figure 8.11. As can be seen, the outbound flight is composed of two legs, Earth-Mars and Mars-Asteroid, having the former one revolution and the latter zero. In addition, it can be appreciated that the gravity assist maneuver is a leading-side flyby. The results for the outbound flight are summarized in Table 8.3. Please notice that the second leg of the transfer describes an orbit very similar to that of the asteroid and that hence it is not so visible in the trajectory plot.

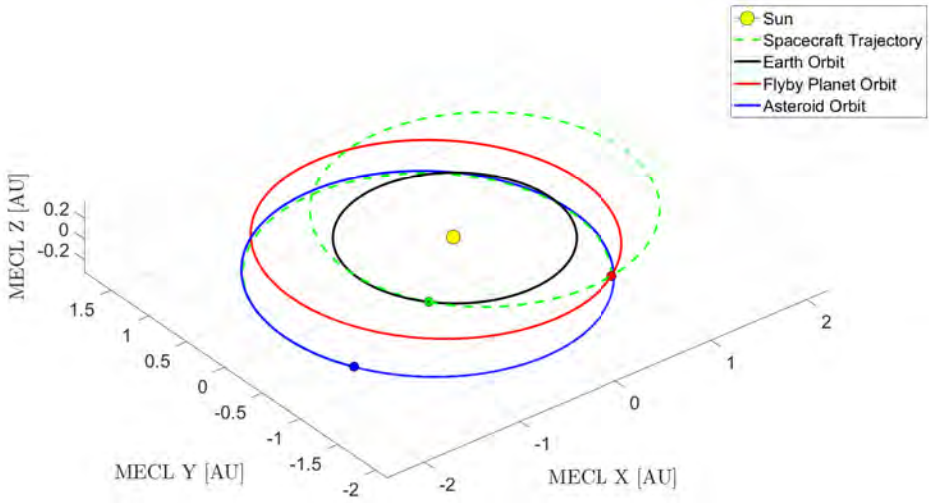

Figure 8.10: Outbound flight trajectory for asteroid Didymos with minumum m_0, showing the gravity assist maneuver in Mars.

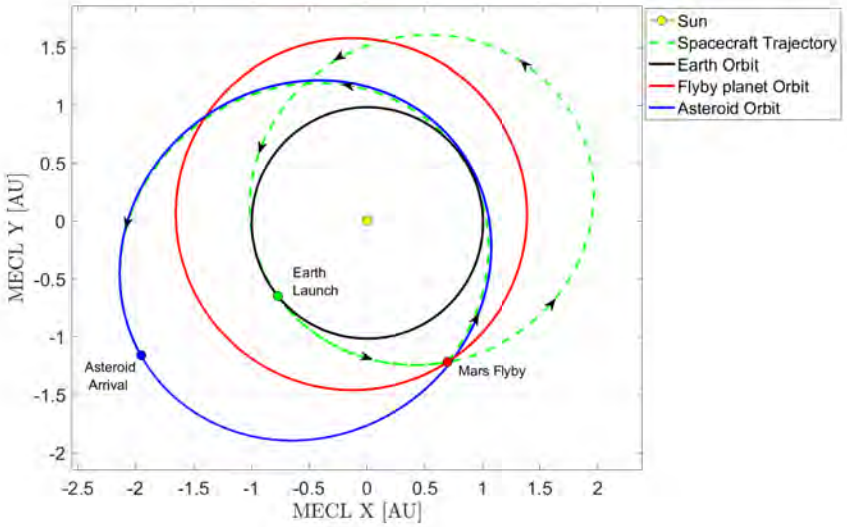

Figure 8.11: Trajectory projected onto the mean ecliptic frame showing the outbound flight corresponding to the chemical propulsion mission with minimum m_0.

Variable	Result
Earth Launch	30 - Apr - 2018
Mars Flyby	06 - Jun - 2020
Asteroid Arrival	23 - Sep - 2021
Asteroid Landing	22 - Jan - 2022
$V_{\infty_{dep}}$ $[km/s]$	5.26
TOF 1st leg $[days]$	768
nº of revs 1st leg	1
TOF 2nd leg $[days]$	474
nº of revs 2nd leg	0
$V_{\infty_{arr}}$ $[km/s]$	0.24
Sun phase angle [°]	84.72
Range to Earth at asteroid arrival $[AU]$	3.18
Approach angle [°]	124.4
Declination of the launch asymptote [°]	-34.43

Table 8.3: Results obtained for the outbound flight to asteroid Didymos. Data provided includes both legs of the trajectory.

With respect to the gravity assist maneuver, the characteristic values are presented in Table 8.4 below. As can be seen both in the trajectory plots provided above and in the value of the turn angle δ below, the gravity assist maneuver is a leading-side flyby.

Variable	Flyby altitude $[km]$	B-plane angle ζ [°]	Turn angle δ [°]
Value	250	54.29	11.8

Table 8.4: Summary of the results for the variables involved in the Mars flyby.

Once the outbound flight has been discussed results for the inbound trajectory can be presented. In this case, this flight is direct and does not involve any revolutions, as can be seen in Figures 8.12 and 8.13. In addition, it is a transfer which almost follows the asteroid orbit and in which the spacecraft has to raise in order to counteract the approximately 3 ° inclination of the asteroid's orbital plane, with the rendez-vous occurring when the Earth comes closest to the asteroid orbit.

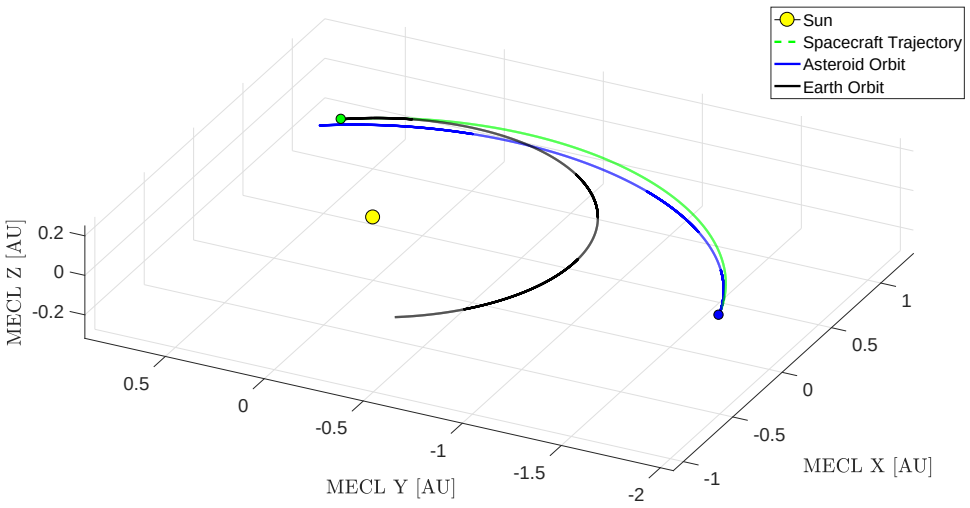

Figure 8.12: Three-dimensional view of the inbound trajectory belonging to the Mars flyby mission to Didymos.

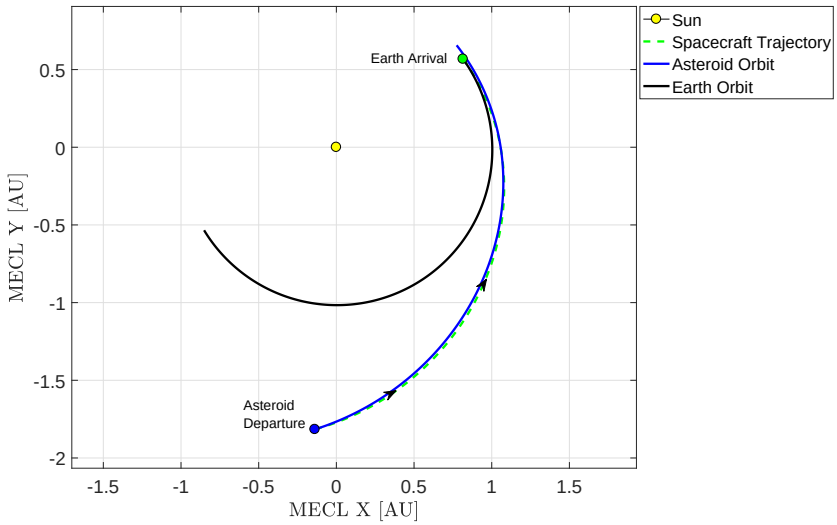

Figure 8.13: Projected view of the asteroid - Earth transfer.

A summary of the variables that characterize the inbound flight is provided in Table 8.5. Finally, Table 8.6 also shows the information regarding spacecraft initial mass, mined mass and mission duration associated to the asteroid mining mission analyzed in this section.

Variable	Value
Asteroid Departure	22 - Apr - 2022
Earth Arrival	28 - Oct - 2022
$V_{\infty_{dep}}$ $[km/s]$	1.32
$V_{\infty_{arr}}$ $[km/s]$	4.99
TOF $[days]$	189
nº of revs	0
Sun phase angle [°]	92.83
Approach angle [°]	6.95

Table 8.5: Summary of the parameters that define the inbound flight for the mission with minimum m_0 for asteroid Didymos.

Spacecraft Initial Mass $[kg]$	**Mined Mass** $[kg]$	**Total Mission Duration** $[days]$
6826	810	1642

Table 8.6: Mass and time information for the mission analyzed.

Having explained and completely defined the trajectories involved in the mission, the last thing to analyze is whether such mission could be launched from Earth, since this was the main limitation usually encountered during the optimization process. To that end, one must recall the values of the spacecraft initial mass $m_0 = 6826\ kg$ and of the infinity departure velocity, $V_{\infty_{dep}} = 5.26\ km/s$. Then, using Table 4.1 and Figure 4.2, where the launcher capacities are found, shows that the mission discussed in this section is completely feasible and that, in fact, there are several launchers capable of performing the Earth departure, such as the SLS's Block 1B and 2 as well as the Falcon Heavy. The Delta IV rocket could possibly perform the launch also, but it would be close to its maximum performance capability and hence further detailed analysis is required in order to ensure the feasibility.

8.4 Optimized Mission with Low-Thrust

The analysis of the mission opportunities that exist to perform asteroid mining operations in Didymos is completed by providing the optimized transfer for the case of low-thrust propulsion. Following the criteria already used, the mission with minimum initial spacecraft mass will be the one selected.

The reader can appreciate in Figure 8.14 a zero revolutions trajectory corresponding to the outbound flight. As it was explained in the previous chapters, low-thrust missions are

considered to be two-dimensional and hence plots are given as projections on the ecliptic plane. In addition, the reader will be able to distinguish the thrust arc and the coast arc that define this trajectory. Nevertheless, please recall that this mission is based on the assumption that a chemical propulsion system performs the rendez-vous maneuver with the asteroid, and that, as a result, the final thrust arc that was shown in Figure 4.7 does not appear in this case.

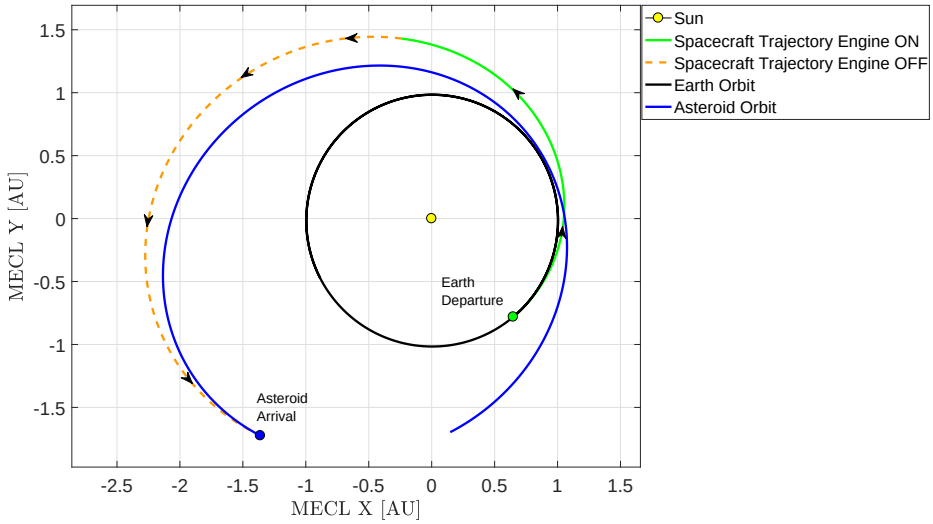

Figure 8.14: Outbound trajectory plot for the low-thrust mission to asteroid Didymos.

Table 8.7 on the next page presents the results for the characteristic parameters of the outbound flight. $V_{\infty_{arr}}$ is the infinity arrival velocity that has to be counteracted by the chemical propulsion system in order for the rendez-vous to occur. No value for $V_{\infty_{dep}}$ is given since it was assumed that the initial impulse was provided by the launcher. Similarly, the value of ΔV represents the velocity change which is obtained during the cruise phase due to the ion thruster. As expected, a large time of flight is obtained for a trajectory which does not have any revolutions due to the small amounts of thrust that the NEXT-C engine is capable of providing and which forces the mission to employ longer transfer times.

Variable	Value
Earth Launch	02 - Aug - 2026
Asteroid Arrival	18 - Apr - 2028
Asteroid Landing	17 - Aug - 2028
$V_{\infty_{arr}}$ $[km/s]$	1.16
ΔV_{ion} $[km/s]$	4.55
TOF $[days]$	624
Number of revolutions	0
Range to Earth at asteroid arrival $[AU]$	1.34

Table 8.7: Parameters characterizing the outbound flight for the low-thrust mission.

Similarly, the trajectory describing the asteroid - Earth flight is presented in Figure 8.15. As can be appreciated, this transfer involves performing one revolution, being this the reason for the orange dashed line representing the coast arc to look continuous. The parameters defining this trajectory are found in Table 8.8. It is important to remark that for both flights the infinity arrival velocities are acceptable, as the values are small and the chemical propulsion system would be able to perform the rendez-vous maneuvers.

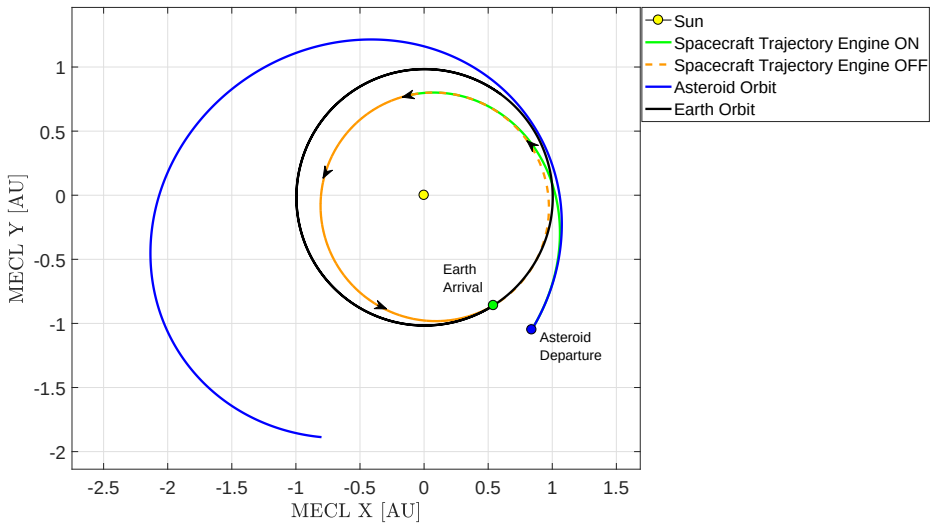

Figure 8.15: Inbound transfer plot for the low-thrust mission to asteroid Didymos.

Variable	Value
Asteroid Departure	15 - Nov - 2028
Earth Arrival	25 - Jul - 2030
$V_{\infty_{arr}}$ $[km/s]$	2.07
ΔV_{ion} $[km/s]$	7.30
TOF $[days]$	618
Number of revolutions	1

Table 8.8: Data characterizing the comeback flight.

Results are completed by stating that the spacecraft initial mass required for this mission is $m_0 = 2615\ kg$, while the amount of mined material is $m_{mined} = 810\ kg$ and the mission lasts 1453 days. As expected, the spacecraft initial mass has experienced a considerable reduction compared to that required for the chemical propulsion mission of Section 8.3, being this caused by the reduced amount of propellant that the spacecraft has to carry. In addition, the small value of m_0 ensures that all the launchers considered in Table 4.1 and Figure 4.2 are capable of performing the Earth departure.

Finally, one must verify that the NEXT-C engine is capable of fulfilling the velocity changes required for this mission to take place. To that end, the procedure described in Section 4.7.2.3 is followed. Information regarding required ΔV and the capacity of the engine are provided in Table 8.9. As can be seen, the mission is unfeasible with just one engine. However, if two NEXT-C engines were used then it could be possible, although further studies would have to be conducted to determine this point.

$\Delta V_{req_{out}}$ $[km/s]$	$\Delta V_{NEXT_{out}}$ $[km/s]$	$\Delta V_{req_{back}}$ $[km/s]$	$\Delta V_{NEXT_{back}}$ $[km/s]$
5.71	3.31	9.37	5.98

Table 8.9: ΔV required in both flights and actual output of one NEXT-C engine.

Comparing the results with those found in Table 8.6 shows that the low-thrust mission described in this section would be the best option possible to mine asteroid Didymos if studies proved that using two NEXT-C engines would be sufficient to ensure the feasibility of the mission, since the same amount of material is obtained with smaller spacecraft mass and mission duration. Nevertheless, in case this option is not possible, it has been shown that there is still a chemical propulsion mission with a Mars flyby which could be performed.

CHAPTER 9

ANALYSIS OF THE SOCIO-ECONOMIC IMPACT

As in any economic venture, profitability is a key factor for private investors to enter into the market. As was explained in Chapter 1, there are several reasons that raise interest in asteroid mining, since profit could come from selling metals on Earth or from building structures and refueling spacecraft in space. Nevertheless, the number of private companies that have entered such activity is very reduced and this has had as a main cause the fact that there are still many questions with unknown answers regarding asteroid mining.

This chapter will now begin by presenting a study regarding the profitability of the two asteroid mining missions studied in detail in Chapters 7 and 8. Then, focus will be placed on explaining the main social and environmental impacts that a burst on asteroid mining operations could provoke.

9.1 Economic Evaluation of Asteroid Mining Missions

Performing the analysis of the economic viability of any project in general, and of an asteroid mining mission in particular, can be reduced to computing the so-called Net Present Value, NPV. Such indicator will be given by the following expression

$$NPV = R \cdot (1+i)^{-n} - C \tag{9.1}$$

where R is the income cash flow received at a certain future time, i is the discount rate, n is the number of years that will pass until the expected income flow is received and C is the initial capital which has to be invested for the project to take place.

Looking at Equation 9.1 clearly shows that the NPV of an asteroid mining missions is going to depend on three main aspects: the cost of the mission (including development and launch), the amount of mined material retrieved and the value at which it can be sold and finally the time that it takes for the mission to be completed.

With respect to the cost, determining the amount of money required to launch the mission can be calculated easily, since the initial spacecraft mass m_0 is known and the price per kg can be assumed to be of 5000 $\$/kg$ [42]. More complicated is to estimate the amount of money that would be necessary to develop the spacecraft and the systems and equipment required for asteroid mining. As a result, the estimated cost of the *Hayabusa-II* mission has been used as an approximated value for C, which will then be equal to 150 million dollars [77].

The time used in the NPV equation is also known and corresponds to the mission duration. With respect to the income received from selling the products, it can be computed by using the value of the mined mass and considering that the market price is of 50,000 $\$/kg$ [42]. Finally, the discount rate has been assumed to be of 3% per year [78]. With all of these values, the NPV analysis for Ryugu and Didymos can be performed by re-expressing Equation 9.1 as follows:

$$NPV = 50{,}000 \cdot m_{mined}(1+0.03)^{\frac{-duration}{365.25}} - (5000 \cdot m_0 + 150{,}000{,}000) \tag{9.2}$$

9.1.1 NPV Analysis for Ryugu

with the values presented in the previous section one can now compute the NPV for the trajectories presented in Chapter 7 using Equation 9.2. Table 9.1 below summarizes the variables and the NPV result obtained for the chemical and low-thrust missions to asteroid Ryugu.

	Initial Mass $[kg]$	**Mined Mass** $[kg]$	**Duration** $[days]$	**NPV** [$]
Chemical	5452	810	1465	-141,287,921
Low-Thrust	1222	810	2399	-122,756,701

Table 9.1: Summary of the variables and NPV for the asteroid mining missions to Ryugu.

As can be seen, both trajectories lead to negative NPV results, therefore meaning that the economic venture is not profitable. As expected, the NPV for the low-thrust mission is more favorable due to the fact that the costs associated to launching are smaller, since m_0 is greatly reduced by using an ion-engine.

Nevertheless, despite the unpromising results obtained, one can find out that, in fact, performing profitable asteroid mining missions is simply a matter of being able to extract more material. To that end, the value of mined mass that is required to make the current trajectories profitable can be obtained by setting Equation 9.2 equal to zero and solving for m_{mined}. This yields that the chemical propulsion mission would be profitable if m_{mined} was greater than 3991 kg, while the low-thrust mission would achieve a positive return if m_{mined} was greater than 3791 kg.

Being able to mine those quantities in the same time as the missions presented in Chapter 7 (so as to not change the epochs, TOF's etc of the trajectories) implies having an extraction and processing rate bigger than 9 kg/day, something which can be perfectly possible since the mentioned extraction rate was arbitrarily assumed due to the lack of information about the aspect.

It is true that mining more material would also lead to increasing the value of m_0 and hence the launch costs, which would then in turn imply having to mine more mass for the mission to be profitable. Nevertheless, the factor multiplying m_{mined} is much grater than the factor multiplying m_0 in Equation 9.2 and, as a result, the increase in launching costs could be rapidly compensated with some more kilograms of mined material.

9.1.2 NPV Analysis for Didymos

The procedure described in the previous section can be also applied for asteroid Didymos. Doing so yields the following results, shown in Table 9.2.

	Initial Mass	**Mined Mass**	**Duration**	**NPV**
Chemical	6826	810	1642	-148,669,518
Low-Thrust	2615	810	1453	-127,068,970

Table 9.2: Summary of the objective variables and NPV for the asteroid mining missions in Didymos.

Once again, although the missions have a negative NPV, profitability could be achieved if 4205 kg were mined for the chemical propulsion mission and 3668 kg were mined for the mission with low-thrust. The same discussion as the one carried out for Ryugu applies to this asteroid.

9.2 Social and Environmental Impact of Asteroid Mining

If asteroid mining became a consolidated industry, big changes would be caused not only in the way humanity explores space but also in the economic and labor markets. For instance, the terrestrial mining industry would have to completely adapt to the appearance of new actors which could pose a threat to its existence.

In addition, the labor market could also be transformed with the expectable boost in the demand for engineers and technicians that would be required to design, test, manufacture and operate the different systems employed in an asteroid mining mission. Furthermore, the creation of this high-tech and well remunerated jobs would strengthen the economy of those countries which take the lead on asteroid mining.

With respect to the legal aspects, the birth of these sector would probably force governments to pass laws regulating this activity, and also new taxes could be created. In any case, since space is a supranational domain, legislation from an organism such as the United Nations would probably be required. Furthermore, congestion in space could become a problem and a new legislation or control center could be required to manage all the spacecraft and flight operations being performed.

Finally, it is expectable that the number of launches would considerably increase. Depending on the frequency, current space ports could not be able to absorb the demand for new launches and this could lead to the creation of new ones, with the corresponding environmental impact on the region where the construction takes place. Furthermore, legislation on the waste products produced by asteroid mining operations should also be developed so as to ensure that asteroids, and space in general, do not become dump sites.

CHAPTER 10

CONCLUSION

10.1 Summary and Results Overview

Near-Earth asteroids, commonly known as NEA's, are small celestial bodies which are characterized by having orbits close to Earth. This feature, together with the results of telescopic reflectance spectroscopy, has lead to nowadays seeing asteroids as promising targets for mining operations.

As a result, and under the scope of the European Space Agency, this thesis has aimed at performing a preliminary design of the optimal trajectories that spacecraft could follow in order to carry out mining missions in ten selected asteroids. To that end, both chemical and low-thrust propulsion methods have been considered.

To perform this study, impulsive trajectories were first designed with the objective of minimizing the change in velocity required to carry out the mission, since achieving the smallest ΔV implied optimizing propellant consumption. Such task was performed by means of a MATLAB code that used the SPICE Toolkit and Vallado's Lambert solver based on universal variables.

The aforementioned approach yielded the so-called pork-chop plots characterizing the transfer possibilities as well as the values for the trajectories optimized according to the mentioned criteria. Whenever possible, results were compared and validated with those

available in the *JPL Mission Design Tool*.

The asteroid mining missions obtained according to the procedure described in the previous paragraphs presented one main drawback: time was not being considered for establishing the optimum mission, and this was therefore creating big intervals between the outbound and inbound flights in which the spacecraft would just wait on the asteroid surface. Indeed, from the point of view of the profitability of the mission, time and mass of mined material should be two factors to take into account.

As a result, the asteroid mining missions had to undergo a multi-objective optimization process in which the aim was be placed on minimizing launch mass and mission duration while maximizing the amount of mined material. In order to implement this, a multi-objective optimization tool had to be used and, in particular, focus was placed on employing a genetic algorithm.

To that end, the Non-dominated Sorting Genetic Algorithm II, *NSGA-II*, was selected for performing the mentioned optimization process. Doing so not only enabled the author to consider three objectives but also provided the possibility of introducing new types of trajectories into the equation. In particular, with the use of *NSGA-II*, multi-revolution transfers and gravity assist maneuvers in Mars and Venus could be analyzed for the cases of chemical propulsion systems, while multi-revolution trajectories were also studied for low-thrust propulsion. Furthermore, since trajectory design for low-thrust missions is performed by means of a shape-based method, a criteria was developed in order to verify if the ion engine would be able to satisfy the thrust profile required.

Results for asteroids Ryugu and Didymos were subjects of a complete analysis, which included not only the determination of the optimal trajectories but also an economic study based on the Net Present Vale, *NPV*, while the optimum trajectories involving chemical and low-thrust propulsion for the rest of asteroids where provided in Annex A.

From the obtained results, several conclusions could be drawn. On the one hand, all asteroids have feasible missions involving chemical propulsion, while on the other hand, in the case of low-thrust there are some asteroids that require two NEXT-C engines and others for which the trajectories are inviable. In particular, access to asteroids 1992 TC, 2001 SG10 and 2002 DO3 appears to be the most complicated, since the low-thrust missions have to be discarded and chemical propulsion missions involve big masses at Earth departure.

Secondly, it was also proven that, for those missions in which it was viable, low-thrust propulsion presents the best option. This is due to the fact that it implies lower spacecraft initial masses (and hence smaller launching costs) while maintaining the amounts of mined material and presenting competitive mission durations.

Thirdly, results also show that performing gravity assist maneuvers in Mars is better than in Venus, where none of the optimal trajectories carried out the flyby. This result is logical and is related with the fact that all of the asteroids being considered in this thesis fall into the categories of *Amor's* or *Apollo's* types of asteroids, being therefore Mars the planet which is closest to their orbits.

Finally, the economic analysis based on *NPV* showed that the trajectories obtained did not present profitable missions. However, it was proven that in order for the missions to generate profits, the amount of mined material only had to increase up to values which are feasible of being obtained.

10.2 Future Work

This thesis performs a preliminary study of the trajectories that can be considered for asteroid mining. The results obtained open a wide variety of options and improvements which can be studied in the future. Examples of these research topics are:

- Having discarded Venus as a candidate for a gravity assist maneuver, future works could analyze the possibility of performing the flyby using Earth.
- This work only considers a maximum of one gravity assist maneuver per mission. As a result, projects could study the possibility of performing more flybys, including also resonant ones.
- This thesis assumes that the spacecraft is directly placed in orbit by means of the launchers. Future works could analyze the possibility of decomposing the departure from Earth into two phases: launching into LEO and then performing the hyperbolic escape.
- In this project it is considered that the spacecraft cannot refuel in the asteroid. Further studies could take this possibility into account, as it would have a great impact on the whole mission.

- Furthermore, future projects could also introduce gravity assist maneuvers into the optimization analysis of low-thrust missions.

Part IV

APPENDICES

APPENDIX A

RESULTS FOR THE REST OF ASTEROIDS

This annex contains the pork-chop plots, trajectory diagrams and tables for the other eight asteroids considered in this thesis, being the results provided following the same structure as the one found in chapters 7 and 8. No discussion for the obtained values is presented, but in any case the reader can use the approach already followed to derive the associated conclusions to each body.

In addition, for the sake of simplicity, only the trajectories projected onto the ecliptic plane for the transfers obtained via the genetic algorithm are presented. Low-thrust missions are only provided in those cases in which the ΔV criteria shows that, with a maximum of two NEXT-C engines, the mission could be feasible. As a result, no low-thrust values are given for asteroids Nereus, 1992 TC, 2001 SG10 and 2002 DO3.

A.1 Asteroid 1989 ML : ID - 2010302

A.1.1 Pork-Chop plots

Outbound Flight

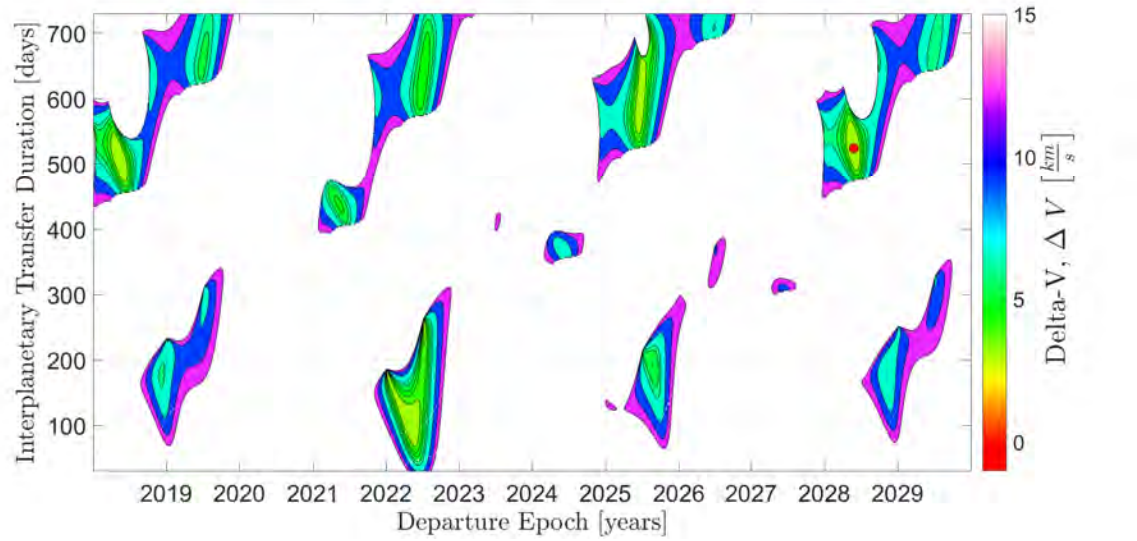

Figure A.1: Pork-chop plot for the outbound flight to asteroid 1989 ML.

Variable	MATLAB	JPL
Launch Date	25 - May - 2028	30 - May - 2028
TOF $[days]$	524	520
C3 $[km^2/s^2]$	5.34	5.70
$V_{\infty_{dep}}$ $[km/s]$	2.31	2.4
$V_{\infty_{arr}}$ $[km/s]$	2.23	2.2
Total ΔV $[km/s]$	4.54	4.6
Sun phase angle [°]	77.95	76.8
Range to Earth $[AU]$	1.234	1.234
Approach angle [°]	138.42	139.9
Declination of the launch asymptote [°]	-58.05	-58.2

Table A.1: Results obtained for the outbound transfer with minimum ΔV to asteroid 1989 ML, compared to the values retrieved from the *JPL*.

Inbound Flight

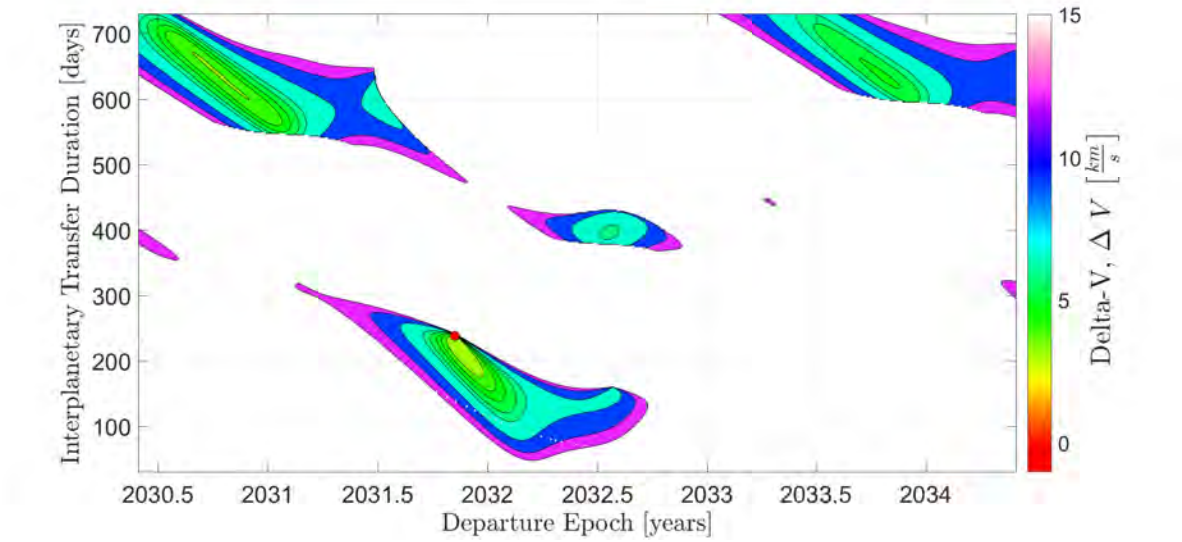

Figure A.2: Pork-chop plot for the inbound trajectory 1989 ML - Earth.

Variable	Result
Launch Date	08 - Nov - 2031
TOF $[days]$	238
C3 $[km^2/s^2]$	2.69
$V_{\infty_{dep}}$ $[km/s]$	1.64
$V_{\infty_{arr}}$ $[km/s]$	2.81
Total ΔV $[km/s]$	4.45
Sun phase angle [°]	83.23
Approach angle [°]	14.41

Table A.2: Table summarizing the results for the inbound trajectory for 1989 ML.

A.1.2 Optimized mission for chemical propulsion

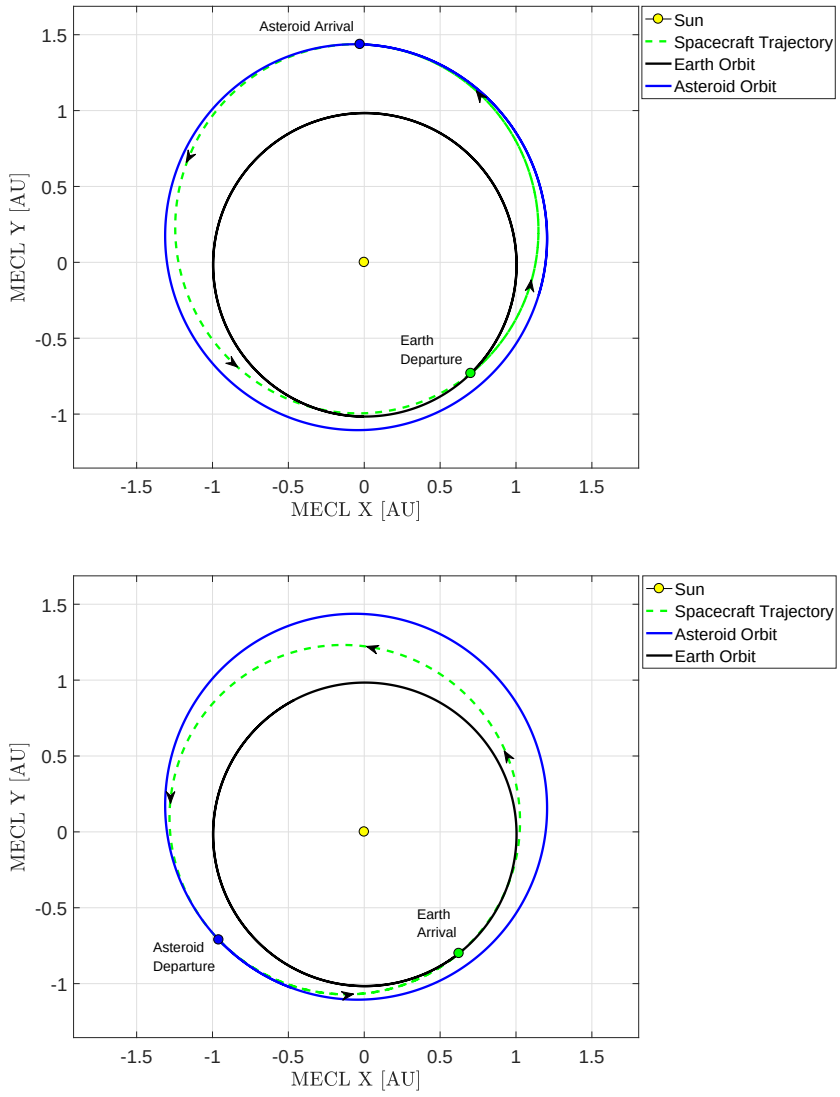

Figure A.3: Outbound (up) and inbound (down) 2D trajectories for the multi-revolution mission that yields minimum m_0 for asteroid 1989 ML.

Spacecraft Initial Mass $[kg]$	**Mined Mass** $[kg]$	**Total Mission Duration** $[days]$
5356	810	1455

Table A.3: Mass and time information for the optimum chemical propulsion mission to asteroid 1989 ML.

Variable	Result
Earth Launch	06 - Aug - 2025
Asteroid Arrival	21 - Jun - 2027
Asteroid Landing	20 - Oct - 2027
TOF [$days$]	684
nº of revolutions	1
$V_{\infty_{dep}}$ [km/s]	3.91
$V_{\infty_{arr}}$ [km/s]	1.45
Sun phase angle [°]	91.98
Range to Earth [AU]	2.45
Approach angle [°]	120.3
Declination of the launch asymptote [°]	-13.35

Table A.4: Results for the outbound flight of the optimum chemical mission to 1989 ML.

Variable	Value
Asteroid Departure	18 - Jan - 2028
Earth Arrival	31 - Jul - 2029
$V_{\infty_{dep}}$ [km/s]	1.50
$V_{\infty_{arr}}$ [km/s]	3.11
TOF [$days$]	559
nº of revolutions	1
Sun phase angle [°]	109.73
Approach angle [°]	51.83

Table A.5: Results obtained for the flight 1989 ML - Earth.

A.1.3 Optimized result for electric-propulsion

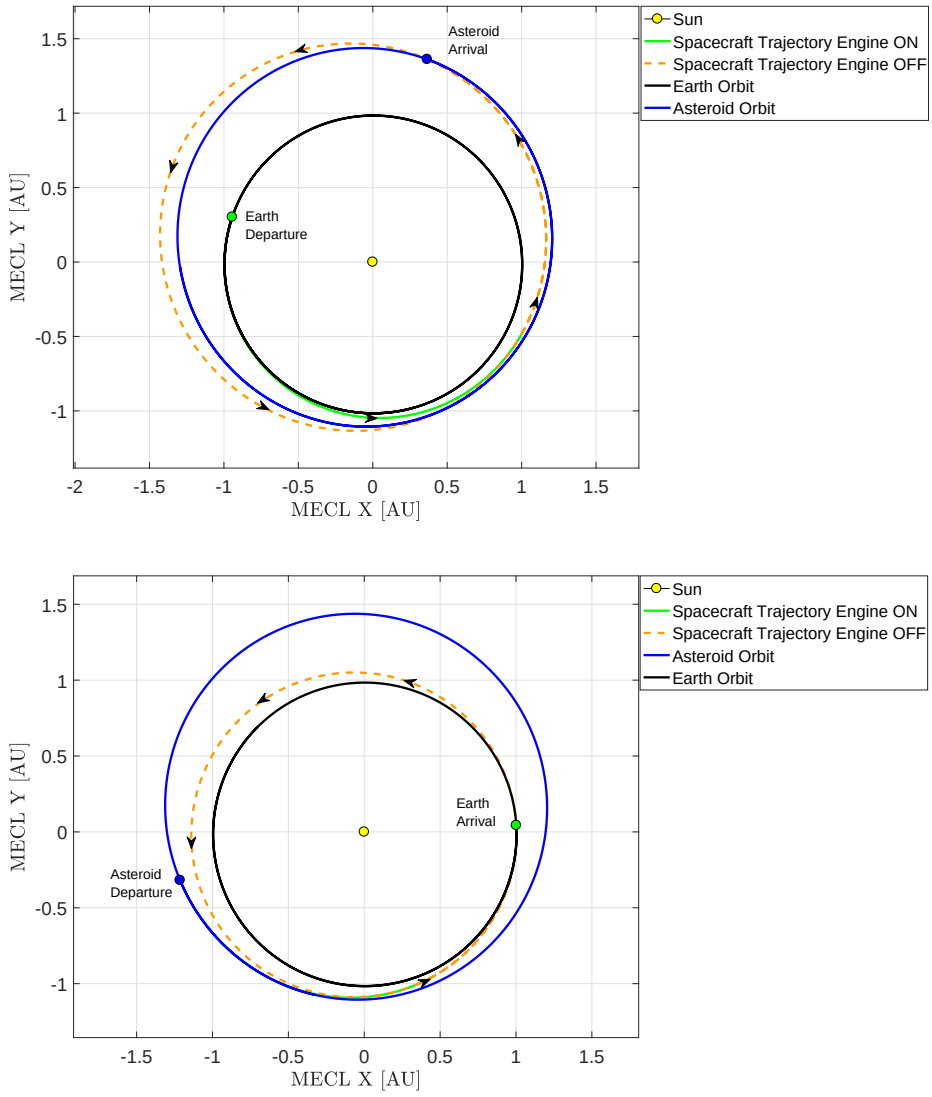

Figure A.4: Outbound (up) and inbound (down) trajectories for the low-thrust mission with minimum m_0 to 1989 ML.

Spacecraft Initial Mass $[kg]$	**Mined Mass** $[kg]$	**Total Mission Duration** $[days]$
1567	810	1668

Table A.6: Mass and time information for the optimum low-thrust mission to 1989 ML.

Variable	Value
Earth Launch	03 - Mar - 2022
Asteroid Arrival	08 - Jul - 2024
Asteroid Landing	06 - Nov - 2024
$V_{\infty_{arr}}$ $[km/s]$	1.43
ΔV_{ion} $[km/s]$	10.83
TOF $[days]$	858
Number of revolutions	1
Range to Earth at asteroid arrival $[AU]$	2.34

Table A.7: Outbound flight parameters for the low-thrust mission to 1989 ML.

Variable	Value
Asteroid Departure	04 - Feb - 2025
Earth Arrival	25 - Sep - 2026
$V_{\infty_{arr}}$ $[km/s]$	1
ΔV_{ion} $[km/s]$	2.79
TOF $[days]$	599
Number of revolutions	1

Table A.8: Data characterizing the low-thrust inbound flight for 1989 ML.

$\Delta V_{req_{out}}$ $[km/s]$	$\Delta V_{NEXT_{out}}$ $[km/s]$	$\Delta V_{req_{back}}$ $[km/s]$	$\Delta V_{NEXT_{back}}$ $[km/s]$
12.27	11.61	3.79	7.69

Table A.9: ΔV required in both flights and actual output of one NEXT-C engine. Mission could be viable with 2 engines.

A.2 Asteroid NEREUS : ID - 2004660

A.2.1 Pork-Chop plots

Outbound Flight

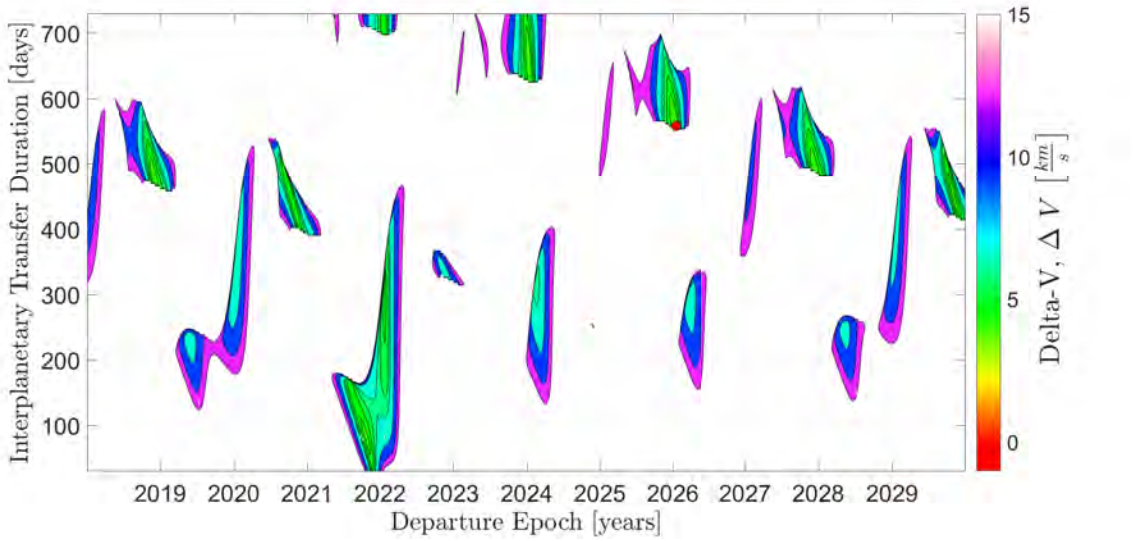

Figure A.5: Pork-chop plot for the outbound transfer to asteroid Nereus.

Variable	MATLAB	JPL
Launch Date	15 - Jan - 2026	16 - Jan - 2026
TOF $[days]$	558	560
C3 $[km^2/s^2]$	8.25	8.38
$V_{\infty_{dep}}$ $[km/s]$	2.87	2.9
$V_{\infty_{arr}}$ $[km/s]$	2.97	3.0
Total ΔV $[km/s]$	5.84	5.9
Sun phase angle [°]	154.02	154.4
Range to Earth $[AU]$	1.947	1.958
Approach angle [°]	127.51	128
Declination of the launch asymptote [°]	-18.75	-17.5

Table A.10: Comparison between the results for the outbound transfer with one revolution and minimum ΔV to asteroid Nereus and the values from the *JPL*.

Inbound Flight

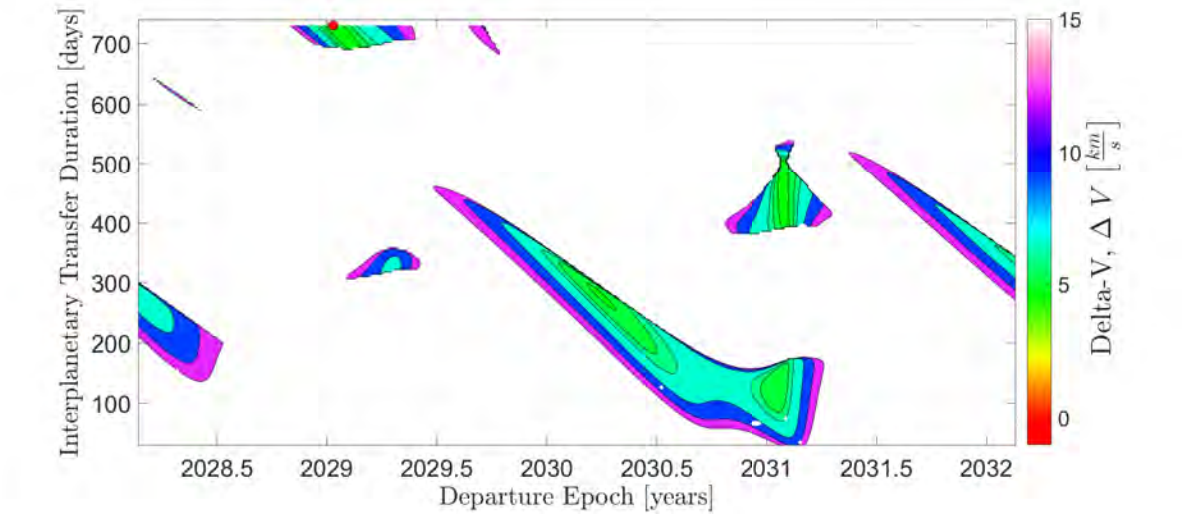

Figure A.6: Pork-chop plot for the comeback trajectory Nereus - Earth.

Variable	Result
Launch Date	12 - Jan - 2029
TOF $[days]$	730
C3 $[km^2/s^2]$	0.865
$V_{\infty_{dep}}$ $[km/s]$	0.93
$V_{\infty_{arr}}$ $[km/s]$	4.41
Total ΔV $[km/s]$	5.34
Sun phase angle [°]	89.66
Approach angle [°]	11.25

Table A.11: Characteristic values for the inbound trajectory with one revolution to asteroid Nereus.

A.2.2 Optimized mission for chemical propulsion

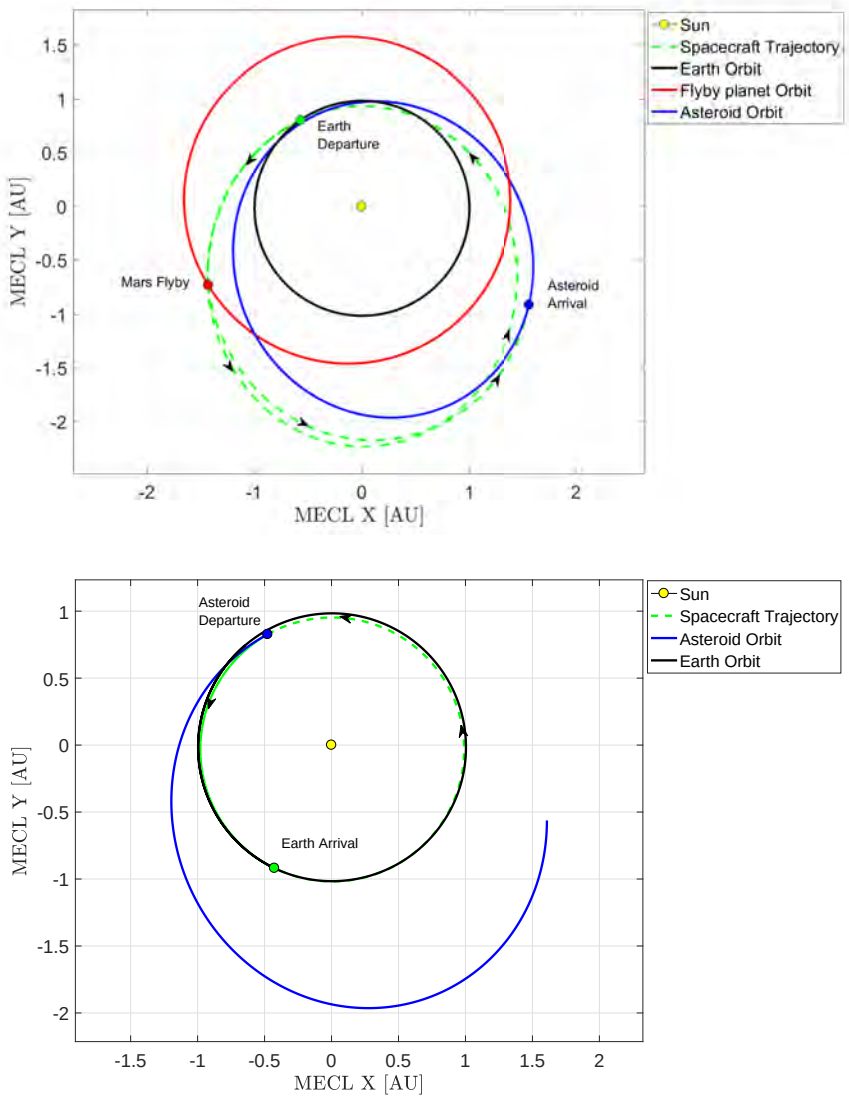

Figure A.7: Outbound (up) and inbound (down) projected trajectories for the chemical propulsion mission with minimum m_0 to Nereus.

Spacecraft Initial Mass $[kg]$	**Mined Mass** $[kg]$	**Total Mission Duration** $[days]$
6897	810	1947

Table A.12: Mass and duration vales for the minimum m_0 chemical propulsion mission to asteroid Nereus.

Variable	Result
Earth Launch	25 - Jan - 2027
Mars Flyby	13 - May - 2029
Asteroid Arrival	04 - Jul - 2030
Asteroid Landing	02 - Nov - 2030
$V_{\infty_{dep}}$ $[km/s]$	7.33
TOF 1st leg $[days]$	838
nº of revs 1st leg	1
TOF 2nd leg $[days]$	417
nº of revs 2nd leg	0
$V_{\infty_{arr}}$ $[km/s]$	1.68
Sun phase angle [°]	132.6
Range to Earth at asteroid arrival $[AU]$	1.355
Approach angle [°]	45.1
Declination of the launch asymptote [°]	9.77

Table A.13: Values characterizing the outbound flight to asteroid Nereus, with data for both legs of the trajectory.

Variable	Flyby altitude $[km]$	B-plane angle ζ [°]	Turn angle δ [°]
Value	4532.4	-87.34	4.56

Table A.14: Mars flyby parameters for the outbound flight to Nereus.

Variable	Value
Asteroid Departure	31 - Jan - 2031
Earth Arrival	26 - May - 2032
$V_{\infty_{dep}}$ $[km/s]$	4.71
$V_{\infty_{arr}}$ $[km/s]$	0.388
TOF $[days]$	481
nº of revs	1
Sun phase angle [°]	49.9
Approach angle [°]	122.9

Table A.15: Inbound flight parameters for the mission with minimum m_0 for asteroid Nereus.

A.3 Asteroid 2011 UW158: ID - 2436724

A.3.1 Pork-Chop plots

Outbound Flight

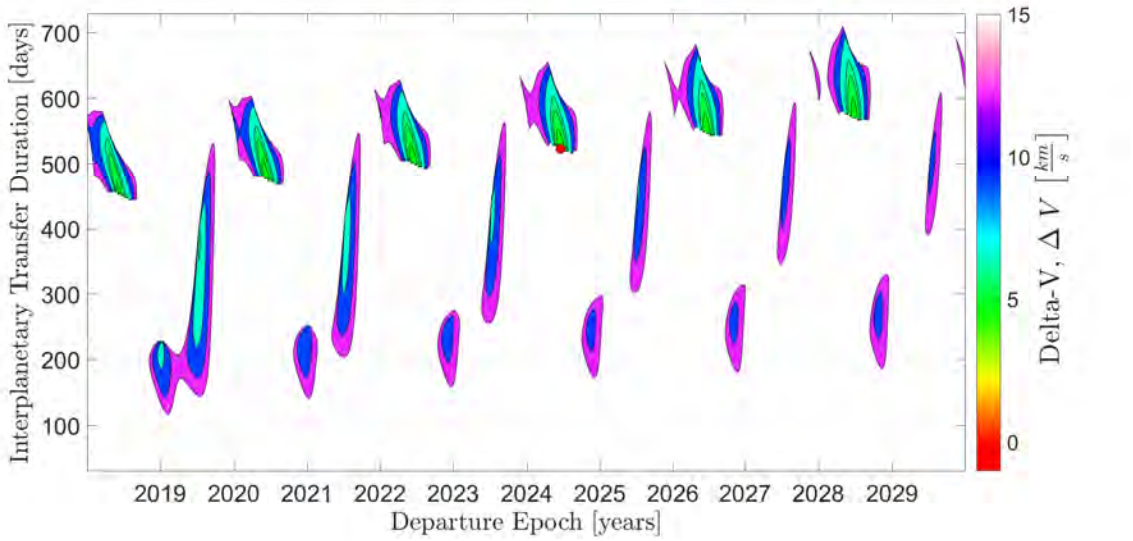

Figure A.8: Pork-chop plot for the outbound transfer to asteroid 2011 UW158.

Variable	MATLAB	JPL
Launch Date	18 - Jun - 2024	19 - Jun - 2024
TOF $[days]$	522	520
C3 $[km^2/s^2]$	10.54	10.44
$V_{\infty_{dep}}$ $[km/s]$	3.25	3.2
$V_{\infty_{arr}}$ $[km/s]$	3.16	3.2
Total ΔV $[km/s]$	6.41	6.4
Sun phase angle [°]	102.78	99.5
Range to Earth $[AU]$	1.656	1.657
Approach angle [°]	156.04	155.9
Declination of the launch asymptote [°]	37.69	36.6

Table A.16: Results obtained for the outbound transfer with minimum ΔV to asteroid 2011 UW158, compared with the values obtained from the *JPL*.

Inbound Flight

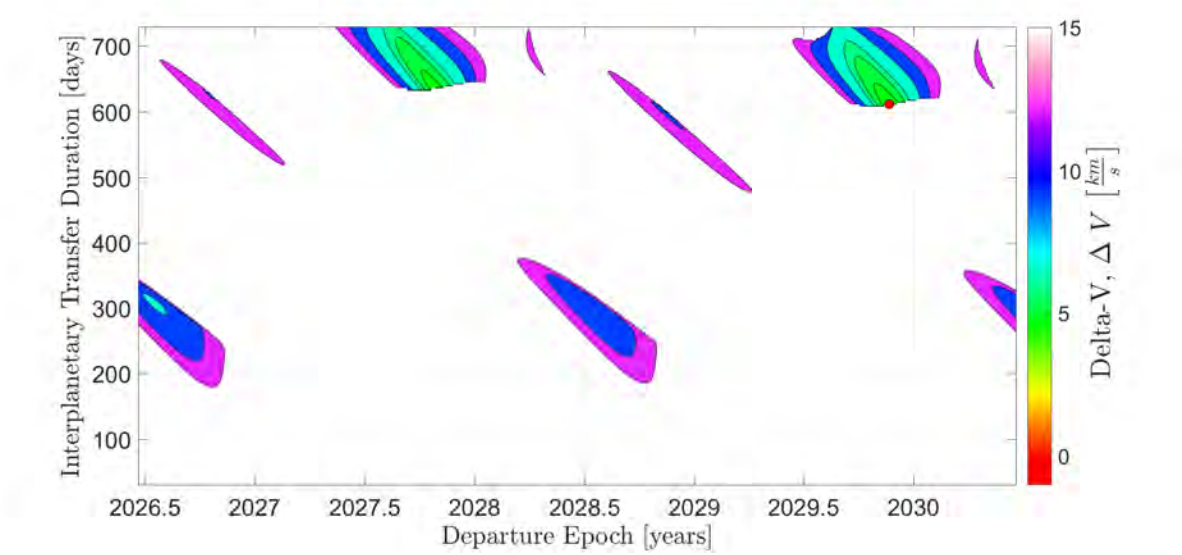

Figure A.9: Pork-chop plot for the comeback trajectory 2011 UW158 - Earth.

Variable	Result
Launch Date	21 - Nov - 2029
TOF $[days]$	612
C3 $[km^2/s^2]$	5.47
$V_{\infty_{dep}}$ $[km/s]$	2.34
$V_{\infty_{arr}}$ $[km/s]$	4.02
Total ΔV $[km/s]$	6.36
Sun phase angle [°]	84.25
Approach angle [°]	27.43

Table A.17: Characteristic values for the inbound trajectory for 2011 UW158.

A.3.2 Optimized mission for chemical propulsion

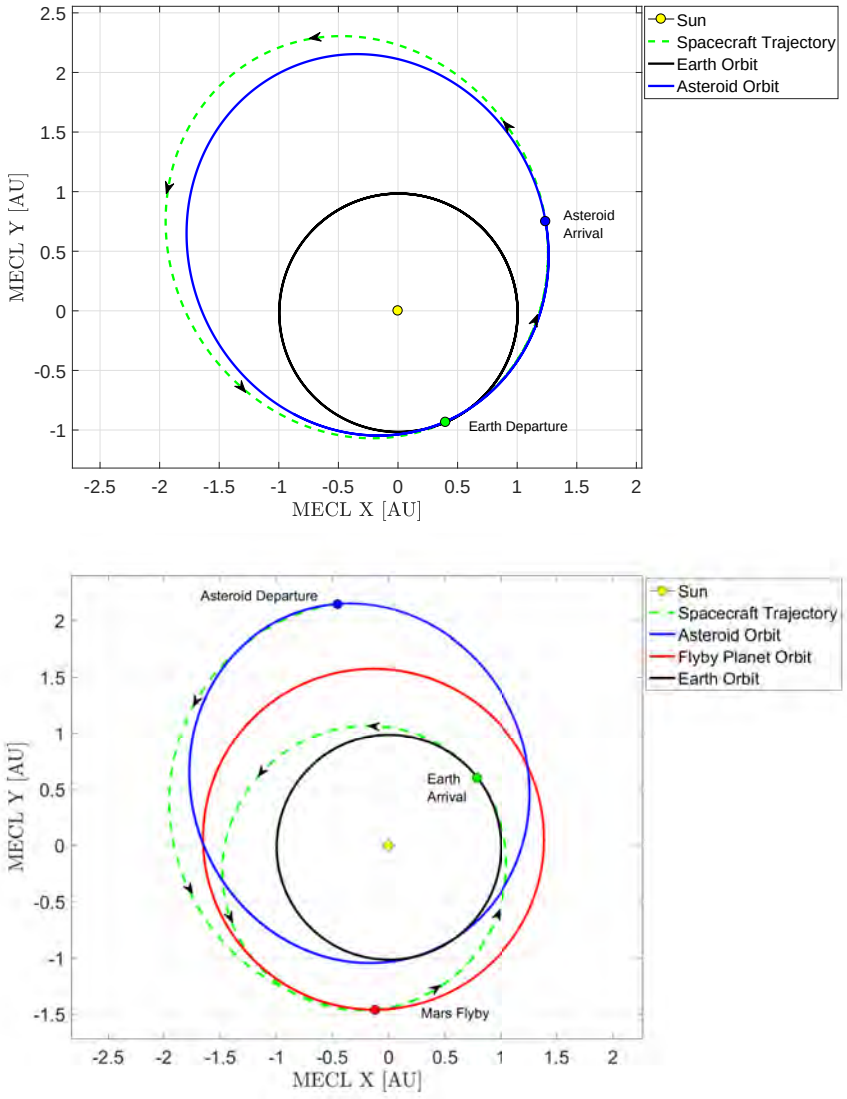

Figure A.10: Outbound (up) and inbound (down) 2D trajectories for the mission with minimum m_0 to 2011 UW158.

Spacecraft Initial Mass $[kg]$	**Mined Mass** $[kg]$	**Total Mission Duration** $[days]$
6055	810	2299

Table A.18: Mass and duration information for the minimum m_0 chemical propulsion mission.

Variable	Result
Earth Launch	15 - Jul - 2021
Asteroid Arrival	06 - Feb - 2024
Asteroid Landing	06 - Jun - 2024
TOF $[days]$	936
nº of revolutions	1
$V_{\infty_{dep}}$ $[km/s]$	6.35
$V_{\infty_{arr}}$ $[km/s]$	0.89
Sun phase angle [°]	28.48
Range to Earth $[AU]$	1.967
Approach angle [°]	46.96
Declination of the launch asymptote [°]	36.11

Table A.19: Results for the outbound flight for optimum chemical mission to 2011 UW158.

Variable	Result
Asteroid Departure	04 - Sep - 2024
Mars Flyby	29 - Nov - 2025
Earth Arrival	31 - Oct - 2027
$V_{\infty_{dep}}$ $[km/s]$	2.2
TOF 2nd leg $[days]$	451
nº of revs 2nd leg	0
TOF 3rd leg $[days]$	701
nº of revs 3rd leg	1
$V_{\infty_{arr}}$ $[km/s]$	3.2
Sun phase angle [°]	93.28
Approach angle [°]	15.48

Table A.20: Results obtained for the flight 2011 UW158 - Earth. Data provided includes both legs.

Variable	Flyby altitude $[km]$	B-plane angle ζ [°]	Turn angle δ [°]
Value	911.12	136.75	73.94

Table A.21: Characteristic values of the Mars flyby found in the inbound flight from 2011 UW158.

A.3.3 Optimized results for low-thrust

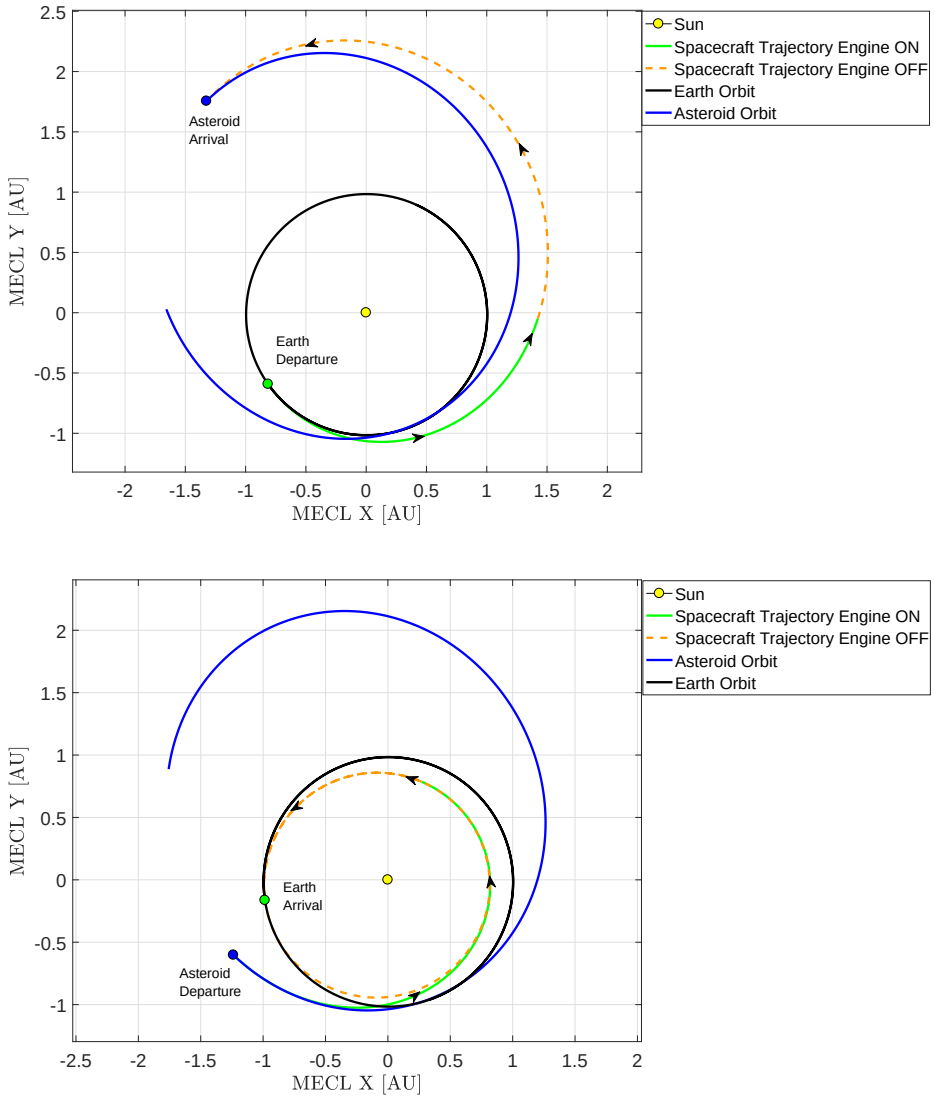

Figure A.11: Outbound (up) and inbound (down) transfers for the low-thrust mission with minimum m_0 to 2011 UW158

Spacecraft Initial Mass $[kg]$	**Mined Mass** $[kg]$	**Total Mission Duration** $[days]$
2854	946	1434

Table A.22: Objectives for the low-thrust asteroid mining mission to 2011 UW158.

Variable	Value
Earth Launch	26 - Apr - 2021
Asteroid Arrival	27 - Nov - 2022
Asteroid Landing	28 - Mar - 2023
$V_{\infty_{arr}}$ $[km/s]$	1.31
ΔV_{ion} $[km/s]$	4.72
TOF $[days]$	581
Number of revolutions	0
Range to Earth at asteroid arrival $[AU]$	1.94

Table A.23: Outbound flight parameters for the low-thrust mission to 2011 UW158

Variable	Value
Asteroid Departure	12 - Jul - 2023
Earth Arrival	30 - Mar - 2025
$V_{\infty_{arr}}$ $[km/s]$	1.69
ΔV_{ion} $[km/s]$	8.76
TOF $[days]$	627
Number of revolutions	1

Table A.24: Low-thrust inbound flight results for 2011 UW158

$\Delta V_{req_{out}}$ $[km/s]$	$\Delta V_{NEXT_{out}}$ $[km/s]$	$\Delta V_{req_{back}}$ $[km/s]$	$\Delta V_{NEXT_{back}}$ $[km/s]$
6.03	3.0	10.45	5.38

Table A.25: ΔV comparison for both flights for 2011 UW158. Mission could be feasible using two NEXT-C engines and slightly adjusting the trajectory.

A.4 Asteroid ANTEROS: ID - 2001943

A.4.1 Pork-Chop plots

Outbound Flight

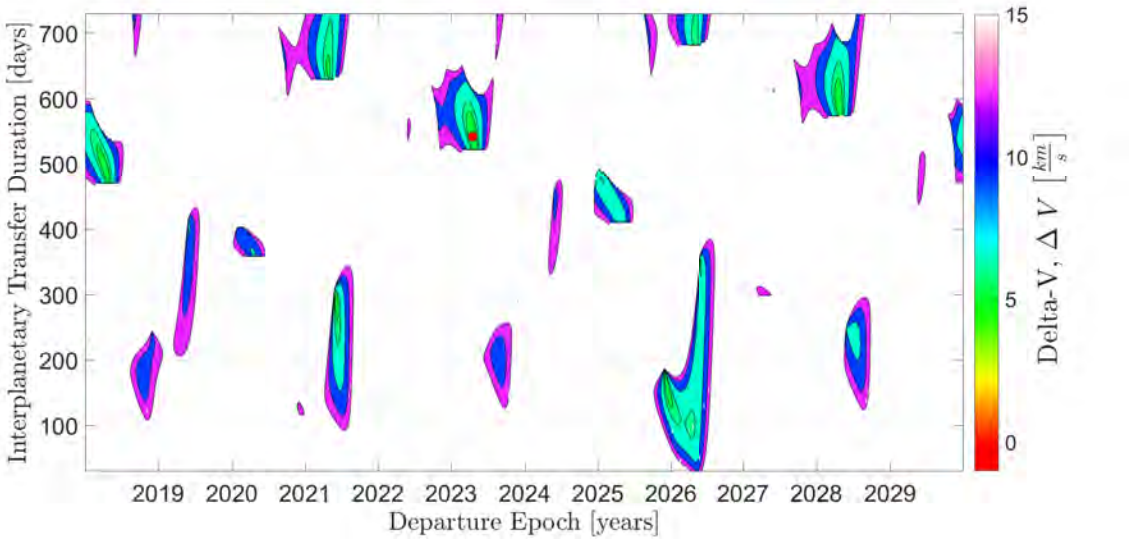

Figure A.12: Pork-chop plot for the outbound transfer to asteroid Anteros.

Variable	MATLAB	JPL
Launch Date	16 - Apr - 2023	21 - Apr - 2023
TOF $[days]$	542	540
C3 $[km^2/s^2]$	10.07	11.54
$V_{\infty_{dep}}$ $[km/s]$	3.17	3.4
$V_{\infty_{arr}}$ $[km/s]$	3.86	3.7
Total ΔV $[km/s]$	7.03	7.1
Sun phase angle [°]	90.46	91.5
Range to Earth $[AU]$	1.73	1.736
Approach angle [°]	124.97	126.8
Declination of the launch asymptote [°]	16.98	18.2

Table A.26: Results obtained for the outbound transfer with minimum ΔV to asteroid Anteros, compared with the values obtained from the *JPL*.

Inbound Flight

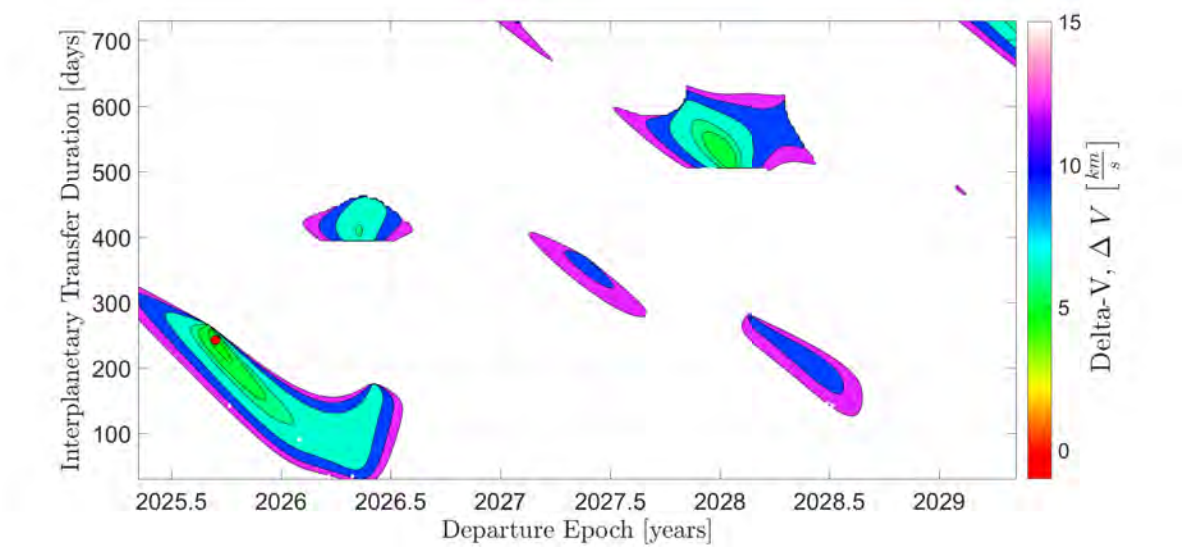

Figure A.13: Pork-chop plot for the comeback trajectory Anteros - Earth.

Variable	Result
Launch Date	14 - Sep - 2025
TOF $[days]$	242
C3 $[km^2/s^2]$	5.34
$V_{\infty_{dep}}$ $[km/s]$	2.31
$V_{\infty_{arr}}$ $[km/s]$	4.2
Total ΔV $[km/s]$	6.51
Sun phase angle [°]	84.87
Approach angle [°]	17.74

Table A.27: Inbound trajectory parameters for Anteros.

A.4.2 Optimized mission for chemical propulsion

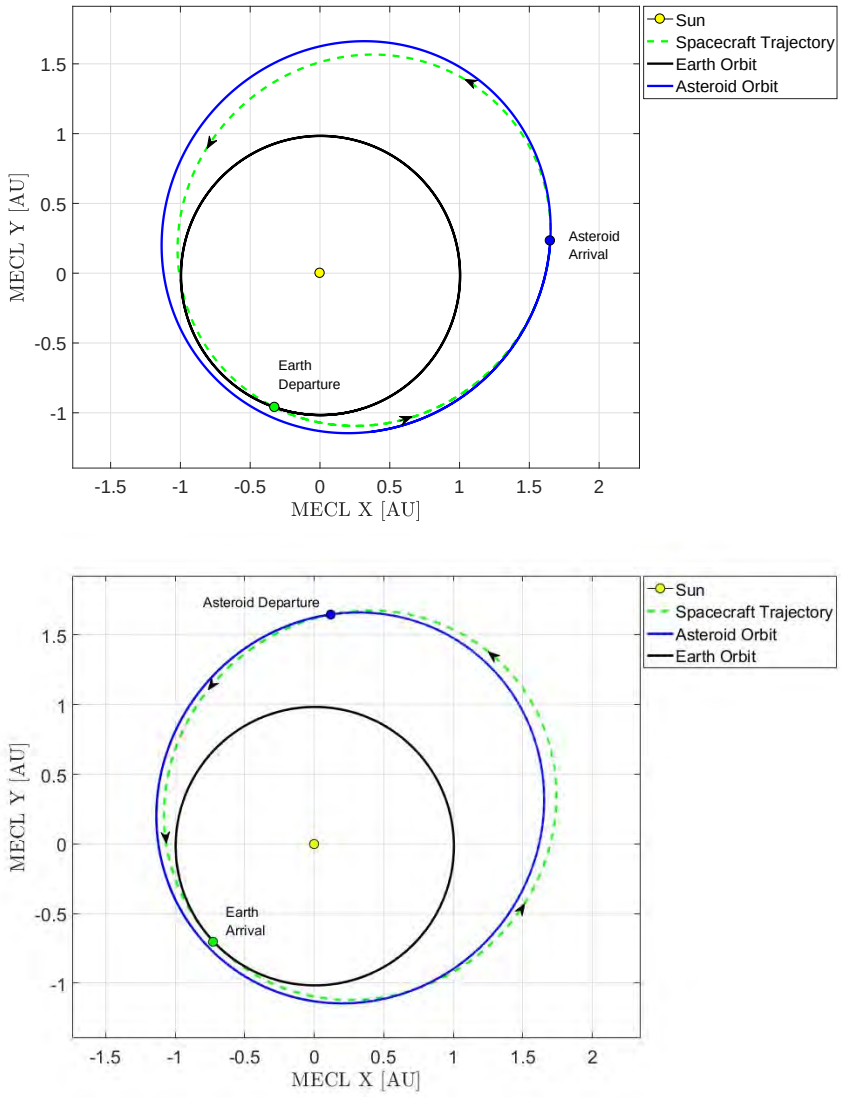

Figure A.14: Outbound (up) and inbound (down) projected trajectories for the chemical multi-revolution mission that yields minimum m_0 for asteroid Anteros.

Spacecraft Initial Mass $[kg]$	**Mined Mass** $[kg]$	**Total Mission Duration** $[days]$
10438.5	810	1798

Table A.28: Mass and time information for the optimum chemical propulsion mission to asteroid Anteros.

Variable	Result
Earth Launch	01 - Jun - 2021
Asteroid Arrival	10 - Jul - 2023
Asteroid Landing	08 - Nov - 2023
TOF [$days$]	768
nº of revolutions	1
$V_{\infty_{dep}}$ [km/s]	7.04
$V_{\infty_{arr}}$ [km/s]	0.76
Sun phase angle [°]	111.06
Range to Earth [AU]	1.82
Approach angle [°]	154.32
Declination of the launch asymptote [°]	19.89

Table A.29: Results for the outbound flight of the optimum chemical mission to Anteros.

Variable	Value
Asteroid Departure	06 - Feb - 2024
Earth Arrival	04 - May - 2026
$V_{\infty_{dep}}$ [km/s]	2.19
$V_{\infty_{arr}}$ [km/s]	4.92
TOF [$days$]	818
nº of revolutions	1
Sun phase angle [°]	88.61
Approach angle [°]	31.73

Table A.30: Results obtained for the comeback flight Anteros - Earth.

A.4.3 Optimized mission for low-thrust

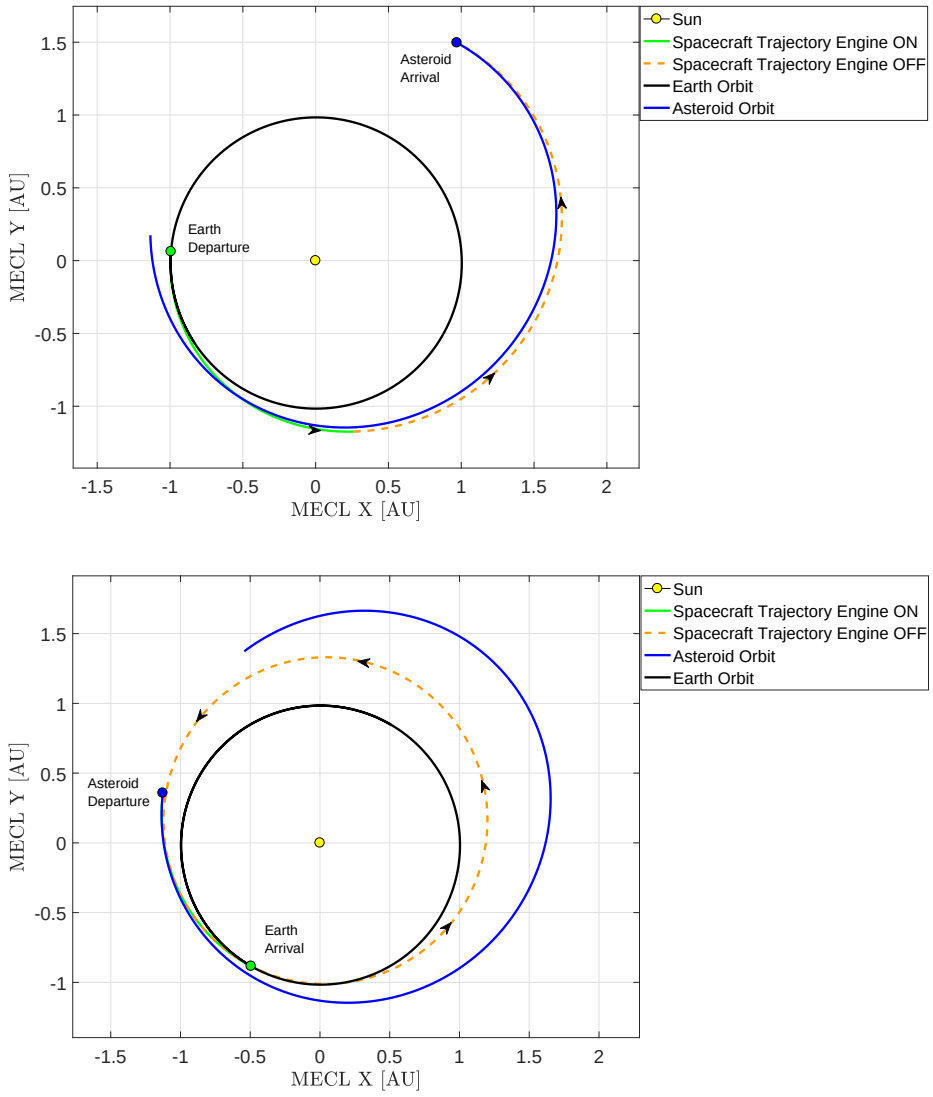

Figure A.15: Outbound (up) and inbound (down) transfers for the low-thrust mission with minimum m_0 to Anteros

Spacecraft Initial Mass $[kg]$	**Mined Mass** $[kg]$	**Total Mission Duration** $[days]$
2070	810	1162

Table A.31: Objectives for the low-thrust asteroid mining mission to Anteros.

Variable	Value
Earth Launch	17 - Mar - 2026
Asteroid Arrival	24 - Apr - 2027
Asteroid Landing	23 - Aug - 2027
$V_{\infty_{arr}}$ $[km/s]$	0.481
ΔV_{ion} $[km/s]$	3.31
TOF $[days]$	404
Number of revolutions	0
Range to Earth at asteroid arrival $[AU]$	2.74

Table A.32: Outbound trajectory parameters for the low-thrust mission to Anteros.

Variable	Value
Asteroid Departure	21 - Nov - 2027
Earth Arrival	21 - May - 2029
$V_{\infty_{arr}}$ $[km/s]$	2.52
ΔV_{ion} $[km/s]$	2.05
TOF $[days]$	547
Number of revolutions	1

Table A.33: Low-thrust inbound flight results for Anteros.

$\Delta V_{req_{out}}$ $[km/s]$	$\Delta V_{NEXT_{out}}$ $[km/s]$	$\Delta V_{req_{back}}$ $[km/s]$	$\Delta V_{NEXT_{back}}$ $[km/s]$
3.788	3.702	4.57	4.19

Table A.34: ΔV comparison for the inbound and comeback flights to Anteros. Mission could be feasible using two NEXT-C engines.

A.5 Asteroid 2001 CC21: ID - 2098943

A.5.1 Pork-Chop plots

Outbound Flight

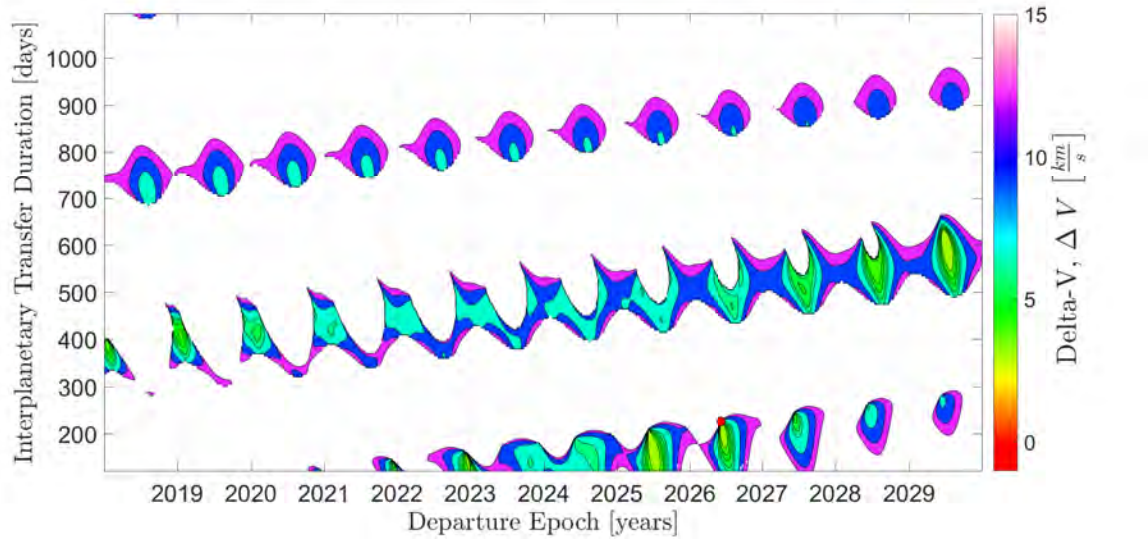

Figure A.16: Pork-chop plot for the outbound transfer to asteroid 2001 CC21.

Variable	MATLAB	JPL
Launch Date	07 - Jun - 2026	10 - Jun - 2026
TOF $[days]$	225	220
C3 $[km^2/s^2]$	4.36	4.74
$V_{\infty_{dep}}$ $[km/s]$	2.09	2.2
$V_{\infty_{arr}}$ $[km/s]$	2.14	2.1
Total ΔV $[km/s]$	4.23	4.3
Sun phase angle [°]	108.4	111.9
Range to Earth $[AU]$	0.878	0.857
Approach angle [°]	42.34	41.8
Declination of the launch asymptote [°]	-38.68	-42.2

Table A.35: Results obtained for the outbound transfer with minimum ΔV to asteroid 2001 CC21, compared with the values obtained from the *JPL*.

Inbound Flight

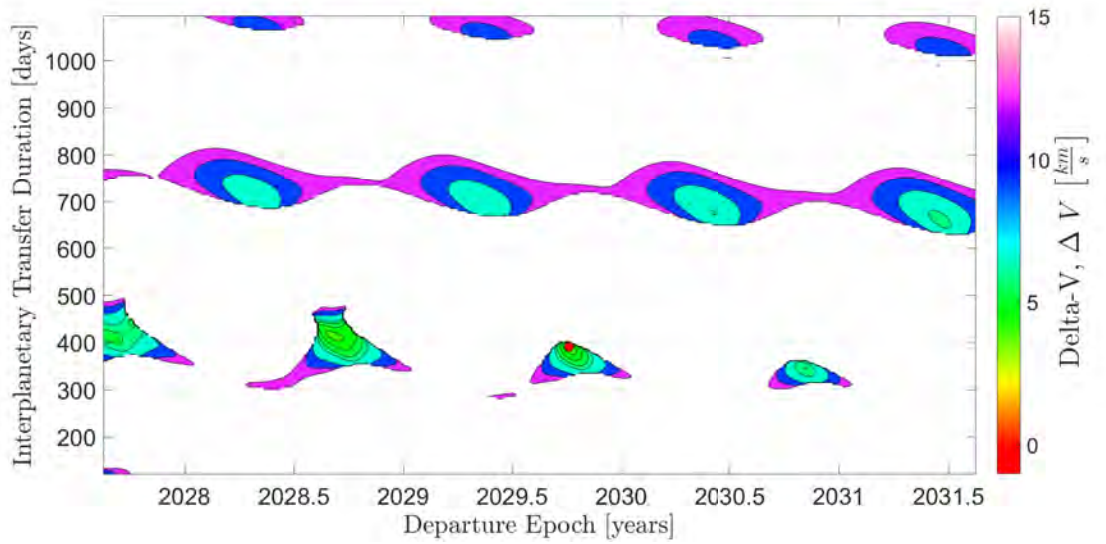

Figure A.17: Pork-chop plot for the inbound transfer 2001 CC21 - Earth.

Variable	Result
Launch Date	06 - Oct - 2029
TOF $[days]$	390
C3 $[km^2/s^2]$	8.79
$V_{\infty_{dep}}$ $[km/s]$	2.97
$V_{\infty_{arr}}$ $[km/s]$	2.92
Total ΔV $[km/s]$	5.89
Sun phase angle [°]	92.55
Approach angle [°]	144.5

Table A.36: Parameters characterizing the comeback flight from 2001 CC21.

A.5.2 Optimized mission for chemical propulsion

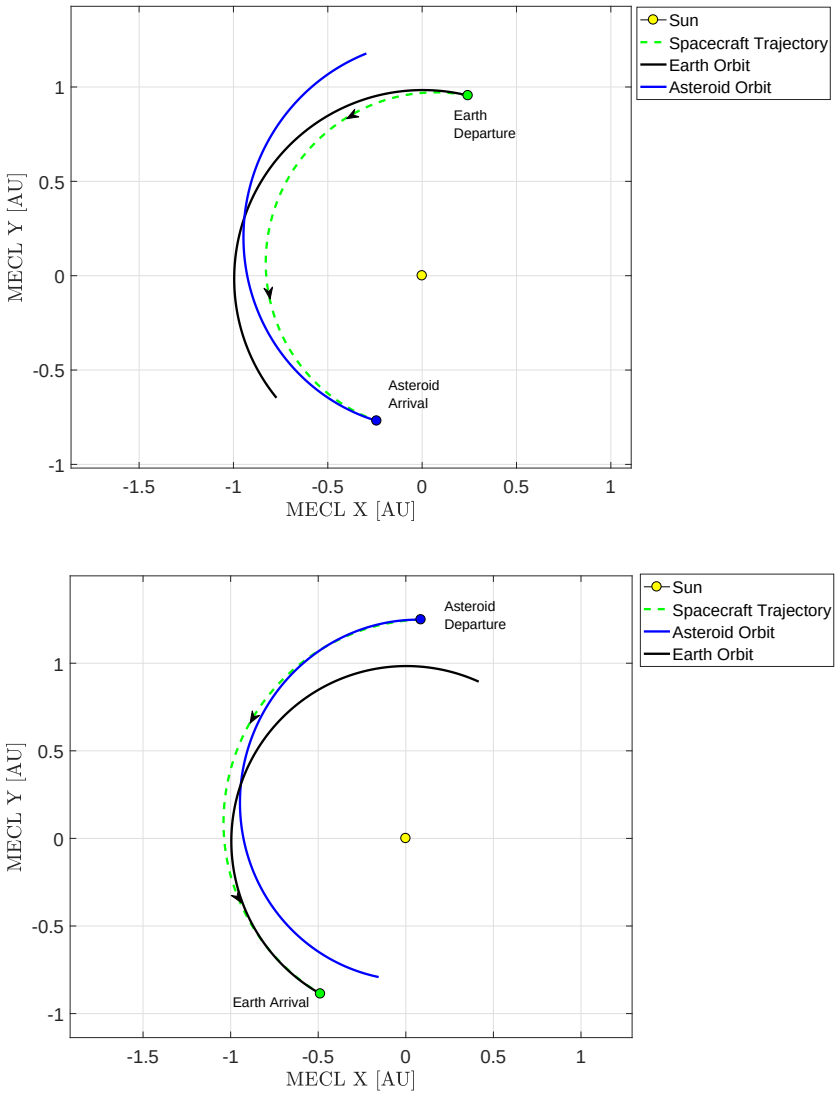

Figure A.18: Outbound (up) and inbound (down) projected trajectories for the chemical zero mission that yields minimum m_0 for asteroid 2001 CC21.

Spacecraft Initial Mass $[kg]$	**Mined Mass** $[kg]$	**Total Mission Duration** $[days]$
7826	810	531

Table A.37: Mass and time information for the optimum chemical propulsion mission to asteroid 2001 CC21.

Variable	Result
Earth Launch	07 - Dec - 2021
Asteroid Arrival	30 - Apr - 2022
Asteroid Landing	29 - Aug - 2022
TOF $[days]$	144
nº of revolutions	0
$V_{\infty_{dep}}$ $[km/s]$	3.18
$V_{\infty_{arr}}$ $[km/s]$	2.45
Sun phase angle [°]	47.97
Range to Earth $[AU]$	0.545
Approach angle [°]	138.11
Declination of the launch asymptote [°]	25.70

Table A.38: Outbound flight results for the optimum chemical mission to 2001 CC21.

Variable	Value
Asteroid Departure	27 - Nov - 2022
Earth Arrival	22 - May - 2023
$V_{\infty_{dep}}$ $[km/s]$	2.45
$V_{\infty_{arr}}$ $[km/s]$	2.36
TOF $[days]$	176
nº of revolutions	0
Sun phase angle [°]	69.99
Approach angle [°]	36.08

Table A.39: Results obtained for the comeback flight 2001 CC21 - Earth.

A.5.3 Optimized mission for low-thrust

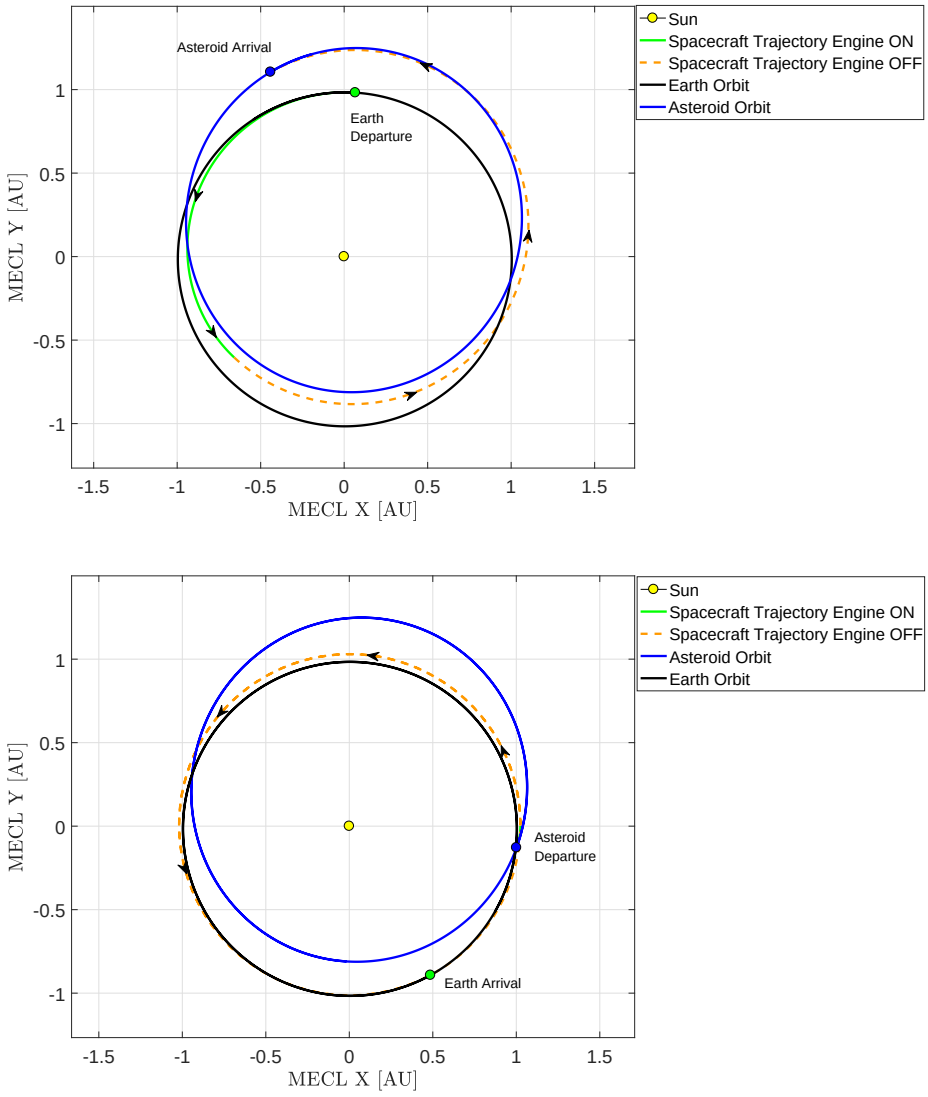

Figure A.19: Outbound (up) and inbound (down) transfers for the low-thrust mission with minimum m_0 to asteroid 2001 CC21

Spacecraft Initial Mass $[kg]$	**Mined Mass** $[kg]$	**Total Mission Duration** $[days]$
1244.3	810	1311

Table A.40: Objectives for the low-thrust asteroid mining mission to 2001 CC21.

Variable	Value
Earth Launch	18 - Dec - 2022
Asteroid Arrival	24 - Jan - 2024
Asteroid Landing	24 - May - 2024
$V_{\infty_{arr}}$ $[km/s]$	1.02
ΔV_{ion} $[km/s]$	12.95
TOF $[days]$	402
Number of revolutions	1
Range to Earth at asteroid arrival $[AU]$	0.309

Table A.41: Outbound trajectory parameters for the low-thrust mission to 2001 CC21.

Variable	Value
Asteroid Departure	22 - Aug - 2024
Earth Arrival	21 - Jul - 2026
$V_{\infty_{arr}}$ $[km/s]$	0.46
ΔV_{ion} $[km/s]$	6.31
TOF $[days]$	698
Number of revolutions	1

Table A.42: Low-thrust inbound flight results for 2001 CC21.

$\Delta V_{req_{out}}$ $[km/s]$	$\Delta V_{NEXT_{out}}$ $[km/s]$	$\Delta V_{req_{back}}$ $[km/s]$	$\Delta V_{NEXT_{back}}$ $[km/s]$
13.98	7.14	6.77	10.06

Table A.43: ΔV comparison for the inbound and comeback flights to 2001 CC21. Mission could be feasible using two NEXT-C engines.

A.6 Asteroid 1992 TC: ID - 2007474

A.6.1 Pork-Chop plots

Outbound Flight

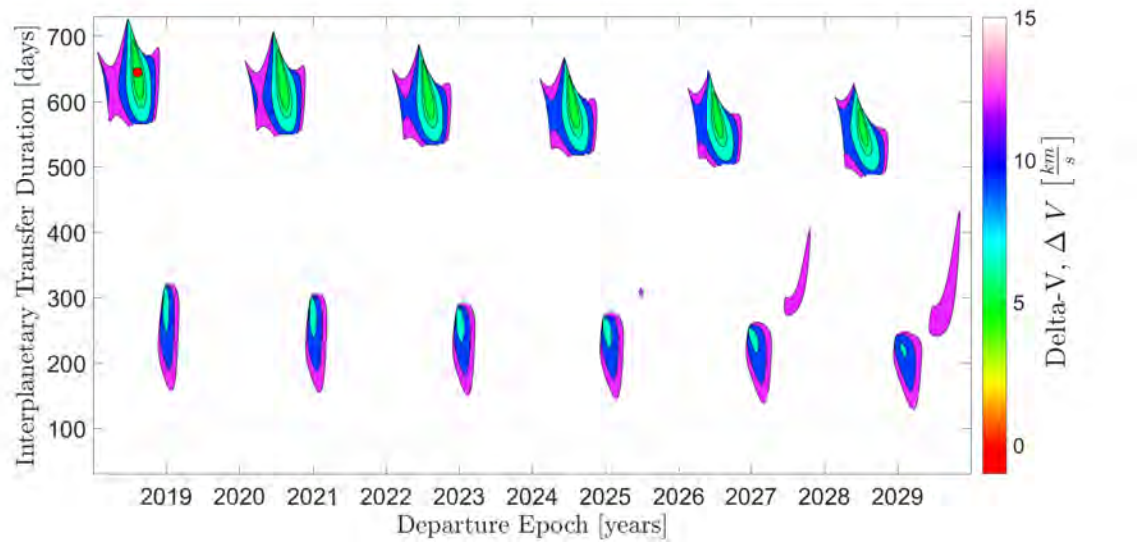

Figure A.20: Pork-chop plot for the outbound transfer to 1992 TC for a 12-year launch window.

Variable	MATLAB	JPL
Launch Date	11 - Aug - 2018	09 - Aug - 2018
TOF $[days]$	644	640
C3 $[km^2/s^2]$	11.30	12.55
$V_{\infty_{dep}}$ $[km/s]$	3.36	3.5
$V_{\infty_{arr}}$ $[km/s]$	3.68	3.5
Total ΔV $[km/s]$	7.05	7.1
Sun phase angle [°]	109.13	103.2
Range to Earth $[AU]$	2.266	2.239
Approach angle [°]	133.61	134.2
Declination of the launch asymptote [°]	-5.65	-8.7

Table A.44: Results obtained for the outbound transfer with minimum ΔV to asteroid 1992 TC, compared with the values obtained from the *JPL*.

Inbound Flight

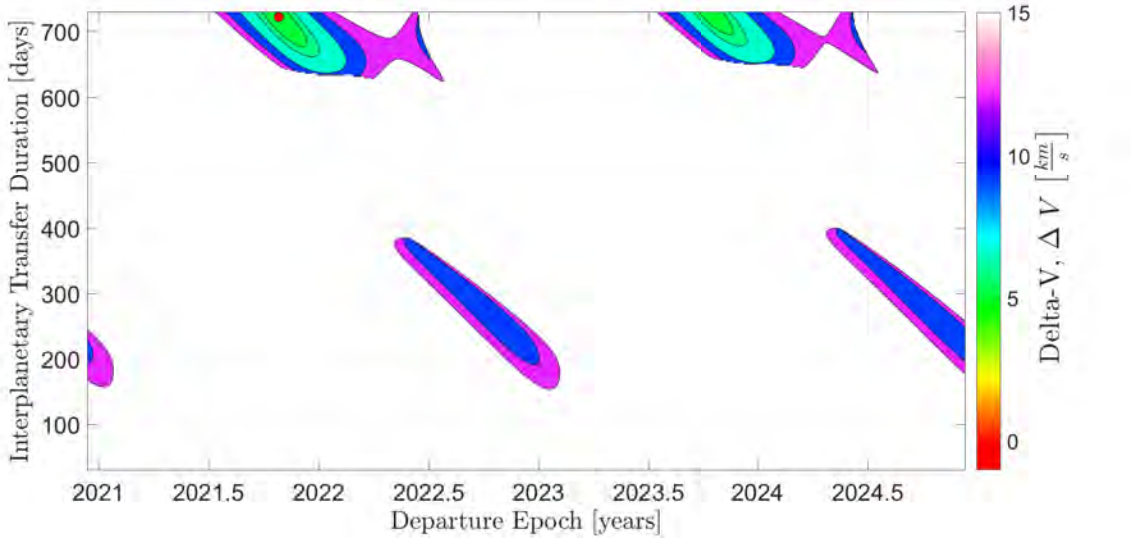

Figure A.21: Pork-chop plot for inbound transfers 1992 TC - Earth.

Variable	Result
Launch Date	27 - Oct - 2021
TOF $[days]$	722
C3 $[km^2/s^2]$	10.61
$V_{\infty_{dep}}$ $[km/s]$	3.26
$V_{\infty_{arr}}$ $[km/s]$	3.83
Total ΔV $[km/s]$	7.09
Sun phase angle [°]	88.57
Approach angle [°]	7.18

Table A.45: Characteristic values for the inbound trajectory for 1992 TC.

A.6.2 Optimized mission for chemical propulsion

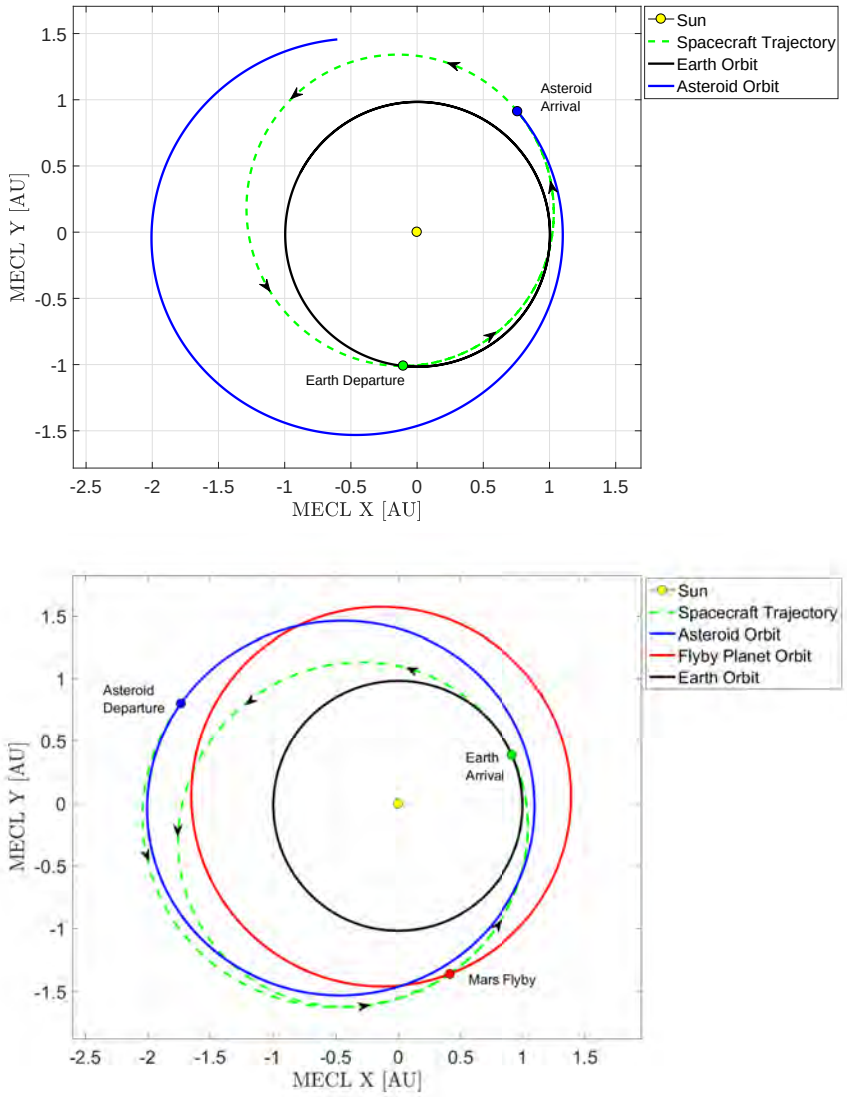

Figure A.22: Outbound (up) and inbound (down) 2D trajectories for the mission with minimum m_0 to asteroid 1992 TC.

Spacecraft Initial Mass $[kg]$	**Mined Mass** $[kg]$	**Total Mission Duration** $[days]$
10942	810	1949

Table A.46: Masses and duration information for the minimum m_0 mission.

Variable	Result
Earth Launch	15 - Jun - 2026
Asteroid Arrival	22 - Feb - 2028
Asteroid Landing	22 - Jun - 2028
TOF $[days]$	617
nº of revolutions	1
$V_{\infty_{dep}}$ $[km/s]$	5.86
$V_{\infty_{arr}}$ $[km/s]$	3.22
Sun phase angle [°]	96.74
Range to Earth $[AU]$	1.707
Approach angle [°]	171.39
Declination of the launch asymptote [°]	-26.24

Table A.47: Results for the outbound flight associated to the optimum chemical mission for 1992 TC.

Variable	Result
Asteroid Departure	20 - Sep - 2028
Mars Flyby	11 - Oct - 2029
Earth Arrival	17 - Oct - 2031
$V_{\infty_{dep}}$ $[km/s]$	0.763
TOF 2nd leg $[days]$	386
nº of revs 2nd leg	0
TOF 3rd leg $[days]$	736
nº of revs 3rd leg	1
$V_{\infty_{arr}}$ $[km/s]$	4.32
Sun phase angle [°]	104.72
Approach angle [°]	18.75

Table A.48: Results obtained for the flight 1992 TC - Earth. Data provided includes both legs.

Variable	Flyby altitude $[km]$	B-plane angle ζ [°]	Turn angle δ [°]
Value	3008.81	50.6	17.39

Table A.49: Values characterizing the Mars flyby found in the inbound flight for 1992 TC.

A.7 Asteroid 2001 SG10: ID - 2194006

A.7.1 Pork-Chop plots

Outbound Flight

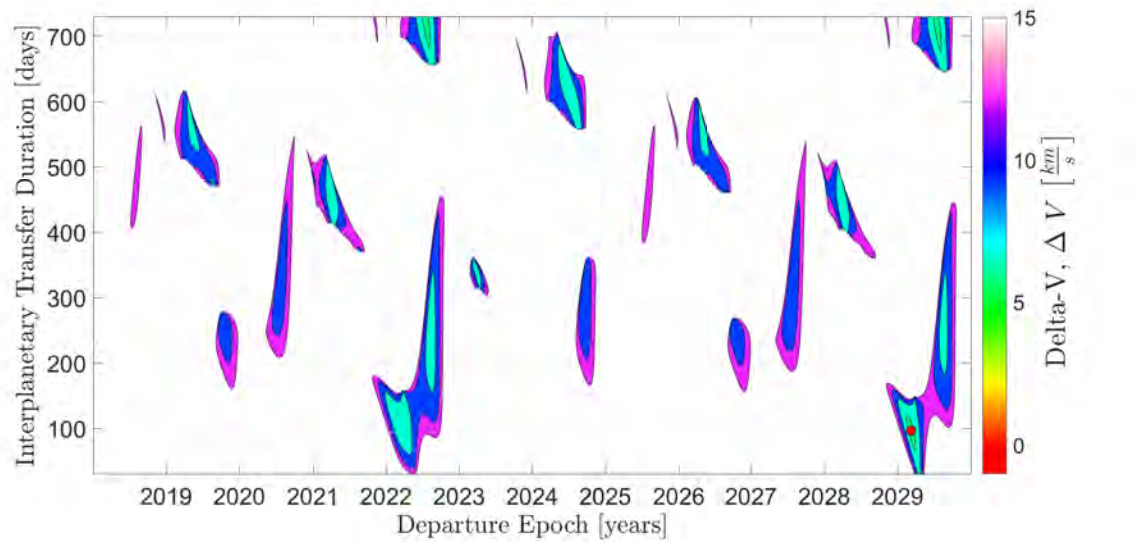

Figure A.23: Pork-chop plot for the outbound flight to 2001 SG10 for the 12-year launch window being considered.

Variable	MATLAB	JPL
Launch Date	07 - Mar - 2029	02 - Mar - 2029
TOF $[days]$	96	100
C3 $[km^2/s^2]$	10.94	9.57
$V_{\infty_{dep}}$ $[km/s]$	3.31	3.1
$V_{\infty_{arr}}$ $[km/s]$	5.1	5.3
Total ΔV $[km/s]$	8.41	8.4
Sun phase angle [°]	88.4	83.8
Range to Earth $[AU]$	0.276	0.261
Approach angle [°]	170.98	168.5
Declination of the launch asymptote [°]	48.76	54.4

Table A.50: Parameters obtained for the outbound transfer with minimum ΔV to asteroid 2001 SG10, compared with values from the *JPL*.

Inbound Flight

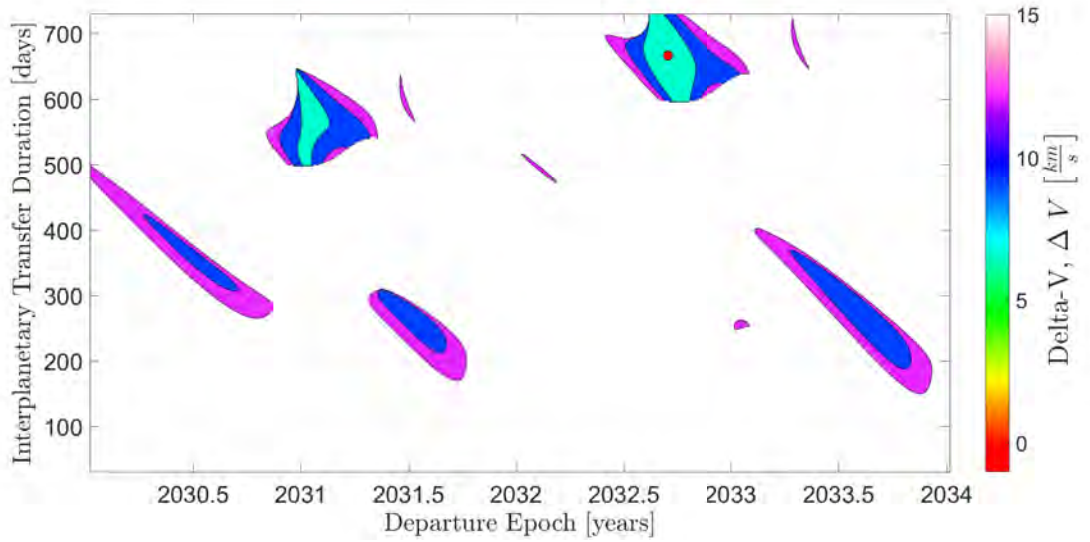

Figure A.24: Pork-chop plot for inbound transfers 2001 SG10 - Earth.

Variable	Result
Launch Date	15 - Sep - 2032
TOF $[days]$	666
C3 $[km^2/s^2]$	33.42
$V_{\infty_{dep}}$ $[km/s]$	5.78
$V_{\infty_{arr}}$ $[km/s]$	3.45
Total ΔV $[km/s]$	9.23
Sun phase angle [°]	79.73
Approach angle [°]	10.39

Table A.51: Characteristic values for the inbound trajectory for 2001 SG10.

A.7.2 Optimized mission for chemical propulsion

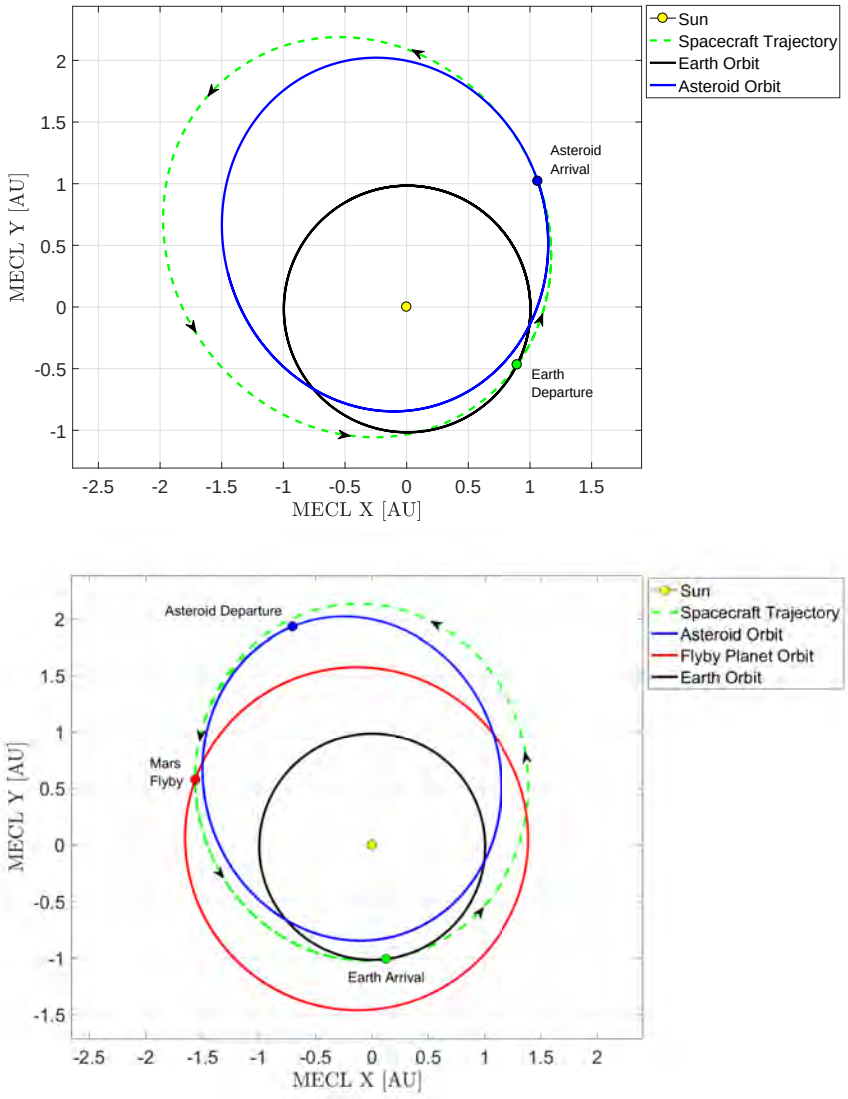

Figure A.25: Outbound (up) and inbound (down) projected flights for the mission with minimum m_0 to asteroid 2001 SG10.

Spacecraft Initial Mass $[kg]$	**Mined Mass** $[kg]$	**Total Mission Duration** $[days]$
13494	810	2134

Table A.52: Masses and duration information for the minimum m_0 mission.

Variable	Result
Earth Launch	25 - Aug - 2025
Asteroid Arrival	21 - Jan - 2028
Asteroid Landing	21 - May - 2028
TOF $[days]$	879
nº of revolutions	1
$V_{\infty_{dep}}$ $[km/s]$	7.49
$V_{\infty_{arr}}$ $[km/s]$	2.0
Sun phase angle [°]	87.33
Range to Earth $[AU]$	1.572
Approach angle [°]	36.55
Declination of the launch asymptote [°]	-5.39

Table A.53: Outbound flight results associated to the chemical mission with minimum m_0 for 2001 SG10.

Variable	Result
Asteroid Departure	19 - Aug - 2028
Mars Flyby	28 - Jan - 2029
Earth Arrival	29 - Jun - 2031
$V_{\infty_{dep}}$ $[km/s]$	1.51
TOF 2nd leg $[days]$	162
nº of revs 2nd leg	0
TOF 3rd leg $[days]$	882
nº of revs 3rd leg	1
$V_{\infty_{arr}}$ $[km/s]$	5.24
Sun phase angle [°]	92.89
Approach angle [°]	13.28

Table A.54: Parameters defining the 2001 SG10 - Earth return flight. Data provided includes both transfer legs.

Variable	Flyby altitude $[km]$	B-plane angle ζ [°]	Turn angle δ [°]
Value	5140.8	23.19	7.95

Table A.55: Parameters defining the Mars flyby found in the inbound flight for 2001 SG10.

A.8 Asteroid 2002 DO3: ID - 3114075

A.8.1 Pork-Chop plots

Outbound Flight

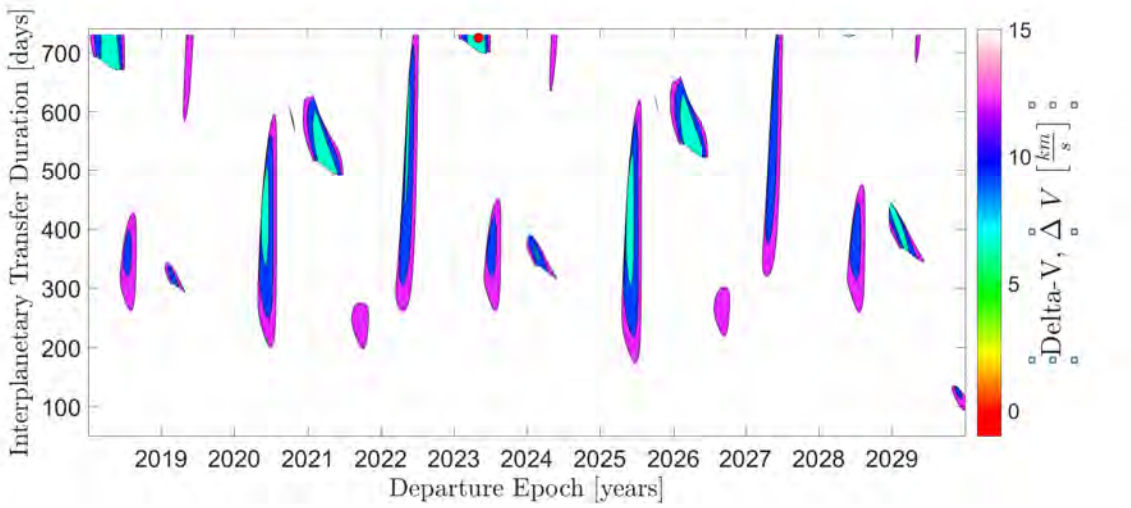

Figure A.26: Pork-chop plot for the outbound transfers to 2002 DO3.

Variable	MATLAB	JPL
Launch Date	04 - May - 2023	01 - May - 2023
TOF $[days]$	724	730
C3 $[km^2/s^2]$	23.82	23.96
$V_{\infty_{dep}}$ $[km/s]$	4.88	4.9
$V_{\infty_{arr}}$ $[km/s]$	4.27	4.3
Total ΔV $[km/s]$	9.15	9.2
Sun phase angle [°]	168.36	167.6
Range to Earth $[AU]$	1.367	1.372
Approach angle [°]	122.2	122.5
Declination of the launch asymptote [°]	-39.44	-38.5

Table A.56: Parameters defining the outbound one revolution transfer with minimum ΔV to asteroid 2002 DO3, compared with values from the *JPL*.

Inbound Flight

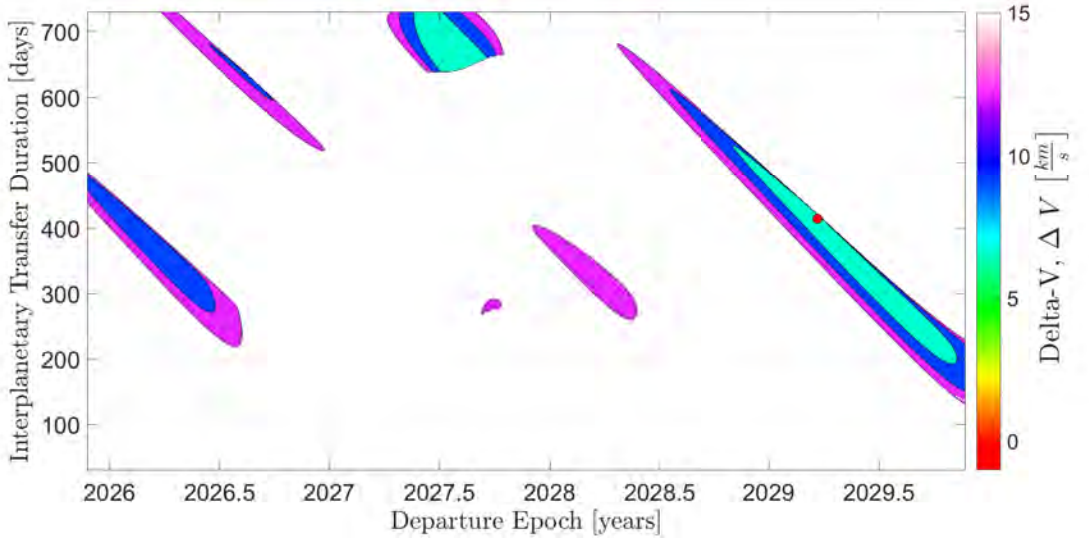

Figure A.27: Pork-chop plot for inbound transfers 2002 DO3 - Earth.

Variable	Result
Launch Date	22 - Mar - 2029
TOF $[days]$	414
C3 $[km^2/s^2]$	3.33
$V_{\infty_{dep}}$ $[km/s]$	1.83
$V_{\infty_{arr}}$ $[km/s]$	6.31
Total ΔV $[km/s]$	8.14
Sun phase angle [°]	90.87
Approach angle [°]	3.41

Table A.57: Inbound trajectory values for the zero revolution transfer to 2002 DO3.

A.8.2 Optimized mission for chemical propulsion

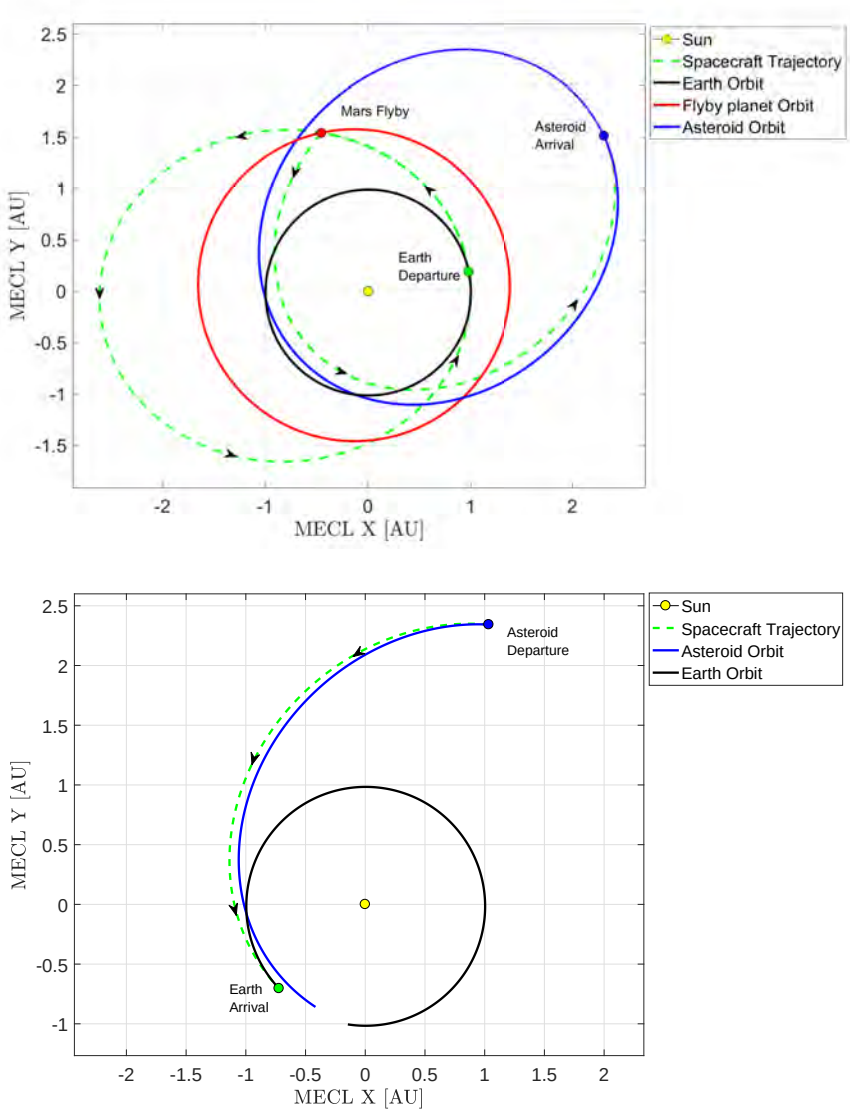

Figure A.28: Outbound (up) and inbound (down) trajectories for the chemical propulsion mission with minimum m_0 to asteroid 2002 DO3.

Spacecraft Initial Mass $[kg]$	**Mined Mass** $[kg]$	**Total Mission Duration** $[days]$
11253.9	810	2039

Table A.58: Mass and duration vales for the minimum m_0 chemical propulsion mission to asteroid 2002 DO3.

Variable	Result
Earth Launch	04 - Oct - 2029
Mars Flyby	05 - Jul - 2032
Asteroid Arrival	14 - Nov - 2033
Asteroid Landing	15 - Mar - 2034
$V_{\infty_{dep}}$ $[km/s]$	6.37
TOF 1st leg $[days]$	1005
nº of revs 1st leg	1
TOF 2nd leg $[days]$	497
nº of revs 2nd leg	0
$V_{\infty_{arr}}$ $[km/s]$	0.88
Sun phase angle [°]	75.65
Range to Earth at asteroid arrival $[AU]$	1.845
Approach angle [°]	149.36
Declination of the launch asymptote [°]	32.0

Table A.59: Values characterizing the outbound flight to asteroid 2002 DO3, with data for both legs of the trajectory.

Variable	Flyby altitude $[km]$	B-plane angle ζ [°]	Turn angle δ [°]
Value	6031	-103.72	-5.96

Table A.60: Mars flyby parameters for the outbound flight to 2002 DO3.

Variable	Value
Asteroid Departure	13 - Jun - 2034
Earth Arrival	05 - May - 2035
$V_{\infty_{dep}}$ $[km/s]$	0.79
$V_{\infty_{arr}}$ $[km/s]$	6.44
TOF $[days]$	326
nº of revs	0
Sun phase angle [°]	89.19
Approach angle [°]	10.12

Table A.61: Flight parameters for the inbound transfer of the mission with minimum m_0 for asteroid 2002 DO3.

APPENDIX B

THESIS BUDGET

In any engineering project detailing the costs associated to the work is an important analysis which has to be performed. For the case of this thesis, several resources and equipment have been necessary and hence must be taken into account.

Firstly, a computer has been required to write the thesis and to carry out all the computations involved. In this case, such computer has been an *HP ENVY 15-j101ss*, which was bought four years ago for 900 €. Therefore, the depreciation of the equipment in the last year has to be taken into account. Considering that the value of the components at the end of the life cycle can be of 80 €, and assuming that the operative time of the computer will come to an end 8 years after it was bought, one can use a linear depreciation method to calculate that the cost associated to equipment depreciation is 102.5€ per year .

In addition, different softwares have been used, although there are no costs associated to them. This is due to the fact that SPICE is an open free software provided by NASA, while the *NSGA-II* code developed by Lin Song is available for free in the MATLAB File Exchange library. Indeed, MATLAB has been used for this thesis but, since the author has been able to do so under an academic license belonging to Universidad Carlos III de Madrid, no associated costs have to be directly charged into the budget of this project.

With respect to the labor costs this project has, up to now, not incurred in any since, on the one hand, the author has not been paid to carry out the work and, on the other hand, the salaries of the corresponding supervisors (both the UC3M tutor and the engineer from

the European Space Agency) are paid on a normal basis and are not a particularity of this project.

Nevertheless, the internship at the European Space Technology Center, *ESTEC*, that was associated to this thesis and which was initially planned for the current year had to be finally postponed to 2019. Hence, such is a future cost associated to this work which must also be taken into account. To that end, a salary for the author of 600 € per month [1] during a six-month period can be introduced into the budget.

Finally, costs associated to the documentation phase of the thesis have to be taken into account. Among them, one can estimate 100€ from printing articles and technical reports. No costs have to be included for obtaining the mentioned documentation, since these papers were either retrieved from the *NASA Technical Report Server*, which is public and free, from the Bioengineering and Aerospace engineering department of Universidad Carlos III de Madrid or from the internet. Other costs such as electricity are not considered in this budget due to the fact that the author has carried out his work either on public libraries or at the universities of Liège and Carlos III de Madrid.

As a result, the project budget amounts to a total of 3802.5 €. The decomposition of the costs that yield this value can be seen in Table B.1.

	PC Depreciation	**Salaries**	**Documentation**	**Software**	**Total**
Current Costs [€]	102.5	0	100	0	202.5
Expected Costs [€]	102.5	3600	100	0	3802.5

Table B.1: Summary of the costs associated to this thesis.

[1] Salary for student internships in which the intern is a non-resident, that is, lives 50 km or more away from *ESTEC*.

BIBLIOGRAPHY

[1] T. Brown, N. Idoine, E. Raycraft, R. Shaw, S. Hobbs, P. Everett, E. Deady, and T. Bide, "World Mineral Production 2012-2016," British Geological Survey, United Kingdom, 2018-978-0-85272-882-6, Tech. Rep., February 2018.

[2] J. Desjardins, *A Forecast of When We'll Run Out of Each Metal*, 2014 (accessed September 09, 2018). [Online]. Available: http://www.visualcapitalist.com/forecast-when-well-run-out-of-each-metal/

[3] E. Zapata, "The State of Play: US Space Systems Competitiveness," NASA Kennedy Space Center, Florida, USA, KSC-E-DAA-TN48988, Tech. Rep., October 2017.

[4] D. Smitherman, J. Fikes, S. Roy, M. W. Henley, and S. D. Potter, "Space Resource Requirements for Future In-Space Propellant Production Depots," NASA Marshall Space Flight Center, Futron Corporation and The Boeing Company, USA, 20020016967, Tech. Rep., October 2001.

[5] Center for Near Earth Object Studies, "Sentry: Earth impact monitoring," 2018 (accessed September 11, 2018). [Online]. Available: https://cneos.jpl.nasa.gov/sentry/

[6] Minor Planet Center, "Running tallies of near-earth objects discovered," 2018 (accessed September 12, 2018). [Online]. Available: https://minorplanetcenter.net/

[7] Center for Near Earth Object Studies, "Frequently asked questions," 2018 (accessed September 12, 2018). [Online]. Available: https://cneos.jpl.nasa.gov/faq/

[8] Center for Near Earth Object Studies, "Discovery statistics," 2018 (accessed September 11, 2018). [Online]. Available: https://cneos.jpl.nasa.gov/stats/

[9] Department of Geology, University of Minnesota, *Pyroxene Group of Silicates*, (accessed September 10, 2018). [Online]. Available: https://www.esci.umn.edu/courses/1001/minerals/pyroxene.shtml

[10] H. M. King, *Olivine*, (accessed September 10, 2018). [Online]. Available: https://geology.com/minerals/olivine.shtml

[11] Hobart M. King, *Plagioclase*, (accessed September 10, 2018). [Online]. Available: https://geology.com/minerals/plagioclase.shtml

[12] M. L. Nelson, D. Britt, and L. Lebofsky, "Review of asteroid compositions," *Resources of near-earth space*, pp. 493–522, January 1993.

[13] Jet Propulsion Laboratory and California Institute of Technology, *JPL Small-Body Database Browser*, (accessed September 12, 2018). [Online]. Available: https://ssd.jpl.nasa.gov/sbdb.cgi

[14] M. Sonter, "Near earth objects as resources for space industrialization," *Solar System Development Journal*, vol. 1, ISSN: 1533-7405, pp. 1–22, 2001.

[15] Arianespace, "Ariane 5 User's Manual," Arianespace, France, Ariane 5 User Manual Issue 5 Revision 2, Tech. Rep., October 2016.

[16] SpaceX, *Falcon Heavy*, (accessed September 13, 2018). [Online]. Available: https://www.spacex.com/falcon-heavy

[17] M. Wade, *N2O4/MMH*, 2017 (accessed September 07, 2018). [Online]. Available: http://www.astronautix.com/n/n2o4mmh.html

[18] D. A. Herman, G. C. Soulas, and M. J. Patterson, "Performance Evaluation of the Prototype Model NEXT Ion Thruster," Glenn Research Center and ASRC Aerospace Corporation, USA, NASA/TM-2008-215029, Tech. Rep., February 2008.

[19] NASA, "Ion Propulsion System (IPS): Information Summary for New Frontiers Mission," Glenn Research Center, Tech. Rep., January 2017.

[20] The Navigation and Ancillary Information Facility, *The SPICE Concept*, (accessed September 14, 2018). [Online]. Available: https://naif.jpl.nasa.gov/naif/spiceconcept.html

[21] Jet Propulsion Laboratory, *Deep Space 1*, 2017 (accessed September 09, 2018). [Online]. Available: https://www.jpl.nasa.gov/missions/web/deep_space_1.jpg

[22] Jet Propulsion Laboratory, *Topographic Maps of Ceres' East and West Hemispheres*, 2015 (accessed September 10, 2018). [Online]. Available: https://dawn.jpl.nasa.gov/multimedia/images/image-detail.html?id=PIA19607

[23] NASA, *OSIRIS-REx and its Payload Fairing*, 2016 (accessed September 10, 2018). [Online]. Available: https://www.asteroidmission.org/spacecraftfairing-in-cleanroom-ksc/

[24] Planetary Resources, *Arkyd 3 Reflight (A3R) Launches from Cape Canaveral on SpaceX CRS-6*, 2015 (accessed September 10, 2018). [Online]. Available: https://www.planetaryresources.com/2015/04/arkyd-3-reflight-a3r-launches-from-cape-canaveral-on-spacex-crs-6/

[25] Bryan Versteeg and Deep Space Industries, *Harvestor-1*, 2018 (accessed September 10, 2018). [Online]. Available: http://deepspaceindustries.com/media/gallery/

[26] H. D. Curtis, *Orbital Mechanics for Engineering Students*, 3rd ed. Elsevier, 2014.

[27] J. P. R. Scott W. Benson and S. R. Oleson, "NEXT Ion Propulsion System Configurations and Performance for Saturn System Exploration," NASA Glenn Research Center, Cleveland, USA, 20080006604, Tech. Rep., 2007.

[28] NASA, "Space Launch System (SLS) Mission Planner's Guide," National Aeronautics and Space Administration, USA, ESD 30000, Tech. Rep., April 2017.

[29] David Morante, Manuel Sanjurjo Rivo and Manuel Soler, "Multiobjective Low-Thrust Interplanetary Trajectory Optimization Based on Generalized Logarithmic Spirals," Universidad Carlos III de Madrid, Leganés, Spain, Tech. Rep., - 2018.

[30] Javier Roa, Anastassios E. Petropoulus and Ryan S. Park, "Semi-analytic preliminary design of low-thrust missions," *Advances in the Astronautical Sciences Astrodynamics*, vol. 162, AAS 17-623, 2017.

[31] Jet Propulsion Laboratory, *Environmental testing of the NASA/GRC NEXT ion thruster*, Unknown year (accessed September 07, 2018). [Online]. Available: https://sec353ext.jpl.nasa.gov/ep/img/ion_thrusters/next_tvac2.jpg

[32] Kalyanmoy Deb, Amrit Pratap, Sameer Agarwal and T. Meyarivan, "A fast and elitist multiobjective genetic algorithm: Nsga-ii," *IEEE Transactions on Evolutionary Computation*, vol. 6 No.2, pp. 182–197, 2002.

[33] Sentryo, *The 4 industrial revolutions*, 2017 (accessed September 09, 2018). [Online]. Available: https://www.sentryo.net/the-4-industrial-revolutions/

[34] J. Cato, *Raw Materials Used in the Manufacture of Electronic Components*, 2017 (accessed September 09, 2018). [Online]. Available: https://sciencing.com/raw-used-manufacture-electronic-components-8053265.html

[35] United Nations, *World population projected to reach 9.7 billion by 2050*, 2015 (accessed September 09, 2018). [Online]. Available: http://www.un.org/en/development/desa/news/population/2015-report.html

[36] Planetary Resources, *Why Asteroids*, Unknown publication year (accessed September 09, 2018). [Online]. Available: https://www.planetaryresources.com/why-asteroids/

[37] energy4me, *Petroleum – Oil and Natural Gas*, 2015 (accessed September 09, 2018). [Online]. Available: http://energy4me.org/all-about-energy/what-is-energy/energy-sources/petroleum/

[38] A. Mamiit, *The World's First Trillionaire Will Be The One Who Harnesses Space Mining*, 2018 (accessed September 09, 2018). [Online]. Available: https://www.techtimes.com/articles/225886/20180423/the-worlds-first-trilionnaire-will-be-the-one-who-harnesses-space-mining.htm

[39] NASA., "Mars Science Laboratory Launch," NASA Kennedy Space Center and Jet Propulsion Laboratory, Florida and California, USA, Press Kit-November 2011, Tech. Rep., November 2011.

[40] Jet Propulsion Laboratory, *Mars Exploration Rovers*, Unknown publication year (accessed September 09, 2018). [Online]. Available: https://mars.nasa.gov/mer/mission/spacecraft.html

[41] L. Sibille, *Space Resources*, 2012 (accessed September 09, 2018). [Online]. Available: https://isru.nasa.gov/SPACERESOURCES.html

[42] M. D. Hogue, L. Sibille, R. P. Mueller, P. E.Hintze, and D. J. Rasky, "Regolith Derived Heat Shield for Planetary Body Entry and Descent System with In Situ Fabrication," NASA Kennedy Space Center and NASA Ames Research Center, Florida and California, USA, KSC-2013-055R, Tech. Rep., November 2012.

[43] NASA, *NEAR Shoemaker*, 2018 (accessed September 08, 2018). [Online]. Available: https://solarsystem.nasa.gov/missions/near-shoemaker/in-depth/

[44] NASA Space Sciences Data Coordinated Archive, *Deep Space 1*, 2017 (accessed September 09, 2018). [Online]. Available: https://nssdc.gsfc.nasa.gov/nmc/spacecraftDisplay.do?id=1998-061A

[45] NASA Space Sciences Data Coordinated Archive, *Hayabusa*, 2017 (accessed September 10, 2018). [Online]. Available: https://nssdc.gsfc.nasa.gov/nmc/spacecraftDisplay.do?id=2003-019A

[46] NASA Space Sciences Data Coordinated Archive., *Dawn*, 2017 (accessed September 10, 2018). [Online]. Available: https://nssdc.gsfc.nasa.gov/nmc/spacecraftDisplay.do?id=2007-043A

[47] NASA Space Sciences Data Coordinated Archive, *Hayabusa II*, 2017 (accessed September 10, 2018). [Online]. Available: https://nssdc.gsfc.nasa.gov/nmc/spacecraftDisplay.do?id=2014-076A

[48] NASA, University of Arizona and Lockheed Martin, *OSIRIS-REx Asteroid Sample Return Mission*, 2018 (accessed September 10, 2018). [Online]. Available: https://www.asteroidmission.org/objectives/

[49] Planetary Resources, *Planetary Resources and the Government of Luxembourg Announce €25 Million Investment and Cooperation Agreement*, 2016 (accessed September 10, 2018). [Online]. Available: https://www.planetaryresources.com/2016/11/planetary-resources-and-the-government-of-luxembourg-announce-e25-million-investment-and-coop

[50] Deep Space Industries, *Comet Water-based SmallSat Propulsion*, 2018 (accessed September 10, 2018). [Online]. Available: http://deepspaceindustries.com/comet/

[51] Deep Space Industries, *Xplorer Low Cost Deep Space Exploration Spacecraft*, 2018 (accessed September 10, 2018). [Online]. Available: http://deepspaceindustries.com/xplorer/

[52] C. Jamasmie, "Luxembourg shoots for the stars with fresh space mining deal," July 2017 (accessed September 10, 2018). [Online]. Available: http://www.mining.com/luxembourg-shoots-stars-fresh-space-mining-deal/

[53] United Nations Office for Outer Space Affairs, "Committee on the peaceful uses of outer space," 2018 (accessed September 10, 2018). [Online]. Available: http://www.unoosa.org/oosa/en/ourwork/copuos/index.html

[54] United Nations Office for Outer Space Affairs, "Treaty on principles governing the activities of states in the exploration and use of outer space, including the moon and other celestial bodies," 2018 (accessed September 10, 2018). [Online]. Available: http://www.unoosa.org/oosa/en/ourwork/spacelaw/treaties/outerspacetreaty.html#a

[55] United Nations Office for Outer Space Affairs, "Agreement governing the activities of states on the moon and other celestial bodies," 2018 (accessed September 10, 2018). [Online]. Available: http://www.unoosa.org/pdf/gares/ARES_34_68E.pdf

[56] Space Resources Luxembourg, "A space development agency and a space investment fund are part of luxembourg's strategy to realize the country's space resources vision," 2018 (accessed September 10, 2018). [Online]. Available: https://spaceresources.public.lu/en/actualites/2018/Space-Forum-2018.html

[57] Center for Near Earth Object Studies, "Neo basics," 2018 (accessed September 11, 2018). [Online]. Available: https://cneos.jpl.nasa.gov/about/basics.html

[58] S. Writers, *NEXT-C Advanced Electric Propulsion Engine Cleared to Begin Production*, 2018 (accessed September 07, 2018). [Online]. Available: http://www.spacedaily.com/reports/NEXT_C_Advanced_Electric_Propulsion_Engine_Cleared_to_Begin_Production_999.html

[59] J. S. Lewis, "Asteroid Resources," Lunar and Planetary Laboratory, University of Arizona and NASA, USA, 19930007691, Tech. Rep., January 1992.

[60] R. E. Gertsch, "Asteroid Mining," Colorado School of Mines, Colorado, USA, 19930007695, Tech. Rep., January 1992.

[61] J. J. K. Daemen, "Mining Nonterrestrial Resources: Information Needs and Research Topics," Department of Mining and Geological Engineering, University of Arizona, Tucson, USA, 19930007696, Tech. Rep., January 1992.

[62] S. D. Ross, "Near Earth Asteroid Mining," California Institute of Technology, California, USA, Space Industry Report, Tech. Rep., December 2001.

[63] European Space Agency, *Rosetta Swingby Update*, 2007 (accessed September 08, 2018). [Online]. Available: http://www.esa.int/About_Us/ESOC/Rosetta_swingby_update_-_03_13_CET_25_February

[64] NASA, *MESSENGER Completes Second Flyby of Venus*, 2007 (accessed September 08, 2018). [Online]. Available: https://web.archive.org/web/20081005102038/http://sse.jpl.nasa.gov/news/display.cfm?News_ID=21335

[65] Javier Roa and Jesús Peláez, "Introducing a degree of freedom in the family of generalized logarithmic spirals," *26th Spaceflight Mechanics Meeting*, vol. AAS 16-317, 2016.

[66] European Space Agency, *Electric versus Chemical Propulsion*, 2004 (accessed September 06, 2018). [Online]. Available: http://sci.esa.int/smart-1/34201-electric-spacecraft-propulsion/?fbodylongid=1535

[67] NASA, *Space Shuttle Propulsion System*, Unknown publication year (accessed September 07, 2018). [Online]. Available: https://www.nasa.gov/pdf/466750main_AP_ST_Chem_ShuttlePROP.pdf

[68] M. J. Turner, *Rocket and Spacecraft Propulsion: Principles, Practice and New Developments*, 3rd ed. Springer and Praxis, 2009.

[69] NASA, *Ion Propulsion*, 2016 (accessed September 07, 2018). [Online]. Available: https://www.nasa.gov/centers/glenn/about/fs21grc.html

[70] The Navigation and Ancillary Information Facility, *Index of public generic kernels*, (last accessed September 15, 2018). [Online]. Available: https://naif.jpl.nasa.gov/pub/naif/generic_kernels/

[71] D. A. Vallado, *Fundamentals of Astrodynamics and Applications*, 4th ed. Microcosm Press and Springer, 2013.

[72] J. R. Vicens, *JPL Small-Body Mission-Design Tool*, 2018 (accessed May 05, 2018). [Online]. Available: https://ssd.jpl.nasa.gov/?mdesign_welcome

[73] European Space Agency, *Rosetta Timeline*, 2016 (accessed May 07, 2018). [Online]. Available: http://www.esa.int/Education/Teach_with_Rosetta/Rosetta_timeline

[74] N. Srinivas and Kalyanmoy Deb, "Multiobjective optimization using nondominated sorting in genetic algorithms," *Evolutionary Computation*, vol. 2 No.3, pp. 221–248, 1994.

[75] Shubham Jain, *Introduction to Genetic Algorithm and their application in data science*, July 2017 (last accessed September 16, 2018). [Online]. Available: https://www.analyticsvidhya.com/blog/2017/07/introduction-to-genetic-algorithm/

[76] Lin Song, *NGPM– A NSGA-II Program in Matlab*, June 2011 (last accessed September 16, 2018). [Online]. Available: https://nl.mathworks.com/matlabcentral/fileexchange/31166-ngpm-a-nsga-ii-program-in-matlab-v1-4

[77] Elizabeth Howell, *Hayabusa2: Japan's 2nd Asteroid Sample Mission*, July 2018 (last accessed September 24, 2018). [Online]. Available: https://www.space.com/40161-hayabusa2.html

[78] Impact Data Source, *Choosing a Discount Rate*, September 2011 (last accessed September 24, 2018). [Online]. Available: https://impactdatasource.com/choosing-a-discount-rate/